1971

Electrical Conductivity And Thermal Decomposition Of Ammonium Perchlorate

Wee Lam Ng

ELECTRICAL CONDUCTIVITY AND THERMAL DECOMPOSITION OF AMMONIUM PERCHLORATE

by

Wee Lam Ng

Department of Chemistry

Submitted in partial fulfillment
of the requirements for the degree of
Doctor of Philosophy

Faculty of Graduate Studies
The University of Western Ontario
London, Canada
August, 1971

ABSTRACT

The kinetics of the solid state thermal decomposition of ammonium perchlorate (AP) has been studied using both pellets and single crystals over a wide temperature range from about 200° to 300°C. The effect of visual crystal faults and of doping with the divalent ions Ba^{2+} and SO_4^{2-} on the chemical reactivity of AP have also been examined. Kinetic analysis of the decomposition curve by a non-linear least-squares method using computing techniques has revealed some important findings: (i) the decomposition consists of four distinct stages, (ii) the major part of the entire reaction ($0.01<\alpha<1.00$, where α is the fractional decomposition) is described by the exact Avrami equation, (iii) the so-called "induction period" comprises a linear process plus an exponential process and involves the first 1% of the total decomposition, and (iv) the induction period is usually preceded by an instantaneous desorption of previously adsorbed species.

The three decomposition steps have been identified with the following processes. The linear inward growth of surface nuclei gives rise to the linear process. Branching of surface nuclei along preferred crystallographic directions

is associated with the exponential process. Formation and growth of nuclei in the bulk of the crystal are responsible for the Avrami process. These kinetic interpretations may be correlated with the most recent microscopic observations by Herley, Jacobs and Levy on the formation and growth of decomposition nuclei in AP.

The topochemical nature of the reaction was further emphasized when doped samples were investigated. The rate of the bulk reaction was enhanced in both Ba^{2+} and SO_4^{2-}-doped AP crystals. Whereas Ba^{2+} ions shortened the time for the completion of the surface reaction, doping with SO_4^{2-} ions prolonged it. Based on the above results, a step-wise proton transfer mechanism which involved the participation of lattice defects (cation vacancies and dislocations) was proposed.

Extensive measurements have been made of the a.c. electrical conductivity of both compressed pellets and single crystals of AP. The mechanism of conduction is proposed to be proton transfer over the whole temperature range. The effects of adsorbed water and ammonia were investigated and the results support the proposed proton transfer mechanism.

ACKNOWLEDGMENT

I would like to express my sincere gratitude to my supervisor Professor P. W. M. Jacobs for his constant guidance, patience and invaluable help throughout the course of this work.

I would also like to thank Professor J. M. Thomas for several useful conversations with him during his three-week stay as a Visiting Professor in this Department. I am also indebted to the graduate students, post-doctoral fellows, faculty members, visitors and technical staff who have contributed to my education at Western.

For the supply of some ammonium perchlorate crystals, I would like to thank Dr. P. J. Herley of Brookhaven National Laboratory, New York.

Lastly, I must also thank my wife not only for typing this thesis but also for her constant encouragement, understanding and help.

TABLE OF CONTENTS

LIST OF TABLES

LIST OF FIGURES

FIGURES

CHAPTER 1

INTRODUCTION

1-1 Solid State Reactions

The study of the reactivity of solids is a branch of solid state chemistry which includes the decomposition of solids, reaction between solids, and reaction between a solid and a gas. This thesis deals primarily with the decomposition of a simple ionic solid, ammonium perchlorate. The mechanism of its decomposition into gaseous products will however be seen to be anything but simple. Some general features of solid state reactions will be reviewed briefly. It will be seen that the sites for and the initial rate of reaction are, to a large extent, determined by the surface states and the defect structure of the solid. The decomposition of solids has received considerable attention in recent times since the pioneering work of Garner[1] and of Tompkins[2] and their co-workers. The first stage of an investigation is usually a kinetic study; the final objective a complete understanding of the physics and chemistry involved in the mechanism of the reaction. While this is undoubtedly of the greatest interest and importance to the solid state chemist, it is seldom possible to deduce a complete mechanism from kinetic data alone. Direct observations with the optical and electron

microscopes and the measurement of physical properties such as optical absorption spectra and electronic or ionic conductivity are of the utmost help and importance in deducing mechanisms.

The decomposition curve is always represented by a plot of fractional decomposition α against time t. The curve has in general a sigmoid shape and this is characteristic of all solid state decompositions. It comprises an initial "induction period" during which the change of α with t is virtually zero. This is then followed by an acceleratory region ($d\alpha/dt$ increasing with t) which is later succeeded by a decay period ($d\alpha/dt$ decreasing) until the completion of the reaction. However, it is not necessarily true that all three stages should occur during the course of a particular reaction. The induction period, for example, may be prolonged, shortened or even entirely absent (lead azide)[3]. The shape of the decomposition curve therefore depends vastly on the solid decomposed, and the temperature at which reaction occurs.

It is nowadays generally accepted that reaction in the solid phase commences only at certain selective locations, called potential nucleus forming sites where the free energy for reaction is least and steric considerations favourable. These locations are most probably related to lattice defects which are always present in any crystalline solid. Jacobs and Tompkins[2] pointed it out that when fluctuations in the local energy of the crystal are sufficiently large to provide

the necessary activation energy, formation of a nucleus (nucleation) takes place. This process is irreversible because in a solid state decomposition (in contrast to a phase change), the free energy change associated with the chemical transformation is generally very large. When nuclei are formed, growth of nuclei can occur in λ dimensions (λ=1, 2, or 3). Normally preferential growth takes place along certain crystallographic planes, resulting in nuclei of a distinct shape, e.g. horn shaped $(CuSO_4 \cdot 5H_2O)$[4], spherical (BaN_6)[5], or hexagonal $(KHC_2O_4 \cdot H_2O)$[6]. Because reaction in a solid is of a topochemical nature, the traditional concepts of order and molecularity, as generally applied in gas phase and liquid phase reaction kinetics, are of little use in interpreting the kinetics of solid state reactions. Because chemical decomposition is confined to the interface between the solid product and the reactant phase, the reaction kinetics can be described in terms of the rate of nucleation and the rate of growth of these nuclei. The overall rate of the reaction is then governed by the equations controlling the formation and growth of nuclei.

The most general law of nucleation is that described by equations 1-1, 1-2

$$\frac{dN}{dt} = k_1(N_o - N) \qquad 1\text{-}1$$

or, $$N = N_o[1 - \exp(-k_1 t)] \qquad 1\text{-}2$$

where, N is the number of nuclei formed in time t, k_1 is the rate constant for nucleus formation, and N_o is the number of potential nucleus forming sites. It is based on the assumption that nucleation is random at a finite number of sites N_o. Microscopic observation during the decomposition of solids has generally revealed[2] that nuclei grow at a constant rate, at least when they are of visible dimensions. Let G(x) be the rate of growth in the x-direction. The size of a nucleus which commences growth at t=t' is, at time t, if the growth is isotropic,

$$v(t,t') = \sigma\left[\int_{t'}^{t} G(x)dx \right]^{\lambda} \qquad 1\text{-}3$$

where σ denotes the shape factor for the nuclei (=4/3 for spherical nuclei). The total size of all nuclei $\bar{V}(t)$ is then given by

$$\bar{V}(t) = \int_{o}^{t} \sigma\left[\int_{t'}^{t} G(x)dx \right]^{\lambda} \left[dN/dt\right]_{t=t'} dt' \qquad 1\text{-}4$$

where $\bar{V}(t) = V(t)/V(\infty)$. If overlapping of growth nuclei is neglected, α is simply proportional to $\bar{V}(t)$. Equation 1-4 predicts that $\bar{V}(t)=\infty$ at $t=\infty$. Clearly overlapping of nuclei cannot be neglected during the decay period. This is because as nuclei grow larger, they must eventually impinge on one another resulting in a cessation of growth when nuclei touch. This consideration can be expressed in terms of the "extended" fractional decomposition α_{ex} which is the total fractional

decomposition without overlapping. The actual fractional decomposition α in which overlapping is included[7] is then related to α_{ex} by equation 1-5

$$d\alpha/d\alpha_{ex} = 1 - \alpha \qquad 1\text{-}5$$

so that α_{ex} can be replaced by $-\ell n\ (1-\alpha)$. Equation 1-4 therefore provides a direct link of the rate of nucleation and of the rate of nucleus growth to the fractional decomposition. In general, it is not easy to find empirically the appropriate forms of the equations for nucleation and nucleus growth from direct microscopic observation. Rather, an indirect approach is usually adopted. This is done by analysing the experimental decomposition curve $\alpha(t)$ using the existing expressions derived by substituting in eqn. 1-4 appropriate expressions for dN/dt and G(x). The expression that gives the best fit to the curve suggests, but does not prove, a topochemical mechanism for the reaction.

There are two kinetic equations that had been found most useful by previous workers on the decomposition of ammonium perchlorate. They are the Avrami equation[8] (1-6) and the Prout-Tompkins[9] equation (1-7)

$$-\ell n\ (1-\alpha) = \frac{6\sigma N_o k_2^3}{k_1^3}\left\{ e^{-k_1 t} - 1 + k_1 t - \frac{k_1^2 t^2}{2} + \frac{k_1^3 t^3}{6} \right\} \qquad 1\text{-}6$$

$$\ell n\ (\alpha/1-\alpha) = k_3 t + c \qquad 1\text{-}7$$

where k_1, k_2, k_3 are respectively the rate constants for nucleation, nucleus growth, and branching of nuclei, and c is a constant. The Avrami equation is based on random nucleation followed by isotropic three-dimensional nucleus growth. Both impingement (overlapping) of growth nuclei and the ingestion of nucleus forming sites by growing nuclei are included. The derivation of eqn. 1-6 has been discussed in detail in the literature[2,10]. Because of its complex mathematical structure, only its approximate form has been used previously[8]; this is often referred to as the Avrami-Erofeev (AE) equation (1-8).

$$\left[-\ell n\ (1-\alpha)\right]^{1/n} = \bar{k}_n t \qquad 1\text{-}8$$

where n=3 for $k_1 t \gg 1$ and n=4 for $k_1 t \ll 1$, respectively; $\bar{k}_n$ is the rate constant for a particular n.

The Prout-Tompkins equation[2] is based on a model in which the branching of nuclei is considered a more important event than the formation of fresh nuclei. The interference of branching nuclei is also taken into account in the derivation.

1-2 Physical Properties of Ammonium Perchlorate (AP)

AP is an ionic crystalline solid in which the constituent ions are NH_4^+ and ClO_4^-. They form an orthorhombic crystal structure which undergoes a phase transition at 240°C to a cubic form. This is associated with the onset of free rotation of the anion[11]. Another transition occurs at much lower temperature which is associated with the onset of cation

rotation at -190°C. The NH_4^+ ions are not involved in hydrogen bonding[11]. The orthorhombic form has cell dimensions a_o=9.202 Å, b_o=5.816 Å, c_o=7.449 Å, and a crystal density of 1.95 g/cm^3; whereas the cubic form has a cube edge of 7.63 Å and a crystal density of 1.76 g/cm^3. The transition at 240°C therefore gives rise to a slight increase in volume. The heat of transition[11] is 2.3±0.2 kcal mole^{-1}. The vapor pressure[12] at room temperature is 10^{-11} torr. The solubility[13] of AP at 30°C is 26.0 g per 100 ml of H_2O. The cleavage planes for the orthorhombic form are (210) and (001). The cleaved crystal has two rhombic (c) faces and four rectangular (m) faces.

1-3 Low Temperature Thermal Decomposition of AP

The chemical decomposition of AP in the solid state has been investigated intensively during the past two decades. The motivation for this undoubtedly stems from two facts: (i) the decomposition is involved in the combustion of a large class of composite propellants in which AP is used as the oxidizer; and (ii) the mechanism by which AP decomposes has not yet been fully elucidated.

Measurable decomposition of AP commences at about 150°C, it is accompanied by dissociative sublimation. The sublimate is chemically pure AP although traces of decomposition products have been reported as contaminants[9]. The decomposition products are all gaseous. The reaction can be further classified[11] into (i) the high temperature (HT) reaction which occurs above 300°C according to equation 1-9

$$2NH_4ClO_4 \longrightarrow Cl_2 + 2NO + O_2 + 4H_2O \qquad 1\text{-}9$$

(ii) the low temperature (LT) reaction which occurs below 300°C and proceeds according to equation 1-10

$$4NH_4ClO_4 \longrightarrow 2Cl_2 + 2N_2O + 3O_2 + 8H_2O \qquad 1\text{-}10$$

These equations[11] only represent the approximate stoichiometry. The differences between these two reactions are that, whereas the high temperature reaction takes place in the gas phase and proceeds to completion, the low temperature reaction is confined only to the solid phase and decomposition is incomplete. The reaction always ceases after roughly 30% decomposition[9] (the actual percentage depends on conditions, particularly, temperature, ambient pressure and the presence of catalysts) leaving a residue which is a spongy and highly porous mass[9,14], chemically identical to the unreacted salt[9], but with a much greater specific surface area[8]. Its chemical reactivity can be restored[11] by sublimation, recrystallization or mechanical deformation.

The decomposition curve has a slightly distorted sigmoid shape. The rate of the reaction has been followed by measuring the pressure build-up in a constant volume system[8,9] or by measuring the weight loss[15] during the course of the reaction. Initial studies on AP by pressure measurements[9] suggested that the Prout-Tompkins equation (1-7) described the decomposition curve fairly well but later workers have

generally preferred the Avrami-Erofeev (AE) equation (1-8) with n=2,3,4, as it gave a better fit to the data over a wider range of α[8,15-17]. In a recent study by Jacobs and Russell-Jones[15], using weight loss measurement, they found a single value for the activation energy of ~30 kcal mole^{-1} for low- and high-temperature reactions and for sublimation. A unified mechanism[15,18] as represented by equations 1-11, was then proposed for the reaction, and is now generally accepted.

$$\begin{array}{ccccc} NH_4ClO_4(s) & \rightleftharpoons & NH_3(a) + HClO_4(a) & \rightsquigarrow & \text{LT prod.} \\ & & \downarrow\uparrow \quad\quad \downarrow\uparrow & & \\ \text{Sublimate} & \longleftarrow & NH_3(g) + HClO_4(g) & \rightsquigarrow & \text{HT prod.} \end{array} \qquad 1\text{-}11$$

The primary process involves a proton transfer which requires much of the 30 kcal mole^{-1} activation energy. The fact that $HClO_4$ accelerated the reaction[18] while NH_3 retarded it[18], probably implies that the low temperature reaction proceeds by the decomposition of adsorbed $HClO_4$ followed by the oxidation of adsorbed NH_3.

The effect on the decomposition of various catalysts[19-21] and of pre-irradiation with x-[22,23] and γ-radiation[24,25] has also been studied, but a detailed description and review of all the previous work in the decomposition of AP is unnecessary in this thesis as there are three recent and readily available review papers[11,12,26] in the literature.

Despite the progress that had been made in understanding the mechanism of the primary process during decomposition,

there still remained certain features of the reaction to be explored. (i) When $-\ell og\ (1-\alpha)^{1/n}$, with n=2, 3, or 4 is plotted against t, there is always a finite intercept t_o, called the "induction period" on the time axis. The length of this period decreased as the temperature was raised. So far no satisfactorily explanation for the occurence of this induction period, prior to significant decomposition, has been advanced. (ii) The AE equation did not fit over the entire range of the acceleratory and decay period. Also, different values of α appeared to be required for AP in different physical forms. For single crystals of orthorhombic AP, Galwey and Jacobs[8] found n=4 for $0.02 \leq \alpha \leq 0.20$ and n=3 for $0.20 \leq \alpha \leq 0.90$. This is consistent with three dimensional growth of randomly formed nuclei. The activation energies E_n were E_4=21 and E_3=17 kcal $mole^{-1}$. For orthorhombic powder the best fit was obtained with n=4, E_4=25 kcal $mole^{-1}$ ($0.03 \leq \alpha \leq 0.70$); for pellets the corresponding values were n=3 and E_3=30 kcal $mole^{-1}$ ($0.05 \leq \alpha \leq 0.75$). These values of n can be explained by assuming that the nucleation stage is prolonged in powdered material but shortened in pellets. This implies a connection between nucleus forming sites and strained regions of the crystal. However, the variations in activation energy are hard to understand. For cubic AP the best fit was found with n=2 for crystals, powder and pellets, E_2 being 25, 25 and 30 kcal $mole^{-1}$ respectively.

Herley and Levy[17] also divided the decomposition

curve for single crystals into two sections: in the accelerating period ($0.07 \leq \alpha \leq 0.25$) n=4 and the activation energy is 27 kcal $mole^{-1}$; in the decay period ($0.40 \leq \alpha \leq 0.98$) n=3 and the activation energy is 25 kcal $mole^{-1}$. These activation energies are significantly different to those found by Galwey and Jacobs[8] for the same material (small single crystals of orthorhombic AP). A possible explanation would be the certain arbitrariness in deciding when n=4 ceases to apply and n=3 commences. Both these versions of the AE equation are approximate forms of the complete Avrami equation (1-6), valid for $k_1t \ll 1$ and $k_1t \gg 1$ respectively. Thus a change-over period, where neither version fits should occur. It is at least reasonable to suspect that the variations in activation energy could be the result of using the approximate form of the complete Avrami equation (1-6). The activation energies found for pellets made from powdered AP are more consistent. Davies, Jacobs and Russell-Jones[18] have carried out least-squares fits to the Arrhenius equation using rate constants derived by various members of their group under a wide variety of experimental conditions. They were unable to resolve the problem of whether there is a discontinuity at the transition point in the rate constant of decomposition of pellets. Fitting data above and below the transition point separately gave E=33.9 kcal $mole^{-1}$ for the orthorhombic structure and E=27.0 kcal $mole^{-1}$ for the cubic modification. If data over the whole temperature range are used then E=26.6 kcal $mole^{-1}$. All these rate constants were obtained from the AE equation

with n=2, but for decomposition carried out at low ambient pressures n=3 fitted the data at lower values of α than did n=2.

The variations in activation energy found for whole crystals, possible difficulties associated with the interpretation of the value of n less than 3, and particularly the need for using different values of n for different physical forms and crystal modifications[8] all lead to the conclusion that the AE equation is probably an oversimplified description of the kinetics of decomposition of AP.

The profound effect of impurities[27-30] on the kinetics of decomposition perhaps explain the discrepancies found in the literature[11]. Maycock et al.[27] recently showed that decomposition is enhanced by doping with SO_4^{2-} while retarded by Ca^{2+}. The activation energy is not altered by the impurities. In another study using Cu^{2+} as impurity, Solymosi and Dobo[29] showed that the decomposition below the transition point was greatly enhanced, whereas Savintsev et al.[28] showed that only the nucleation step is enhanced. The effect of various cation and anion impurities was also studied[30] using differential scanning calorimetry (DSC). The doped samples were prepared by rapidly cooling a saturated aqueous solution of AP and the impurity ion. Both Ba^{2+} and SO_4^{2-} were found to have no effect on the decomposition rate. These experiments, however, are rather inconclusive as it is doubtful whether the impurities can be incorporated

effectively into the lattice of AP by rapid coprecipitation. Polyvalent anions (PO_4^{3-} and SO_4^{2-}) were found to retard the decomposition and cations (Ca^{2+} and Mg^{2+}) were found to accelerate it[31]. It appears that before the effect of impurities can be assessed, it must first of all be established, whether the impurities have in fact been incorporated in the lattice.

1-4 Electrical Conductivity of AP

The thermal instability of AP restricts considerably the working range over which the electrical conductivity can be measured accurately. The first investigation was that of Zirkind and Freeman[32] who used pellets of AP in the temperature range of 25° to 125°C. Irreproducibility from sample to sample of about a factor of 2 was always encountered, even when samples were annealed overnight at 110°C prior to measurements. An activation energy of about 1 eV was deduced from the plot of log σ vs. 1/T, where σ is the specific conductivity. Owing to the lack of information regarding the conducting species, no detailed conclusions could be drawn at that stage.

More recently, both Maycock et al.[27] and Wise[33] have independently investigated the electrical conductivity of AP over a wider temperature range. Maycock et al. used single crystals of AP grown at the Naval Research Laboratory at China Lake. Surprisingly, they found a complex temperature dependence of σ in the temperature range 25°C to 350°C. A d.c.

method of measurement was employed with 40 V across the sample. The conductivity curve (log σT vs. 1/T) showed three distinct changes of slope occuring at 92°, 171°, and 255°C. It was suggested that conducting species were Frenkel defects in the orthorhombic region but Schottky defects in the cubic modification. The activation energy of migration was tentatively assigned as 0.5 eV and the energies of formation of Frenkel and Schottky defects were deduced to be 0.6 eV and 3.0 eV respectively. On the other hand, Wise[33] found the plot of log σT vs. 1/T to be a straight line between 225° and 325°C with no discontinuity on passing through the transition point. He concluded that the conduction process involved protons, as the conductivity showed a linear increase with the partial pressure of ammonia. The activation energy in the presence of N_2 was found to be 1.4 eV, and in the presence of NH_3, 0.87 eV. These values were interpreted as the energy required for defect migration (0.87 eV) and the enthalpy for defect formation (1.0 eV). These results[27,33] are in contradiction with one another, and hence complicate efforts to understand the mechanism of conductivity and its possible relevance to thermal decomposition.

Before any judgement can be made, it is of the utmost importance to identify the charge-carrier. The most elegant work of Boldyrev et al.[34] on the electrolysis of AP has resolved this problem. When a d.c. current was applied to AP, only hydrogen was detected at the cathode, the amount produced

being in accord with Faraday's law. This implied that both the discharging and conducting species were the proton. The conductivity plot was found[31] to be composed of two straight lines below the transition temperature, with a change of slope at 72°C. The activation energies found were 0.48 eV between 30° and 72°C and 0.87 eV between 72° and 170°C. The mechanism by which protons were produced in and migrated through the crystal could not, however, be elucidated.

1-5 Objectives of this Research

The preceding summary has shown that the decomposition of AP is not fully understood; apart from discrepancies between various estimations of E, there are the shortcomings of the AE equation (the most successful one to be applied so far) and above all the mystery of the induction period. Also there are serious disagreements in conductivity measurements made by various previous investigators which have not been explained. Recent work on AP has tended to focus on the induction period and it is now recognized that the term, "induction period" cannot be taken in a literal sense. It implies more than merely the time required to bring the sample to the decomposition temperature, or the time taken for the germ nuclei to grow into stable growth nuclei. Irradiation studies[17,35-38] have confirmed that the induction period was considerably shortened when the sample was exposed to γ- or x-radiation, and that this shortening was directly proportional

to the logarithm of dose[35-37]. Irradiation therefore presumably produced a large number of nuclei in the solid. Direct observations of nucleation and nucleus growth have also been made[39,40] during the early stages of decomposition at low temperatures. Spherical nuclei[39], 20-30 μm beneath the crystal surface, and also holes[40] which appeared to reflect the shape of the crystal face under investigation were observed. As nuclei cannot be seen when first formed, the nuclei as seen under the microscope were presumably ones that had already grown considerably. No assessment could therefore be made as to whether nucleation and nucleus growth occur during the induction period.

The aims of this research were, therefore: (i) to explore the nature of the induction period by making careful measurements of α using pressure measurements; (ii) to search for equations which would describe accurately the kinetics of the low temperature reaction; (iii) to study the effect on the kinetics of the reaction and on the duration of the induction period, of doping AP crystals with the divalent impurity ions Ba^{2+} and SO_4^{2-}, which would be expected to produce cation vacancies and anion vacancies respectively; (iv) to look for any correlation between the electrical conductivity and the decomposition of AP; and (v) to investigate the mechanism of protonic conduction in AP to resolve, if possible, the disagreement between the results of previous workers. As the proposed experiments would involve the use of single

crystals of good quality, considerable effort would also have to be devoted to the preparation of sufficiently large single crystals of both pure AP and Ba^{2+}- and SO_4^{2-}-doped AP.

CHAPTER 2

EXPERIMENTAL

As described in Chapter 1, this research involves an attempt to acquire a deeper understanding of the mechanism of the thermal decomposition of ammonium perchlorate (AP), and its correlation with electrical conductivity. This chapter consists of a general description on the experimental technique used (i) in measuring the pressure build-up as a function of time when a sample of AP is decomposed isothermally, and (ii) in measuring the electrical conductivity when the temperature is increased continuously from room temperature to the transition temperature. The importance of using single crystals, whenever possible, in solid state chemistry was well appreciated. However, compressed pellets were frequently used not only in preliminary studies, but also to provide a comparison between the behavior of single crystals and pellets, which have often been employed in previous work.

2-1 Sample Preparation

Ammonium Perchlorate in the form of anhydrous powder of 99.99% purity was obtained from the Fisher Scientific Co.. The only stated impurity was 0.002% by weight of chlorate ion. The powder was first ground thoroughly in an agate motar

and then compressed using a manual press into small cylindrical pellets of diameter 3.195 mm, and height about 4 mm. These pellets had a density equal to 93.6% crystal density and were of an average weight of 40 mg, suitable for decomposition experiments. Disc-like pellets of diameter 12.78 mm and height about 4 mm, a size more suitable for conductivity measurements were also made manually, but these had a density of only 79.3% crystal density. Pellets of diameter 12.96 mm and height about 2.2 mm were made using a hydraulic press and a pressure of 14,000 p.s.i.. These had a higher density of 98.6% crystal density. All pellets were stored in a desiccator over silica gel for several days before use.

Some small plate-like single crystals were obtained through the courtesy of Dr. P. J. Herley of Brookhaven National Laboratory. These small crystals had many visual faults within the crystal bulk. They had an average weight of ~10 mg and were usable only for decomposition studies. They are referred to in this thesis as BNL crystals.

An apparatus was built with the object of growing large single crystals of good quality both of pure AP and also of AP doped with Ba^{2+} and with SO_4^{2-} ions. The dopants were respectively A.R. $(NH_4)_2SO_4$ from British Drug Houses and analytical grade $Ba(ClO_4)_2 \cdot 3H_2O$ from Alfa Inorganics. The technique used for growing these crystals will be described along with the general description of apparatus

in a later section. These crystals were used mainly for conductivity measurements, but small cleaves from them were also used in decomposition studies so as to compare rate data with the more imperfect BNL crystals and thus provide information about effect of gross visual crystal faults on the chemical reactivity of AP.

2-2 Apparatus

2-2-1 Crystal Growth

Single crystals of AP were grown from aqueous solution using the crystal growing equipment[41] shown in Figs. 1 and 2. The seed crystals were supported on a glass pins by epoxy resin, the pins being inserted into the sockets K at the end of each "arm" or branch of the "tree" (Fig. 1). Two sets, each of four arms, were staggered to allow room for the seeds to grow. To each arm was attached by nylon thread N a glass-plate V, which hung freely in the solution; these plates stirred the solution as the axis bearing the arms rotated. A set of four paddles Q, twisted at an angle of about 45° with respect to the vertical, was attached to the crystal tree about half of an inch below the solution level L. This ensured efficient stirring near the top of the solution and is necessary to remove unwanted nuclei which would otherwise be formed on the surface during concentration of the solution. The seeds were prepared by slow evaporation of a saturated solution from about 10°C above room temperature. Only good quality seeds were

selected and these were cleaved along the cleavage planes, (210) and (001), to yield small rhombic prisms of size about 2×2×1 mm. The seeds were glued with epoxy resin to the glass pins on either the rhombic face (210) or the rectangular face (001) vertically. These were left overnight to allow the epoxy resin to harden and then the pins were inserted in the sockets K. 1.6 litre of an aqueous solution saturated with AP at about 30°C was prepared in a pyrex jar cut from a 2 litre beaker. The jar was covered by perspex lid A to which was attached a mechanical device for rotating the seed. The "crystal tree" was attached to the shaft S of the rotation mechanism via a demountable T-joint by means of a horizontal stainless steel pin going through the shaft. This joint had an open top which hence acted as receiver should any lubricating oil or grease fall down from the ball bearings B. A thermistor P, which was the sensor of the temperature controller, was inserted through the lid. The jar was surrounded by a stainless steel beaker with an air gap of about one inch to cut down heat losses by radiation and convection.

A 25 r.p.m. motor M rotated the "crystal tree" in the solution, anticlockwise for three and a half revolutions and then for a similar period in the reverse direction (Fig. 2). This was essential to ensure equal growth on opposite faces of the crystal seed. The reversible rotation mechanism was made possible by means of a rack and pinion device as shown in Fig. 2. The gear rack R, moved backward and forward by

an eccentric attachment to the motor shaft, imparted through the pinion gear G on the tree shaft, an almost sinusoidal rate of rotation to the crystal tree. This mechanism permitted a gradual deceleration and acceleration on either side of the reversal point. The temperature of the solution was regulated by a Fisher proportional temperature controller and the heating source consisted of two IR lamps situated on the opposite side of the crystal growing tank. The lamps were sited so that the heat first reached the surface of the solution and was then transmitted into the entire bulk because of the stirring of the solution by the paddles as described above. When the crystals were introduced into the solution, the temperature (read by the thermometer T) was raised by half a degree so as to dissolve the surface of the crystals and thus smooth out any surface irregularities. The temperature of the solution was then lowered by about 0.04°C per day.

The rhombic faces grew at a much faster rate than the rectangular faces resulting in plate-like crystals. The crystals eventually reached an average size of 12×12×4 mm after about four weeks. The same result could be achieved by maintaining the temperature constant and allowing the solvent (water) to evaporate slowly through a small gap around the rim of the jar. The crystals thus formed were visually glass clear and could be cleaved easily into any desired size along the (001) and (210) cleavage planes. The crystals were then stored in a desiccator over silica gel until needed.

2-2-2 Thermal Decomposition Apparatus

The vacuum line used in the study of the thermal decomposition of AP is shown in Fig. 3. This consisted of three sections: (i) A reaction vessel V, 18 inches long, fitted with a B24 socket, and immersed up to half its length into an aluminum block furnace F whose temperature was maintained constant by a Hallikainen Thermotrol controller to ±0.02°C; (ii) Two McLeod gauges M, one with a 338 ml bulb and 1 mm bore capillary and the other with a 60 ml bulb and 3 mm bore capillary, capable of measuring pressures in the range from 10^{-6} to 10^{-2} torr and from 10^{-4} to 3 torr respectively; (iii) A U-trap T, situated half-way between the gauges and the reaction vessel, which was maintained at liquid nitrogen temperature to prevent attack by chlorine on the mercury in the gauges. The apparatus could be evacuated to 10^{-6} torr by backing a mercury diffusion pump with a two stage rotary oil pump. The decomposition apparatus could be isolated from the pumping system by means of a mercury cut-off C.

The sample to be decomposed was outgassed in a rotatable spoon R directly above the reaction vessel at least overnight under continuous pumping. This was to ensure the desorption of foreign gases from the solid which might influence the decomposition. When the furnace temperature was steady and outgassing in the usual high vacuum (10^{-6} torr) completed, the reaction could be started by rotating the spoon thus allowing the sample to fall into the reaction

vessel. The rate of the reaction was then followed by measuring the pressure developed in a constant volume system. The height of the mercury in the McLeod gauge capillaries was read using a cathetometer. The temperature of the decomposing solid was assumed to be the same as that of the aluminum block in the furnace whose temperature was measured by a Pt/13%Rh+Pt thermocouple inserted in the block. The validity of this assumption had been confirmed by previous workers[18]. The level of liquid nitrogen in the trap was found to be rather crucial and this was frequently checked and maintained at constant height.

2-2-3 Conductivity Cell

The conductivity cell is shown in Figs. 4,5 and 6. The sample to be investigated was sandwiched between two platinum electrodes in a crystal holder (Fig.4). Each electrode F consisted of a rigid platinum sheet of 0.002" thickness cut into the shape of a rectangle about 14×18 mm. The end of a Pt+13%Rh wire was spot-welded to the centre of the electrode and was insulated from the rest of the platinum by a thin sheet of mica. The electrode was completed by spot-welding a platinum wire at one corner of the rectangular sheet. The two leads acted as a thermocouple so that the temperature of the sample could be measured at each electrode. Any temperature gradient across the sample was removed by adjusting the current through the various sections of the furnace winding. As the physical contact between the electrode

and the sample was of utmost importance, a thin soft platinum sheet of 0.0005" thickness was therefore inserted between the electrodes and the sample so as to give better contact. The electrodes were insulated from the supporting silica plates by discs of recrystallized alumina D. The alumina discs had a central hole and a radial groove to accommodate the thermocouple wires. The body of the crystal holder was made entirely of silica. The sample was maintained under mild spring pressure by screwing down the screw S (Fig. 4) on to the metal plate P_2 to finger tightness. Originally the screw and metal plates were made of brass but as this was found to be corroded fairly easily by chlorine or wet acid vapour, it was replaced by one made of stainless steel. The spring W was made from tungsten wire. The crystal holder was suspended by two tungsten rods T (Figs. 4,5) sealed through top of the glass cell. The conductivity cell was inside a furnace F (Fig. 5) such that the electrode section was situated in the middle of the furnace. The thermocouple leads were brought out through side arms (a, b, c, d) on the top part of the cell through seals made with epoxy resin. Inside the cell, the leads were insulated by quartz tubing. Outside the cell, the leads dipped into four mercury cups in a perspex plate. From the mercury cups Pt or Pt+13%Rh leads continued to the cold junctions situated in ice baths contained in dewar flasks. From this point to the Guildline Type 9160 potentiometer, the leads were of copper. During conductivity measurements, the four leads to the cold junctions were lifted

out of the mercury cups and the two cups containing the platinum leads were connected to a Wayne-Kerr B221 transformer ratio-arm a.c. bridge. The cell could be evacuated by a side-arm V which was connected to the vacuum line (Fig. 6). The line also contained a gas-handling system consisting of a drying column D filled with P_2O_5, a manometer M, two traps T and U, and a facility G for introducing gases (N_2, H_2, NH_3) from cylinders.

In order to eliminate surface conductance, the electrode system was modified slightly. The upper electrode was made of a small circular platinum plate about 7 mm in diameter. This upper electrode was situated on the middle of the sample, the perimeter of which was painted with aqua dag which formed a guard ring. The guard ring was then grounded by means of a platinum wire. The electrode assemblies with and without the guard ring are shown in Fig. 4, for both circular specimens (pellets) and rhombic prisms (single crystals).

The specific conductivity of the samples measured could be as small as 10^{-10} ohm^{-1} cm^{-1}. To minimize electrical interference, coaxial wire was used for all leads outside the cell. The furnace was wound in sections on a silica tube of 70 mm diameter. This tube was separated from the cell by a nickel shield. The exposed part of the cell was covered by aluminum foil. The tungsten rods, the aluminum foil, the nickel shield, and the supporting frame were all grounded to minimize electrical interference.

AP starts to sublime at about 150°C. An inert gas atmosphere was therefore used to suppress sublimation. Generally N_2 was used for this purpose. It was used directly from the cylinder without further purification apart from being passed through the P_2O_5 column. The pressure of gas was measured on a manometer M shown in Fig. 6. Dry NH_3 was prepared by first condensing the gaseous ammonia in a liquid nitrogen trap. The dewar was then lowered allowing the ammonia to vaporize slowly through the P_2O_5 drying column and then into the cell. The amount introduced was again registered by the manometer. The sample was first annealed at a certain temperature until a steady value in σ was reached. Dried ammonia was then admitted until the desired pressure had built up in the cell. The change in σ with time was then recorded until a constant value of σ was obtained. Both the initial and the final (equilibrium) pressure of NH_3 were noted. Desorption could then be carried out by pumping off the ammonia and following the change in σ with time in a similar way.

To study the effect of H_2O on conductivity, a small side arm containing about 3 ml of H_2O was attached to the bottom of the cell. The system was then evacuated so that the water vaporized into the system. N_2 was then admitted until the total pressure reached one atmosphere. The vapor pressure of H_2O was about 22.4 mm at room temperature. The effect of $HClO_4$ was also studied. This was done by moistening one surface of the pellet with one drop of concentrated $HClO_4$

(70%). The run was then performed under one atmosphere of nitrogen.

2-3 Analysis for SO_4^{2-} and Ba^{2+} in the Doped Crystals

Quantitative analysis for SO_4^{2-} and Ba^{2+} at the low concentrations present in the crystals presents some technical difficulties. The conventional gravimetric determination could not be applied here, as the concentrations of impurity were too small. These doped crystals were prepared from solutions each containing 0.1 mole% and 1.0 mole% of SO_4^{2-} and Ba^{2+}, respectively. However, the amounts incorporated into the crystal were considerably smaller. The analysis were done by amperometric titration using 0.001M $Pb(NO_3)_2$ and 0.0018M $(NH_4)_2SO_4$ as titrants for the determination of SO_4^{2-} and Ba^{2+} respectively. This method could detect ion concentrations as low as 10^{-5}M. The procedure used was first to determine a calibration curve using several known solutions containing the same amounts of AP (0.1M) and different concentration of SO_4^{2-} or Ba^{2+}. Generally, the solution to be titrated contained about 60% by volume of ethyl alcohol which effectively suppressed the solubility product of $PbSO_4$ or $BaSO_4$ such that a sharp end-point could be obtained. A preliminary titration was also carried out on solutions with the same amounts of SO_4^{2-} but different concentrations of AP. The results agreed fairly well with each other, showing the actual concentration of AP did not effect the determination significantly. Titration of the dissolved crystal and

interpolation of the calibration curve then gave the required concentration of Ba^{2+} or SO_4^{2-}.

CHAPTER 3

RESULTS ON DECOMPOSITION

In this chapter are described results obtained from measurements of the isothermal decomposition of AP, using (i) pellets made from pure AP (PP); (ii) pure single crystals of good quality (PC); (iii) pure single crystals with visual crystal faults (BNL); (iv) crystals doped with SO_4^{2-} (APS); and (v) crystals doped with Ba^{2+} (APB). The decomposition results will be presented in terms of parameters found by least-squares fitting of the experimental data to various kinetic equations; computing techniques were used extensively for this purpose. The experimental results on the conductivity of AP will be given in the following chpater.

3-1 Low Temperature Decomposition of AP

The term low temperature decomposition refers to the reaction that occurs in the solid state. The high temperature (gas phase) reaction has been studied previously by Galwey and Jacobs[42], and was not studied further in this investigation in which the main interest was on solid state processes. The kinetics of decomposition was therefore studied between 200°C and 300°C with sample weight ranging from 3 mg to 97 mg. The decomposition line had a working volume of 1011 ml. All the condensable gaseous products were condensed by using a liquid

nitrogen trap, leaving oxygen as the only gas contributing to the measured pressure. Pure AP in the form of cylindrical pellets and single crystals in both the orthorhombic and cubic modifications were investigated and their decomposition kinetics compared. The effect of doping single crystals with sulfate and with barium ions was also studied.

3-1-1 Pure Pellets of AP

The average mass of sample used was about 40 mg. As the reaction was rather fast, the highest temperature for which PP could be investigated was 270°C. As found in previous investigations[8,9], at all temperatures studied the reaction did not go to completion, there remaining in the reaction vessel a white, porous, spongy residue. This residue was chemically inert, since on prolonged heating at the same temperature, no further decomposition was detected. Attempts were made to measure both the volume and the weight of this residue but these failed as it was so fragile. It appeared, however, to be completely opaque and to have a very rough surface. The percentage decomposition at the completion of reaction was therefore calculated indirectly. It was assumed that oxygen behaved as an ideal gas and therefore gave rise to 0.108 torr at 25°C for every 1 mg of sample decomposed. The percentage decomposition in the low temperature reaction was then found to range from 18-22%. Furthermore, it was found that the sublimation and decomposition occured simultaneously and were competitive processes. For pellets,

the rates of decomposition (D) and sublimation (S) are comparable such that the ratio S/D is quite constant throughout the whole temperature range. A thin milky layer of sublimate was formed around the interior wall of the reaction vessel directly above the reaction zone. The extent of this layer was observed to be almost the same at all temperatures.

Two runs using pellets of similar mass were carried out at 222°C. The results are shown in Fig. 7; good reproducibility was obtained. Furthermore, the ratio of the final pressure (PF) to the mass (M) was the same in both cases (PF/M=0.019), indicating that the same extent of decomposition had occured. The effect of mass on decomposition kinetics was then investigated by using pellets with masses ranging from 13 mg to 61 mg. The results are shown in Fig. 8. Those with masses close to 40 mg agreed quite well with one another. However, for masses far from 40 mg, deviations became significant. This may perhaps indicate that the pellets differed from one another in density since a manual press was used for sample preparation. Nevertheless, variations were small for masses in between 32.2 and 44.7 mg and samples with masses close to 40 mg were therefore used for all runs at all temperatures.

As the decomposition of pellets was relatively much faster than that of single crystals, only a limited number of experimental points were available during the course of the reaction owing to the time neccessary to read a McLeod gauge.

Readings were taken at intervals of between 3 to 5 minutes at the beginning of the reaction and at 5 to 10 minutes during the decay period. The results so obtained were first analysed graphically by plotting pressure P vs. time t. The final pressure PF corresponded the steady state reading. The fractional decomposition $\alpha(t)$ at each point was then calculated by dividing P(t) by PF. The validity of the Avrami-Erofeev (AE) equation was then tested by plotting $[-\log (1-\alpha)]^{1/n}$ vs. t for n=3 and n=2. These plots are shown in Fig. 9. The rate constants were then evaluated from the slope of the straight line region. These, together with the α-range within which the plot was linear are given in Table 1. The Arrhenius plot, shown in Fig. 10, gave activation energies of 31 kcal $mole^{-1}$ and 24 kcal $mole^{-1}$ for n=2, for the orthorhombic and cubic form respectively. For n=3, the corresponding values were 32 kcal $mole^{-1}$ and 29 kcal $mole^{-1}$. These results are in good agreement with those of previous workers[11]. The fact that the straight line did not pass through the origin indicated clearly that the early stages of the reaction could not be described by the AE equation. Thus the equation could be modified[15] to

$$[-\log (1-\alpha)]^{1/n} = \bar{k}_n (t - t_o) \qquad 3\text{-}1$$

However, this yields no kinetic information other than the value of t_o, which may be thought of rather loosely as an

"induction period" or "time until the reaction is governed by AE kinetics". A more detailed kinetic analysis for $t<t_o$ was handicapped by the small number of data points in this region. It was anticipated that t_o would be greater for the decomposition of single crystals at corresponding temperatures and so the decomposition of single crystals was then studied with the hope that one might get useful information about the beginning stage of the reaction.

3-1-2 Single Crystals of Pure AP

The BNL sample consisted of small single crystals with many visual faults and an average mass of about 10 mg. The crystals were thin and sheet-like with two rhombic faces. Two runs at 222°C were first carried out. Both show a significant reduction in decomposition rate. The induction period t_o was very much prolonged so that this region was then accessible to further kinetic analysis. Plotting log P vs. t was first attempted. Fig. 11 shows that the exponential dependence of P on t was reasonably well obeyed in the later part of the induction period, but not over the beginning section which showed large deviations. However, this could possibly be due to the fact that the pressures measured within this range were relatively small and one may argue that the deviations observed (Fig. 11) simply arise from the low sensitivity of the McLeod gauge. At this stage, the big single crystals grown in these laboratories became available and crystals of large mass were therefore decomposed in the hope that the kinetics of the

early stages of the reaction might be further elucidated. A pure crystal (PC) of 96.7 mg was first decomposed at 222°C. Pressure measurements were taken over the first 3 hours at intervals of 3 to 5 minutes. The final pressure at the completion of the reaction was also taken. A plot of α vs. t, on a large scale, over the initial 70 minutes is shown in Fig. 12; this shows plainly two distinct decomposition regions within the so-called induction period, t_o. Initially, the pressure showed a rather slow increase, varying linearly with time. This was then followed immediately by a steeply-rising section where the pressure increased exponentially with time. A second run using a smaller mass (76.1 mg) was also carried out at the same temperature. The induction period again consisted of a linear part followed by an exponential region. The duration of the linear region was similar for both runs, but the slope differed greatly. The relatively slow rate of decomposition in single crystals permitted the highest temperature studied (290°C) to be close to the upper limit of the low-temperature reaction. The lowest limit studied was 222°C, below which the reaction became too slow to follow manually. For example, the reaction took 20 hours for completion at 230°C. It was remarkable that the plots of α vs. t at all the temperatures studied consistently showed the same behavior, a linear process followed by an exponential process, during the initial reaction. A re-examination of the data for pellets showed the same result to be true for all the

pellets studied, although in some cases, the linear region was very short or completely absent.

The projection of the straight line did not always pass through the origin, and frequently gave an intercept on the positive α-axis. This intercept α_o was usually small ($\alpha_o \sim 10^{-4}$), and presumably arose from an instantaneous (t<1 min) desorption of gases previously adsorbed at room temperature.

The first kinetic analysis of results for AP pellets had indicated that the major part of the reaction (α from 0.1 to 0.85) obeyed the AE equation. The significant discrepancies outside the α-range pointed to the necessity of using the complete Avrami equation rather than its approximate form (the AE equation). The graphical analyses described above have also shown the necessity for accounting for desorption in addition to the Avrami (3 dimensional nucleation and growth) region. The Avrami equation (1-6) is a complicated one which cannot be put into a linear form for graphical display. The test of the validity of this equation in describing the experimental data could therefore only be made with the aid of a computer. A non-linear least-squares program[43] NL1N2 was used throughout for curve fitting using a composite kinetic equation which comprised a linear section, a modified exponential, and the Avrami equation:

linear :

$$P = P_o + k_L t \qquad 0 \le t \le t_L \qquad 3\text{-}2$$

exponential :

$$P = C_3(e^{k_3 t} - 1 - k_3 t) \qquad t_L \leq t \leq t_E \qquad 3\text{-}3$$

Avrami :

$$-\ell n\ (1-\alpha) = C_1(e^{-k_1 t} - 1 + k_1 t - \frac{k_1^2 t^2}{2} + \frac{k_1^3 t^3}{6}) \quad t \geq t_A \qquad 3\text{-}4$$

where C_1, C_3 are constants (see eqns. 1-6 and 5-11 (or 5-14)) k_L, k_1, and k_3 are the rate constants for the linear process, for nucleation, and for branching, respectively. P_o denotes the pressure at t=0 corresponding to the extrapolation of the linear section to t=0 (Fig. 12). Details of the computing procedure will be described later and the numerical results will then be given.

3-1-3 Single Crystals of AP doped with Ba^{2+}(APB) and SO_4^{2-}(APS)

The object of studying the decomposition of AP doped with Ba^{2+} (APB) or with SO_4^{2-} (APS) was to see if the decomposition rate was affected by impurities that would be expected to introduce cation and anion vacancies respectively. However, in order to minimize possible secondary effects arising from these impurities, their concentration incorporated into the AP lattice should be kept small. In order to compare the results with those for pure AP, the decomposition of both the APB and APS single crystals was investigated over the

same temperature range. The results showed the same qualitative picture during the initial reaction, but the addition of both Ba^{2+} and SO_4^{2-} accelerated the overall decomposition. This is shown by the values of $t_{0.5}$, the time for 50% decomposition. At 230°C, $t_{0.5}$ for PC, APS, APB, and PP respectively was 390, 350, 200, and 50 minutes. The entire reaction curve for these four samples at 230°C is exhibited in Fig. 13. The continuous curves are the results of computer fitting to equations 3-2, 3-3, and 3-4.

3-2 Model Used in Least-squares Curve Fitting of Thermal Decomposition Data

Although the behavior during the initial reaction had been characterized and the complete $\alpha(t)$ curve indicated that the reaction involved three consecutive processes, i.e., linear, exponential, and Avrami regions, yet the problem still existed as to when one process should terminate and the next one begin. Three models were therefore tested:

(i) the linear process extended into the exponential region and terminated at the same time as the exponential, the Avrami process then setting in;

(ii) the linear process terminated at the onset of the exponential stage which again ended at the commencement of the Avrami process;

(iii) the linear region terminated at the onset of the exponential, and the Avrami process set in before the exponential terminated, thereby allowing a certain variable

period for overlapping between the tail of the exponential and the beginning of the Avrami process.

These models were studied by suitably varying t_L, t_E and t_A in eqns. 3-2 to 3-4. Whereas model (i) always gave a poor fit over the exponential, and both models (i) and (ii) showed a "kink" at the transition from the exponential to the Avrami process, model (iii) gave the best fit over the entire range of α. The reasons for using the modified exponential (eqn. 3-3) and the validity of model (iii) will be discussed further in Chapter 5. The least-squares routine NL1N2 is available as a share program[43] (No. 14281) and is based on a general model of the form

$$\hat{Y}_i = f(X_{i1}, X_{i2}, \ldots, X_{im}; b_1, b_2, \ldots, b_k) \qquad 3\text{-}5$$

which contains m (maximum number is 10) independent variables $X_{i\ell}$($i=1,\ldots n$; $\ell=1,\ldots m$) and k (maximum number is 50) parameters b_j. The program provides the predicted values $\hat{Y}_i$ for each observation i, by adjusting each of the parameters b_j such that

$$\Phi = \sum_{i=1}^{n} (Y_i - \hat{Y}_i)^2 \qquad 3\text{-}6$$

is a minimum. Y_i is the observed value and $\hat{Y}_i$ the predicted one. Guessed (initial) values for each of the k parameters b_j must be provided. The change of each b_j during iteration is governed by the estimated derivative

$$\frac{\partial Y_i}{\partial b_j} = \frac{f(b_j + \Delta b_j) - f(b_j)}{\Delta b_j} \qquad 3\text{-}7$$

with $\Delta=10^{-5}$ until a specified convergence criterion is satisfied. Usually this criterion was that the fractional changes in all the parameters being varied should be less than 5×10^{-5} in successive iterations. In some cases, constraints must be imposed in order to limit the portion of the $\vec{b}$-vector space which may be searched for the minimum in Φ. However, if the absolute minimum value of Φ is well inside the searchable region, constraints are not necessary. Any of the parameters b_j may be held constant if desired. The out-put of the program also provides statistical information involving the parameter correlation matrix and the confidence limits for each of the parameters.

A subroutine called F CODE was written to enable the model to be analysed. The kinetic equation to be tested (eqns. 3-2 to 3-4) contained a total of ten parameters and one variable (i.e. the time t). $P_o(=b_1)$, $k_L(=b_2)$, $t_L(=b_3)$ and $P_A(=b_7)$ were the only four out of the total of ten parameters for which guessed values could be determined graphically. Guessed values for the other six parameters $C_3(=b_4)$, $k_3(=b_5)$, $t_E-t_L(=b_6)$, $C_1(=b_8)$, $k_1(=b_9)$ and $t_E-t_A(=b_{10})$ were each given a reasonable estimate based on physical intuition. Least-squares fitting was first carried out fixing b_1,b_2,b_3 and b_7 while allowing the remaining parameters to vary. When optimum

value for each of these six parameters were obtained, b_1, b_2, b_3 and b_7 were then allowed to vary and least-squares fitting once more carried out. The final set of parameters chosen must fulfil two requirements; (i) Φ must be a minimum with data points evently scattered around the computed line, and (ii) each of the ten parameters b_j must have a physically reasonable value. Three parameters b_2, b_4 and b_8 involved four rate constants implicitly while b_5 and b_9 were explicitly related to the rate constants for the exponential process and the Avrami process respectively. By comparing equations 5-8, 5-11 (or 5-14), and 1-6, the following relationships follow:

$$k_L = PF\sigma k_{21} N_o \qquad 3\text{-}8$$

$$C_3 = PFN_o\sigma_E k_1 k_2/k_3^2 \quad \text{or,} \quad PF\sigma_E k_2 N_o/k_3 \qquad 3\text{-}9$$

$$C_1 = \frac{6\sigma N_o k_2^3}{k_1^3} \qquad 3\text{-}10$$

By a suitable combination of C_1 and k_1 one obtains a quantity proportional to k_2

$$C_1^{1/3} k_1 \propto k_2 \qquad 3\text{-}11$$

However, k_2 may not be obtained explicity since N_o is unknown. Similar information could be obtained by suitably combining

C_3 with k_3 and k_1, but the accuracy was rather uncertain as the exponential period was relatively much shorter than the Avrami stage and only a few data points were available. The Arrhenius parameters for the three processes were therefore evaluated from four parameters, namely b_2,b_5 and b_9 directly and indirectly from the combination of b_8 and b_9. A list of the parameters showing their significance is given in Appendix I for ready reference.

The parameter b_2 showed so much scatter that an Arrhenius plot could not be made. The activation energy was therefore evaluated from $b_3(=t_L)$ instead. The good fit to the whole $\alpha(t)$ curve is shown in Fig. 13 for the four types of AP studied. Figure 14 shows the good fit over the major part of the $\alpha(t)$ curve for a single crystal, but this means effectively the Avrami process since the linear and exponential regions hardly shown on this scale. Figures 15 and 16 reveal the fitting obtained from eqns. 3-2 and 3-3 over the so-called induction period.

Tables 2 to 10 summarize the values of all the ten computed parameters along with the run number, the temperature of the run and also the mass of the sample used. The number of significant figures given for each of the parameters in the tables is a compromise. The values given fall well within the computed confidence limits for each of the parameters. However, the irreproducibility of kinetic experiments in general and of solid state kinetics in particular is such that

the uncertainty, in an absolute sense, of a rate parameter is greater than the confidence limits that are obtained by analyzing any particular run. Tables 11 to 16 summarize the extent of decomposition corresponding to the termination of the linear process (α_{LT}), the termination of the exponential process (α_{ET}) and the beginning of the Avrami process (α_{AS}). Also appearing in the same table are the logarithm of each of the three parameters, b_3, b_5, b_9, and of the product of $b_8^{1/3} b_9$, together with the ratio PF/M which allows one to calculate the percentage decomposition at the completion of the low temperature reaction. For pellets, PF/M remained quite constant throughout the whole temperature range studied, but the ratio tended to decrease at elevated temperatures for both the pure and the doped single crystals indicating that the extent of decomposition was greatly reduced at elevated temperature.

The Arrhenius plots for the linear process are given in Fig. 17 to 20 for pellets, pure single crystals, Ba^{2+} doped crystals, and SO_4^{2-} doped crystals respectively. The scatter is considerable and was worst of all for the BNL crystals for which no Arrhenius plot for t_L could be made. The lines on all Arrhenius plots are least-squares computed fits to the data. Similar plots for the exponential and Avrami process appear in Figs. 21 to 25. In each case the data above and below the transition point are fitted separately. The corresponding activation energies together with the logarithms

of the pre-exponential factors are tabulated in Tables 17 and 18. Reference may be made to Appendix II for definition of the symbols used. The effect of phase transition at 240°C needs to be emphasized. Figures 23 to 25 clearly indicate that there was always a sudden change in rate constant within the range 240° to 250°C although this change is very small for pellets and possibly negligible for k_1 and k_3 (Fig. 21). During Arrhenius plotting, the values in this region were therefore included to show the changes, but were excluded during the least-squares evaluation of the activation energy for both the orthorhombic and the cubic modifications. For t_L, it is not reasonable to distinguish between points below and above the transition point since any change is of the same order of magnitude as the experimental scatter. For BNL crystals, there were insufficient data below the transition point to establish Arrhenius parameters for this specimen (Fig. 22).

3-3 Attempted Quantitative Determination for Ba^{2+} in APB and of SO_4^{2-} in APS

A saturated solution of APS in 60% ethyl alcohol was prepared and titrated amperometrically with 0.001M Pb^{2+} solution as described in section 2-3. This method can detect SO_4^{2-} ion concentration as low as 10^{-5}M, but failed to analyse the SO_4^{2-} content in APS. Similarly, the barium content in APB could not be detected using 0.0018M of SO_4^{2-} solution as

titrant. The lowest concentration that could be analysed by this method was 10^{-3}M. However the presence of barium in APB and sulfate in APS is shown by their effects on the kinetics of decomposition of AP as described in 3-1-3. It is therefore justified to say that APB and APS each contains $<10^{-4}$ Mole % of Ba^{2+} and $<10^{-6}$ Mole % of SO_4^{2-} respectively.

CHAPTER 4

RESULTS ON CONDUCTIVITY

The work described in this chapter deals mainly with the electrical conductivity of AP both in the form of compressed pellets and solution grown single crystals. The work focuses on three major targets; (i) the temperature-dependence of the conductivity and the effect on it of various gaseous atmospheres; (ii) the time-dependence of the conductivity on annealing; and (iii) the magnitude and kinetics of conductivity changes during adsorption and desorption of dry ammonia. These will be described separately.

4-1 Temperature-dependence of the Conductivity of AP

4-1-1 Pellets in Nitrogen

The a.c. bridge of 1591 Hz frequency was used throughout the conductivity measurements. The thermal instability of AP and the concurrent occurrence of sublimation, as described in Chapter 3, greatly limits the useful temperature range on which conductivity measurements could be made. However, the length of the induction period (e.g. 100 min at 230°C, Fig. 14) meant that measurements, if sufficiently rapid, could be carried out at higher temperatures although in interpreting the results, it will be necessary to recognize that some decomposition has occured. Sublimation

could be reduced by the presence of 1 atmosphere of nitrogen or ammonia. Measurements were made both on heating up and cooling down and these gave consistent results after thorough annealing. However, at lower temperature (<90°C) they showed deviations from one another in runs involving adsorption or desorption. All measurements were taken continuously either on heating up or cooling down the samples. The coincidence of heating and cooling conductivity plots for well-annealed specimens showed that thermal equilibrium was maintained. The need for taking large numbers of measurements (every 1 to 3°C) will be evident from the graphs to be presented. This necessity has not always been appreciated by previous workers (e.g. ref. 27).

Figure 26 shows a plot of log σT vs. $1/T$, where σ is the specific conductance. Successive measurements made while heating up the sample in the presence of 760 torr of nitrogen were taken in the order 1,2,3,4,5 as shown. The temperature range can be divided into two sections: above ~127°C, σ is unaffected by successive thermal cycling, but below this temperature, the plots of log σT against $1/T$ are successively displaced in the direction of lower σ (curves 1,2,3,4). At temperatures close to the phase transition (240°C), σ increased at a much faster rate, presumably because the sample was undergoing significant decomposition. This, however, will be discussed further later. The occurrence of decomposition was reflected by a much higher σ measured over the entire

temperature range (curve 5). In order to study the effect of prolonged annealing, a pellet was kept at 120°C for five days. The plot of log σT vs. 1/T then gave essentially a good straight line region (Fig. 27) between 83° and 174°C. At this point, it was concluded tentatively that the conductivity of an unannealed sample within the low temperature range (120°C) was most probably related to some species that could be completely removed by sufficiently long annealing. To investigate this problem further, two independent lines of investigation were pursued. These are: (i) to study the influence of N_2, NH_3, H_2O, and $HClO_4$ on the conductivity; (ii) to eliminate any possible contribution from surface conduction by means of a guard ring electrode on the top surface of the sample.

4-1-2 Effect of Perchloric Acid (72.4% $HClO_4$ by Weight)

Figure 28 shows the great enhancement in σ which occurs when one surface of the pellet is wetted with a tiny drop of the acid solution before being introduced into the cell. The conductivity was increased ten-thousand fold at room temperature. As the temperature was increased, σ was first increased slightly, then rapidly decreased and finally levelled off at 105°C (curve 1). Annealing within the zero-slope region caused σ to drop. However, when measurements were resumed from room temperature (curve 2), σ had dropped to a much lower value, only about ten times greater than the untreated one.

This implied that the $HClO_4 \cdot H_2O$ must have contributed greatly to the conduction in AP and have been largely removed by the first heating. Curve 2 is quite similar to curves 1,2,3,4 in Fig. 26, except that it levelled off at 105°C. Curve 3 shows qualitative reproducibility after thermal cycling, but also that decomposition is setting in at ~135°C as σ started to increase. At 175°C, σ at first showed a decrease for a short while and then quickly increased (within 240 minutes). This interpretation was felt to be justified by the fact that $HClO_4$ has been shown to shorten the so-called induction period and to accelerate the decomposition of AP[18]. Further indications of partial decomposition are revealed by curves 4 and 5 which show considerable enhancement in the conductivity. Since it was rather difficult to say at this stage whether it was the $HClO_4$ or the H_2O which had enhanced the conductivity, the next experiment was designed to study the effect of H_2O vapor.

4-1-3 Effect of Dry Nitrogen

Before the effect of H_2O can be understood, it should be first of all established whether dry N_2 will have any effect on the conductivity of AP since Zirkind and Freeman[32] had found that both oxygen and argon depressed the conductivity of AP. Figure 29 shows the results. Curve 1 shows a run carried out under vacuum up to 118°C; the pellet was then annealed for 24 hours, σ dropping to a point on curve 2.

Both measurements in vacuum and in 760 torr of N_2 after annealing followed the same route (curve 2) provided no further annealing was carried out. This experiment shows that the presence of dry N_2 does not affect the conductivity.

4-1-4 Effect of Nitrogen Saturated with Water Vapor

Figure 29 also shows the effect of H_2O vapor. Upon further prolonged annealing in nitrogen at 118°C, the conductivity of the previously annealed sample dropped from curve 2 to a point a. In the presence of saturated H_2O vapor (22.4 torr at 25°C), σ increased slightly (ca. 50%). The plot of log σT vs. 1/T above this temperature (118°C) was distinctly parallel to the corresponding section along curve 2. However, on cooling curve 3 resulted. It showed a tremendous increase in σ associated with the adsorption of H_2O beginning at about 60°C. The conductivity was greatly enhanced at room temperature (by about ten-thousand fold!). Upon heating up again, σ at first dropped and then levelled off (curve 4) over a long temperature range. After annealing at 148°C and 120°C for 5 hours and 21 hours respectively, the measurements of σ then followed curve 5 on cooling down. The value of σ at room temperature again increased to the same value as that achieved previously, curve 3. Now when the system was pumped out (still at room temperature) H_2O desorbed from the solid, causing σ to drop considerably over the initial 6 hours (to b). On heating up, the conductivity followed curve 6 in which the behavior was similar to curves 1,

2,3,4 in Fig. 26, except that σ gradually levelled off at about 100°C. Any point along curve 6 did not correspond to the equilibrium value since σ decreased on annealing.

4-1-5 Effect of Ammonia

After the water vapor study, the sample was then annealed in vacuum at 118°C until a steady state (point p in Fig. 30) was reached. NH_3 at a pressure of 760 torr was then admitted when the conductivity again increased but by only 30%. Upon cooling down, it first dropped to a minimum and started increasing at about 50°C, but at a much slower rate than in the presence of saturated water vapor. On standing for 13 hours overnight at room temperature σ increased by a factor of $\sim 10^4$. Upon then heating up the measurements of σ followed curve 2. After 18 hours annealing, σ decreased and on further heating, it gradually increased, reached a maximum, and then abruptly fell to a minimum at 240°C. It rose again on further heating.

Adsorption and desorption of large amount of NH_3 seemed to complicate the study of its effect on σ. Figure 31 shows that when a reduced amount of NH_3 (80 torr) was used, the vast adsorption observed at 760 torr (Fig. 30) did not occur on cooling down to room temperature (curve 3). This curve also shows the hysteresis that occured on heating. Curve 1 was obtained on heating up a fresh sample in vacuum. Curve 2 shows the effect of annealing at 120°C and also that dry N_2 did not affect the conductivity.

4-1-6 Effect of a Guard Ring

In order to test whether surface conductance was dominating the low temperature conductivity, a different electrode system was adopted incorporating an aqua dag guard ring (as described in 2-2-3). This ring electrode was then grounded to remove any effects due to surface conduction. Figure 32 shows results very similar to those obtained without the guard ring so that one may conclude that the low temperature conductivity was not dominated by surface conduction. Figure 33 further emphasizes this points, showing similar results to Fig. 31 when the conductivity is measured under a low pressure of NH_3.

4-1-7 Single Crystals

It was important to see if the complicated behavior of AP pellets would apply also to single crystals. However, Figs. 34 and 35 show the same qualitative picture in that on annealing at a low temperature (arrow B in Fig. 35) the conductivity curve is displaced towards lower values of σ, and the whole curve translated towards the left (Fig. 35). On annealing at high temperature where decomposition would be appreciable, σ increased (arrow A). Curve 2 in Fig. 34 shows again the enhancement in σ which occurs on partial decomposition. This increase in σ could be reduced by thermal cycling. When decomposition was much more extensive, pronounced hysterisis was observed at low temperatures (curve 7, Fig. 35); above this a rather long zero-slope

region persisted until finally further decomposition increased the conductivity.

Measurements made with a guard ring are shown in Fig. 36. Curve 1 shows the effect of NH_3. Curve 2 shows measurements carried out in the presence of dry N_2. The same general features are observed, indicating that the previous results were not due to surface conduction. Perhaps the most significant finding shown in Fig. 36 is that inside the decomposition range, the conductivity curve did not correspond to an activated process (i.e. the system was not in a steady state). After decomposition occured, neither the cooling down nor the heating up measurements (curve 3) traced the same route as curve 2. If the sample was subjected to further decomposition, resulting in more gaseous products considerable adsorption occured at low temperatures (curve 4). On pumping at room temperature, the conductivity fell considerably (arrow C), presumably as the gaseous products (H_2O?) were desorbed.

4-1-8 Summary

1. Results in the low temperature region were not due to surface conduction but rather were influenced by some unidentified adsorbed species, probably H_2O. By desorption upon prolonged annealing at 120°C, virtually a straight line could be obtained when $\log \sigma T$ was plotted against $1/T$.

2. Pellets show a slightly higher conductivity than single crystals when unannealed samples are compared. This

probably indicates that a larger amount of the adsorbed species is present in the pellets.

3. Annealing below the decomposition region always lowered the conductivity, whereas at high temperatures in the decomposition region σ increased on annealing.

4. The effect of gaseous NH_3 and H_2O was to increase slightly the conductivity at high temperatures (>110°C), but as temperature decreased the enhancement in σ became more pronounced. This increase could be as much as a factor of 10^5 at room temperature. The presence of dry N_2, however did not affect significantly the conductivity measurements.

5. Smaller and more readily controlled changes in conductivity are observed if lower pressures of NH_3 are used.

6. Partially decomposed samples also show a big enhancement in conductivity (e.g. 100-fold, curve 2 in Fig. 34) in the low temperature range, while at the same time hysteresis on heating and cooling may be observed if considerable decomposition has occurred.

7. The conductivity of partially decomposed samples was not constant but rather decreased on annealing.

8. Upon heating up through the transition point, σ at first dropped to a minimum and then increased.

9. For unannealed samples a zero-slope region was always observed at low temperature for pellets; this appeared at higher temperature for single crystals. This behavior could be removed by sufficient annealing. However, partially

decomposed samples for both pellets and single crystals always show a zero-slope region when measurements were made over a sufficient wide range at low temperatures. The high temperature slope in plots of log σT vs. 1/T corresponds to an activation energy ranging from 0.6 to 0.9 eV.

4-2 Time Dependence of σ on Annealing

4-2-1 Compressed Pellets of AP

It seems highly possible that the two different types of annealing effects were connected with whether or not the sample underwent decomposition. Because of the relatively longer induction period displayed by single crystals, the demarcation between the two kinds of annealing would be expected to lie at higher temperature (ca. 190°C) in single crystals than in pellets (ca. 180°C). In section 4-1-7 it has been shown that enhancement due to partial decomposition could be reduced by pumping (e.g. arrow C, Fig. 36). This indicated that the conductivity increase on partial decomposition was due to the adsorption of gaseous products. One might then expect that one should be able to study the kinetics of decomposition if the change in σ with time was followed. However, two technical problems restrict such a study: (i) the cell constant would undoubtedly vary and the whole sample might simply collapse should extensive decomposition take place; (ii) the sample could not be raised to the desired temperature under controlled conditions within a very short

time to enable the reaction to start at time effectively equal to zero. Despite this difficulty, experiments on high temperature annealing did show qualitatively the changes in conductivity that occur during the course of decomposition. Figure 37 shows the behavior of σ over the initial 60 minutes of the anneal at 153°C of a partially decomposed pellet (refer to arrow A in Fig. 26). The enhancement in σ did not appear to follow any simple law. However, when annealing was carried out at a low temperature (118°C; refer to arrow A in Fig. 29) in vacuum, the conductivity fell monotonically (Fig. 38). The decay was found to be described by a $t^{\frac{1}{2}}$ law indicating that the rate of removal of the adsorbed species was governed by a diffusion process.

4-2-2 Single Crystals of AP

The high temperature annealing of single crystals exhibited a much more complex behavior than one would expect (Fig. 40). This experiment, although not providing useful quantitative information on the time-dependence of σ during decomposition, nevertheless revealed the importance of restricting measurements of conductivity to temperatures well below the decomposition region if information on transport properties is required (cf. ref. 27). Figure 41 shows two annealing experiments, one at 89°C and the other at 114°C. Both show a gentle decrease in σ over a considerable period of time. The change in σ was in fact rather small but both curves obey a $t^{\frac{1}{2}}$ law as shown in Fig. 42. That the low

temperature conductivity was complicated by the presence of an adsorbed species can no longer be doubted. Furthermore, these results indicate clearly that measurements must be done continually either on heating up or cooling down, and the speed of heating up or cooling down should be as fast as one could manage. Coincident data on thermal cycling or on repeating a given run will be indicative of a true steady state situation.

4-3 Time-dependence of Adsorption and Desorption of Dried Ammonia on AP

It was first noted that in the presence of NH_3, the conductivity at any temperature did not maintain a steady value within the low temperature range. On measurements made during heating up, annealing at any one temperature was accompanied by a decrease in the value of σ, whereas on cooling down σ increased upon annealing. The conductivity ultimately became constant indicating that the system had reached a steady state. The time required to reach a steady state depended on (i) the amount of NH_3 present in the system, and (ii) the temperature at which annealing was carried out. This implied that both adsorption and desorption were not spontaneous process. In order to acquire some insight as to the nature of these process, their kinetics were investigated at three temperatures. It was hoped that from the adsorption isotherms, one would be able to get information as to heat of adsorption and from the temperature-dependence of the kinetics,

the activation energy involved. Also, one hoped to see whether any chemical reaction would occur during adsorption.

4-3-1 Compressed Pellets of AP

Figure 43 is a plot of σ vs. t for a pellet at 83°C under 157 torr of NH_3. Both the adsorption and desorption isotherms were given. For adsorption, σ first increased sharply from σ_o (the steady value of σ in the absence of NH_3), and gradually levelled off. The desorption pattern was approximately its mirror image. That the desorption isotherm finally lead to a value equal to σ_o indicated unambiguously that no chemical reaction was involved. Plots of σ vs. $t^{\frac{1}{2}}$ and log t are shown in Fig. 44. These show that a log t law is obeyed very much better than a $t^{\frac{1}{2}}$ law for both adsorption and desorption of NH_3.

Adsorption isotherms were then carried out at various pressures of NH_3. The enhancement $(\sigma_\infty - \sigma_o)$ calculated from the steady state value (σ_∞) was then plotted against the equilibrium pressure of NH_3 at all three temperatures studied, 83°, 101°, and 120°C. It was found that the equilibrium pressure was not very different from the initial pressure reading, showing at most 1 torr reduction. This pressure reduction would include any contribution from the recrystallized alumina discs in the conductivity cell. The reduction in pressure due to adsorption by the sample, being less than one torr, was therefore neglected when plotting the isotherms in

Fig. 45. The isotherms at 101° and 120°C almost coincide whereas that at 83°C possesses a unique feature being concave upwards. Thus the heat of adsorption could not be calculated from the experimental isotherms. Furthermore, if one was to heat an AP pellet in the presence of about 550 torr of NH_3 as indicated by the vertical line AB, the conductivity from 83°C (point A) would drop considerably until a temperature of 101°C was reached. Further heating up to 120°C would not be accompanied by any further reduction in σ. This qualitative picture is reflected in curve 2 of Fig. 30 in which 760 torr of NH_3 was used. If one was to heat a pellet in a lower pressure of NH_3, say 200 torr along line DC, the conductivity would increased from 83°C upwards until 101°C when again the conductivity would not change very much. This behavior is in accord with curve 3 in Fig. 31.

4-3-2 Single Crystals of AP

Adsorption on and desorption from single crystals were much slower processes and the observed changes in σ were much smaller than for pellets. This is indicated by Fig. 46 which shows a desorption isotherm at 116°C for a crystal which had been equilibrated in 581 torr of NH_3. Plots of σ vs. $t^{\frac{1}{2}}$ and log t (Fig. 47) show that the $t^{\frac{1}{2}}$ law was well obeyed for single crystals. At no time was there a good fit to the log t law. This implies that desorption from the surface was small in comparison with the amount of NH_3

diffusing out of the crystal so that the rate process was solely governed by diffusion ($t^{\frac{1}{2}}$ law). The adsorption isotherms (Fig. 48) were similar to those obtained for compressed pellets.

CHAPTER 5

DISCUSSION

The results as presented in Chapter 3 have revealed some important findings. (i) The "induction period" which is composed of a linear process plus an exponential process comprises only ~1% of the total decomposition. (ii) The remaining part of the reaction ($0.01 \leq \alpha \leq 1.00$) has, for the first time, been successfully described by the exact Avrami equation. (iii) The effect of doping with Ba^{2+} is to shorten the linear process and to enhance drastically the overall reaction rate, while doping with the SO_4^{2-} prolongs the linear section and only slightly shortens the time for complete decomposition.

5-1 Decomposition of Pure AP

5-1-1 Induction Period, t_o

Previous work has indicated that t_o could be greatly reduced by (i) scratching[44] the crystal surface, or crushing and grinding[2] the whole crystal, and (ii) pre-treatment[45-48] with γ- or x-radiation. In AP the induction period could also be reduced by moistening with a drop of $HClO_4$[18] or lengthened by exposure to gaseous ammonia[18]. However, these results only provide a qualitative picture of the effect of

various physical and chemical factors on the duration of t_o. The physical significance and necessity for the occurrence of the induction period prior to the major part of the reaction route has not been explained satisfactorily. This is due in part to lack of information as to whether the induction period involves significant decomposition. Figure 12 provides a positive answer. The termination of the induction period is given by α_{ET} in Tables 11 to 14 for all samples studied. This quantity varies from sample to sample and from temperature to temperature. Nevertheless, it has an average value of around 0.01. This value is small but kinetically significant in the sense that the induction period covers the first 1% of the entire decomposition.

(a) Instantaneous Desorption

Figure 12 further stresses the composite nature of the induction period. An exponential acceleration in α is always preceded by a linear process. The corresponding straight line frequently does not pass through the origin but rather intercepts the α-axis at a positive value of α, α_o. Because the extent of decomposition at the completion of reaction may not be the same for each run (because of the residue phenomenon and of sublimation) it appears to be more appropriate to examine the values of P_o as listed in Tables 2 to 6. The vacuum line was always evacuated to 10^{-6} torr prior to the beginning of the reaction. The difference $\Delta P_o = P_o - 10^{-6}$ torr is therefore the contribution from the instantaneous desorption

of any adsorbed species that were not removed by pumping alone at room temperature. The value of P_o is of the order of 10^{-5} torr. Despite the smallness in its magnitude, its existence is almost indisputable. No further conclusions can be drawn with respect to the types of gases desorbed. The very short duration (less than 1 min) does not allow the kinetics to be explored. It also rules out the possibility of ΔP_o being due to a rapid decomposition at certain special sites since no time-dependence was ever observed, even at the lowest temperature. The pressure rise undoubtedly must be due to non-condensable gases such as N_2 or O_2. Traces of H_2O (moisture) are also most probably desorbed, but the water would not contribute to the pressure increment as it would be readily condensed in the trap.

(b) Linear Process

Tables 2 to 6 also provide two other important facts: (i) the time for completion of the linear process t_L tends to decrease as the temperature increases; (ii) the rate constant k_L associated with this process exhibits a tremendous scatter and thus shows no direct correlation with the temperature. Before these results can be interpreted, the kinetic equation obeyed by this process must be understood. Three models will be considered, all based on random nucleation at N_o potential nucleus forming sites and a constant rate of nucleus growth.

Because the reaction products are all gases, one

would expect that reaction would commence first at the surface. This is confirmed by photomicrographic studies[14]. Nuclei can therefore spread along the surface with rate constants k_{22}, k_{23}, and penetrate into the bulk with rate constant k_{21}. Three separate cases will be distinguished. (i) If $k_{21} \simeq k_{22} \simeq k_{23}$, the nuclei will have the shape of a sphere or parallelopiped. This is the normal 3-D Avrami case and leads to a dependence of α on t which is cubic for $k_{21}t >> 1$ and quartic for $k_{21}t << 1$. Even if $k_{21} > k_{22} \simeq k_{23}$ so that the nuclei are cone- or pyramidal-shaped then a t^3- or t^4-dependence results unless the depth to which the nuclei can grow is limited. (ii) If $k_{21} >> k_{22} \simeq k_{23}$, and the nuclei can only penetrate to a finite depth, then their shape rapidly becomes (approximately) cylindrical and

$$G(x)G(y) = k_{22}k_{23} \qquad 5\text{-}1$$

On integration,

$$\alpha(t) = \bar{V}(t) = 2\sigma N_o \frac{k_{22}k_{23}}{k_1^2}\{1 - k_1 t + \frac{k_1^2 t^2}{2} - e^{-k_1 t}\} \qquad 5\text{-}2$$

This equation 5-2 can be simplified to

$$\alpha(t) = \tfrac{1}{3} N_o \sigma k_{22} k_{23} k_1 t^3 \qquad 5\text{-}3$$

or

$$\alpha(t) = 6 N_o \sigma k_{22} k_{23} t^2 \qquad 5\text{-}4$$

respectively for $k_1 t \ll 1$ and $k_1 t \gg 1$. It is obvious that when growth along the surface is rate-determining, this does not lead to a linear law. (iii) If $k_{21} \ll k_{22} \approx k_{23}$, this would result in pancake or sheet-like nuclei if the area of the nuclei is limited. Photomicrographic investigations[14] have shown that the surface nuclei are approximately circular and remarkably uniform in size. This would imply that rapid surface growth up to a limited size occurs and that thereafter the nuclei penetrate more slowly into the interior of the crystal.

$$G(x) = k_{21} \qquad 5\text{-}5$$

Equation 1-4 then becomes

$$\bar{V}(t) = \sigma N_o k_{21} k_1 \int_o^t (t-t') e^{-k_1 t'} dt'$$

$$\alpha(t) = \bar{V}(t) = \frac{\sigma N_o k_{21}}{k_1} \{e^{-k_1 t} - 1 + k_1 t\} \qquad 5\text{-}6$$

If $k_1 t \ll 1$, equation 5-6 reduces to

$$\alpha = \frac{1}{2} \sigma N_o k_{21} k_1 t^2 \qquad 5\text{-}7$$

If $k_1 t \gg 1$, equation 5-6 becomes

$$\alpha = \sigma N_o k_{21} t \qquad 5\text{-}8$$

Equation 5-8 therefore adequately describes the linear process encountered in the "induction period". This implies that the rate determining step in the linear process is associated with nucleus growth penetrating into the bulk from the surface and that nucleation is instantaneous or at least very rapid.

(c) Exponential Process

Garner and Hailes[49] first introduced the concept of nuclei as linear, branching chains. The formation of additional nuclei by chain mechanism is considered to be a much more important process than the formation of fresh nuclei, so that the initial nucleation law assumed is relatively unimportant. For linear nucleation, the net rate of production of nuclei[2] is

$$dN/dt = k_3N + k_1N_o \qquad 5\text{-}9$$

The length of a nucleus formed at t=t', is at time t,

$$\ell\ (t,t') = k_2(t-t') \qquad 5\text{-}10$$

The kinetic equation is then formulated based on equations 5-9 and 5-10 which give

$$\alpha(t) = \bar{V}(t) = \frac{\sigma_E k_1 k_2 N_o}{k_3^2}\{e^{k_3 t} - k_3 t - 1\} \qquad 5\text{-}11$$

If the number of nucleus forming sites is limited, the linear nucleation law must be replaced by the exponential law. The net rate of production of nuclei becomes

$$dN/dt = k_1(N_o - N) + k_3N$$

or
$$dN/dt = k_1N_o + (k_3 - k_1)N \qquad 5\text{-}12$$

If the nucleus forming sites are rapidly exhausted, equation 5-12 becomes

$$dN/dt = k_3N \qquad 5\text{-}13$$

with the boundary condition $N=N_o$ at $t=0$. Equations 5-10, 5-13 and 1-4 then lead to the kinetic equation

$$\alpha(t) = \overline{V}(t) = \frac{\sigma_E k_2 N_o}{k_3}\{e^{k_3t} - k_3t - 1\} \qquad 5\text{-}14$$

Either eqn. 5-11 or 5-14 describes adequately the later part of the "induction period". It is this equation $P = C_3(e^{k_3t} - k_3t - 1)$, which is referred to in this thesis as the "modified exponential" or, for brevity, simply as the "exponential", which fits the data (cf. eqn. 3-3).

5-1-2 Avrami Process

The complete success of the exact Avrami equation over

a substantial range of α from 0.01 to 1.00 has two valuable implications concerning the low temperature decomposition of AP. (i) At least two different kinetic mechanisms must be operating consecutively. (ii) The activation energies derived from equations other than the complete Avrami equation cannot be justified. The apparent validity of AE equation needs further comment. The AE equation (1-7) may be arrived at in either of two distinct ways. Firstly, it is an equation derived by Erofeev[50] purely from probability considerations. This equation can at best fit the decomposition curve of AP from 0.20 up to 0.89[18], or 0.40 to 0.98[17], for n=3. For n=4, the equation fits the α-range only from 0.02 to 0.20[8] or from 0.07 to 0.25[17]. The limited range of α over which the Erofeev equation fits clearly indicates its inadequacy in accounting for the decomposition kinetics. Since the exact Avrami equation fits the α-range from 0.01 to 1.00, one might expect that its approximate form (the AE equation) should describe the acceleratory and decay periods of the reaction. This is in fact the case[8]. The AE equation with n=4 fits the decomposition curve from 0.02 to 0.20, whereas with n=3, the equation is valid in the α-range of 0.20 to 0.90[8]. However, the splitting of the decomposition curve into two consecutive parts each fitted by the AE equations with n=4 and n=3 should involve an unknown α-range for which neither version fits. This change over period corresponds to $k_1 t \simeq 1$. The difficulty in distinguishing between various powers of n when approximating

the Avrami equation has been stressed in the literature[10]. The superiority of computer fitting to the exact Avrami equation, over graphical methods using an approximate form of this equation as a means of kinetic analysis is clearly displayed in this work. Also the arbitrary use[8] of different powers of n for different physical forms of AP is no longer necessary when the exact Avrami equation is used since both single crystals and compressed pellets have been shown to obey the same equation (1-6).

5-1-3 Physical Interpretation of Linear, Exponential, and Avrami Processes

Equations 5-8, 5-11 (or 5-14), and 1-6 provide a complete fit to the decomposition curve; nevertheless the hypotheses on which they are based require confirmation. Direct observation of nuclei in AP has been made by several workers[9,39,40,51]. The most recent and elegant work of Herley, Jacobs, and Levy[14,52], using optical and electron microscopy, has shown that the same pattern could be obtained on AP crystals by either solution or thermal etching. They[14] concluded that decomposition nuclei on the surface are formed preferentially where dislocations intersect the crystal surface. The resulting nuclei were therefore circular[14] with a shape similar to a pancake[53]. Furthermore, these nuclei were uniform in size with no preferential crystallographic alignment. Nucleation is most probably[14] instantaneous with a constant rate of growth. These observations are in perfect

agreement with equation 5-8 which has been derived to describe the kinetics of the linear process. The time for completion of the surface reaction was also measured approximately[14] (at time intervals of 1 hour) at three temperatures 170°, 190° and 205°C. The results were 600, 240 and 90 minutes respectively. Figure 49 is a plot of $\ell n\ t_S$ vs. $10^3/T$, where t_S is the time for the completion of surface reaction as observed[14]. The dashed line obtained by extrapolating to higher temperatures meets fairly well the two points for t_L (Table 4) at 222° and 227°C. This figure thus reveals the physical meaning for the linear process! That the linear process corresponds to a purely surface reaction whose kinetics are governed by equation 5-8 can no longer be doubted. There remains only the question of the activation energy.

In the linear process, the computed parameter k_L is equal to $PF\sigma k_{21}N_o$. An Arrhenius plot of $\ell n\ k_L$ vs. $1/T$ will therefore give the activation energy for transverse nucleus growth on the surface E_{21}. This is complicated however, by the unknown value for N_o which clearly varies from crystal to crystal, and from one crystal face to another. The trend of k_L is rather irregular as is apparent from Tables 2 to 6. The same situation arises even when k_L is divided by PF. An indirect method therefore has to be used to find the activation energy. The linear process does not continue into the exponential and acceleratory regions. This was checked during the fitting by allowing the linear process to continue

rather than terminate at the beginning of the exponential process. Satisfactory fits could not however, be obtained using this variant of the model. A definite termination of the linear process implies that the nuclei, which are all formed much at the same time, grow to a uniform depth and then cease growing when the branching process takes over. The time required for the completion of the linear process (penetration of surface nuclei) is therefore inversely proportional to k_{21} and independent of how many nuclei are actually growing. A plot of $-\ell n\ t_L$ vs. 1/T should therefore yield the necessary activation energy for the inward growth of the pancake-shaped surface nuclei. Figures 17 and 18 show the actual plot and Table 17 displays the activation energy of 28.1±2.3 kcal $mole^{-1}$ for single crystals. A plausible explanation for the wide spread in the values of t_L is the fact that the crystals decomposed do not always have the same ratio of the area represented by the m face to that by the c face. It has been shown[39,51] that c face is much more reactive than the m face. One should then expect that the scatter in t_L should be minimized when pellets are used, and should not arise at all for cubic crystals. However, because of the very short duration of t_L in both pellets and cubic crystals, the scatter is most probably due to the rather large uncertainty in the values obtained from curve fitting. Furthermore, nucleus growth on pellets is much easier, as indicated by the smaller activation energy involved.

Another remarkable observation[14] is that even when the surface reaction is nearly completed, there is no sign of the appearance of any internal nuclei in the bulk. As the surface nuclei cease growth, branching of nuclei is observed[14]. The branches appear to be aligned along the $[\bar{1}24]$ and $[\bar{1}2\bar{4}]$ directions but these directions are really the projections of the lines of growth on the surface and it is uncertain whether the branches lie on the surface or penetrate into the crystal at an angle. Spherical nuclei were then found[14] to occur along certain crystallographic directions [010] and [510] in the bulk. Perhaps the ease of escape of the gaseous products plays a decisive role and is the reason for slow nucleation in the bulk. The reacted surface layer is so "broken up" that gases can readily find their way out of the reaction sites and this perhaps explains why branching occurs prior to bulk nucleation even though the branching process is associated with a rather high activation energy of 31 to 44 kcal $mole^{-1}$, with the exception of orthorhombic crystals (Table 18). Note that the exponential and Avrami processes do overlap, however, showing that bulk nucleation commences before the branching process is completed.

The bulk reaction is associated with spherical nuclei that occur in bands aligned principally along the [010] direction. They appear to have roughly the same size of about 2 μm in a crystal decomposed at 217°C for 225 min (α=0.15). Nucleus growth is isotropic in three dimensions so that the

rate constants for nucleus growth are each equal to k_2 in the Avrami equation (1-6). The coral-like structure of the resulting residue[14] is a good indication that the growth nuclei finally impinge on each other thereby causing deceleration of the reaction. The fact that nucleation in the bulk is not entirely random indicates the Avrami equation may not be completely adequate; however it certainly gives an excellent fit to the data (Fig. 13). Even though the nuclei are aligned preferentially in bands, nucleation at the possible nucleus forming sites within the bands will be random and this may be a sufficient condition for the Avrami equation to be satisfied. The activation energies for nucleation E_1 and for nucleus growth E_2 are summarized in Table 18. Because of the discontinuity at the transition point, the activation energies will receive separate consideration. In the orthorhombic form, the results for single crystals displays a wide uncertainty in both E_1 and E_2 so that a direct comparison between pellets and single crystals cannot be made. If the numerical values are taken literally then E_1 for a single crystal is much larger than that for pellets. This is quite reasonable since the mechanical deformation brought about by the operations of grinding and pelleting would be expected to introduce many more potential sites at which the activation energy for reaction is lower than at those sites present in the single crystal. Above the transition point the activation energies for PC crystals, BNL crystals, and compressed pellets

(PP) are equal within the confidence limits stated in Table 18 while for both PC and PP they are both less than the corresponding values for the orthorhombic modification. These results imply that the phase transition introduces a sufficient number of dislocations into the crystal to make its original physical form or state of perfection irrelevant.

The activation energies for nucleus growth E_2 are equal, within the confidence limits that can be placed on the values determined, for pellets, PC and BNL crystals in both orthorhombic and cubic modifications. The mean value of E_2 for the cubic form is 26.6 kcal $mole^{-1}$ and for the orthorhombic modification 27.8 kcal $mole^{-1}$; these values are equal within the accuracy with which they may be determined. They are also in satisfactory agreement with the average value of 26.6 ± 0.9 kcal $mole^{-1}$ found by Davies, Jacobs and Russell-Jones[12] using the AE equation with n=2. Thus the activation energy determined from the AE equation approximates that for nucleus growth but the graphical analysis, as emphasized above, does not reveal any of the details of the kinetics, particularly those relating to the induction period. The effect of gross imperfections within the crystal is illustrated by the results for BNL crystals which display higher values for the rate constants k_1 and k_2 (in $C_1^{1/3} k_1$). This enhancement in the chemical reactivity is most probably associated with (i) a reduction in lattice energy in the vicinity of cracks and (ii) the easier escape of gaseous products.

5-1-4 Percentage Decomposition

One of the most remarkable features associated with the low temperature decomposition of AP is that reaction ceases after about 30% decomposition[11] at an ambient pressure of 760 torr of inert gas. The residue is chemically inert and has a large surface area[8]. The cessation of the reaction has been interpreted as due to inhibition of the reaction by an adsorbed layer of NH_3 on the surface. Because the present work on the decomposition of AP was carried out at high vacuum, sublimation occurs simultaneously such that the percentage decomposition is well below 30%. Tables 11 to 12 show that the percentage decomposition in terms of PF/M is fairly constant throughout the whole temperature range studied and corresponds to an average value of 20% decomposition. The implication is that decomposition and sublimation are competitive processes with similar rate constants and activation energy. On the other hand, the crystal shows a high percentage decomposition at low temperature (~28%) which rapidly decreases to about 3% at elevated temperatures. This remarkable result is due to the long "induction period" for single crystals even at high temperatures. Nevertheless, the kinetics of decomposition are not seriously affected, implying that both sublimation and decomposition occur simultaneously but independently.

5-2 Decomposition of Doped Crystals

Although direct microscopic observation[14] has revealed the importance of both screw and edge dislocations in providing reaction sites, the possible role played by vacancies and impurities has not been considered. Since the primary process involves proton transfer[11], one might tentatively suggest that an adjacent cation vacancy would facilitate the transfer process as it has a virtual negative charge. If this is so, an increase in the cation vacancy concentration should increase the rate of reaction. Both cation and anion vacancies are present in all real ionic solids in thermodynamic equilibrium, the product of the concentration of cation vacancies and that of the anion vacancies being constant at constant temperature. When a divalent cation, e.g. Ba^{2+}, is incorporated into the lattice of AP, the impurity ion will occupy a cation lattice site. In order to preserve electrical neutrality, there must be a corresponding cation vacancy in the lattice. If n such Ba^{2+} ions are incorporated in this way, n such cation vacancies will be produced. The concentration of anion vacancies can be increased in a similar way by doping with divalent SO_4^{2-} ions. It is possible that some of the impurity ions are associated with vacancies on nearest neighbour sites in the form of complexes. This would reduce their possible effectiveness for altering the rate of proton transfer. However, if the dopant concentration were high enough, a

direct chemical influence on the reactivity of AP might be expected. At high concentrations the impurities will most probably accumulate in the dislocation cores which have a high affinity for impurities[54]. Ba^{2+} can probably then form complex ion with NH_3 whereas SO_4^{2-} might abstract a proton to form HSO_4^-, so that the proton transfer reaction will be affected in both cases. The effect of the added impurity on the surface reaction and on the bulk reaction will be considered separately. Tables 5 to 10 show that SO_4^{2-} increases t_L, while Ba^{2+} greatly decreases it in comparison with pure AP. This can be understood if a cation vacancy is involved in the proton transfer reaction. The direct transfer of proton from NH_4^+ to ClO_4^- is inhibited by the high proton affinity of NH_3[31] even though the loss in lattice energy as a result of proton transfer would not be so large at the surface. The indirect transfer of a proton via some proton trap T can be envisaged:

$$NH_4^+(\ell) + T \rightleftharpoons NH_3(a)T + H^+(\ell) \qquad 5\text{-}15$$

where (ℓ) denotes a normal lattice site. $H^+(\ell)$ can be considered as a proton trapped in a cation vacancy. When sufficient energy is received, the proton can be removed from the lattice site and combined with a neighboring ClO_4^-, thereby completing the proton transfer process:

$$H^+(\ell) + ClO_4^-(\ell) \longrightarrow \square_+ + HClO_4(a) \qquad 5\text{-}16$$

The cation vacancy $\boxed{\quad}_+$ left behind may function as a further proton trap:

$$NH_4^+(\ell) + \boxed{\quad}_+ \rightleftharpoons \boxed{NH_3}_+ + H^+(\ell) \qquad 5\text{-}17$$

Because surface nucleation occurs at sites where dislocations intersect the surface in deformed crystals, but is apparently random in unstrained crystals[14], it would seem that either dislocations or cation vacancies can function as the initial proton traps T. That Ba^{2+} ions enhance the surface reaction while SO_4^{2-} ions retard it suggests that cation vacancies indeed act as proton traps assisting the surface reaction. This effect is reflected in the fact that the values of t_L lie in the order: APS > PC > APB.

In the bulk reaction, the situation becomes quite different. The internal nuclei are aligned[14] along definite crystallographic directions and are almost certainly associated with the presence of dislocations in the bulk. This implies that in the bulk reaction, it is dislocations rather than cation vacancies that function as the effective traps assisting the proton transfer process. The reason could be simply that dislocations provide relatively easy paths for the escape of gaseous products. The reduction in lattice energy at a dislocation is comparable to that on crystal surface. From equation 5-17, one would therefore expect that both Ba^{2+} and SO_4^{2-} could enhance the reaction effectively by complexing with NH_3 and by abstracting the

H^+, respectively. Alternatively, the cation vacancies created by incorporation of Ba^{2+} to the lattice may accumulate at dislocations cores. The increase in the concentration of cation vacancies will therefore enhance the proton transfer in the neighbourhood of dislocations as evident from equation 5-17. This can be seen from the fact that, in the orthorhombic region, APB shows a tremendous reduction in both E_1 and E_2 as compared with that of PC; APS shows correspondingly higher values. For the cubic modification, E_2 for both APB and APS are reduced, although both show high values in E_1. It appears, therefore, quite difficult to judge the effects from an energetic point of view. Figure 13 perhaps provides the clearest picture. Both Ba^{2+} and SO_4^{2-} shorten the overall reaction time, but, the percentage decomposition in both APB and APS follows the same pattern as in PC. This is in accordance with the proposed model, eqn. 5-17.

5-3 Electrical Conductivity of AP

In Chapter 4, the conductivity results have been described along with some conclusions made in each section in order to reveal the motivation behind the succeeding experiments. In this section emphasis will be laid particularly on the mechanism by which electrical conduction can occur in crystals of AP. Some further interpretation of the results and comparisons with results from other investigators will also be given.

5-3-1 The Conducting Species

Before the conduction process in an ionic solid can be understood, one has first to discover the conducting species involved within the appropriate temperature range in which the conductivity measurements were carried out. This could be achieved by electrolysing the solid and measuring the transport number of both the cation and anion, and also analysing the products of electrolysis. Migration of ionic species in a perfect crystalline lattice would require such a tremendous activation energy that such a process is not energetically feasible. The idea of diffusion via lattice defects was therefore introduced[55,56]. In the alkali and silver halides respectively, the conducting species are cation and anion vacancies, and interstitial Ag^+ ions and cation vacancies.

The d.c. electrolysis[34] of AP yielded only hydrogen at the cathode between 20-100°C. The amount produced obeyed Faraday's law. These results imply that both the discharging and the conducting species are protons. The migration of a proton in the lattice might involve some lattice defects. Conductivity measurements should therefore yield information about the necessary activation energy for the migration and formation of such defects from the plot of log σT vs. $1/T$.

5-3-2 Conductivity of AP Pellets

When a fresh sample was measured, the change of conductivity σ with temperature is shown by curve 1 in

Fig. 26. Successive runs in the number order 1,2,3,4 show that the conductivity curve can be classified into (i) the low temperature region (<127°C) in which σ changes on thermal cycling or annealing; and (ii) the high temperature region in which σ is not affected by annealing. Conductivity in the high temperature region (but still below the decomposition temperature) corresponds to a steady state; whereas in the low temperature region, a non-equilibrium state exists. If a sample is heated into the region of measurable decomposition (~>180°C), σ always increases with time on annealing. Three different types of annealing have been observed: (i) low temperature annealing (Fig. 38) in which σ decreases monotonically with time, and obeys a $t^{\frac{1}{2}}$ law (Fig. 39); (ii) annealing in the intrinsic region (127°C<T<180°C) in which σ is independent of time (point a in Fig. 26); and (iii) annealing in the decomposition region which is accompanied by an increase in σ (not shown in Fig. 26 but marked by arrow A in Fig. 28). These three regions corresponding to the three types of annealing will be discussed separately.

(i) Low temperature region (t<127°C)

A possible cause for the irreproducibility observed upon thermal cycling is that some adsorbed species involved in the conduction process is being gradually removed by heating the crystal. It is thus of importance to find out if the conductivity is due to surface, or bulk conduction.

Figure 32 in which a guard ring electrode was used shows that surface conduction is not predominant. Figure 27 strongly supports the suggestion that some adsorbed species is involved and that this was driven off completely after sufficiently long (five days) annealing. The study of the effect of water vapor (Fig. 29) shows that the enhancement in σ is tremendous (compare point d in curve 4 to point e in curve 2) at room temperature, but only slight (compare c in curves 3,5 with point a in Fig. 29) at high temperatures (118°C). Upon 6 hours pumping in vacuum σ drops from d on curve 4 to b on curve 6, which has the same qualitative features as curves 1,2,3,4 in Fig. 26. This implies that the low temperature conductivity is complicated by the presence of moisture in the AP powder from which the compressed pellets were prepared. In order to understand the role played by adsorbed H_2O, the effect of introducing an ambient pressure of 760 torr of NH_3 was studied and is shown in Fig. 30; the results are broadly similar. The enhancement in conductivity in the presence of H_2O or NH_3 (Fig. 30) undoubtedly must indicate the participation of these adsorbed species in the conduction process. Figure 29 further implies that desorption of moisture during annealing is diffusion-controlled as the water is desorbed out from the bulk of the crystallites in the pellet. The study of NH_3 adsorption and desorption isotherms (Fig. 43) clearly shows that no chemical reaction is involved during the adsorption process since the

initial conductivity value is regenerated upon desorption. Finally, when a pellet has been annealed for a sufficiently long time to remove all the moisture, the conductivity in the low temperature region then merges with that in the higher temperature range in one continuous line (Fig. 27).

(ii) High temperature region

Provided the amount of moisture is not significant or the moisture has been entirely desorbed, the conductivity is steady with time between ~127°C to ~200°C. The activation energy E in this linear region is 0.9 eV (refer to Table 19).

(iii) Decomposition region

Above about 200°C, σ increases with time (not shown in Fig. 26, but appears in curve 3 of Fig. 28 at a much reduced temperature 175°C, an effect due to $HClO_4$ treatment). The slope on log σT vs. 1/T plot deviates upward from that in the "high temperature region". The magnitude of this slope is not significant as one can readily see from Fig. 37 which shows that σ increases with time in a complex ways, so that the slope in Fig. 26 depends on the rate of heating up the sample and the time taken to measure the conductivity. It is likely that this region does not correspond to a process involving a higher activation energy and one should not accept a value calculated from the apparent slope in interpreting the conductivity process. This region is certainly associated with partial decomposition (presumably

the surface reaction) during which the gases produced might influence the conductivity. The effect of partial decomposition is exhibited by curve 5 in Fig. 26. The conductivity at room temperature has been enhanced by a factor of 10^3 (compare curves 5 and 4) but only by a factor of 10 at ~130°C. The low temperature region in curve 4 has also been modified into a fairly flat region (curve 5). The gradual increase in conductivity at about 60°C and the sudden drop at 90°C imply that the values of σ along curve 5 do not correspond to a steady state. This conclusion is confirmed by arrow B at 118°C which shows a drop in σ upon annealing. This type of behavior indicates that the enhancement in σ is due to gaseous products rather than to structural modification, e.g. the introduction of defects into the crystal. Which of the products is influencing σ needs to be explored. The fact that σ increases at 153°C (arrow A, Fig. 26) after partial decomposition shows that $HClO_4$ has been produced which reduces[18] the induction period and accelerates the reaction such that measurable decomposition occurs at 153°C on re-heating. $HClO_4$ probably does not enhance the conductivity. Comparison of Figures 28 and 29 indicates that the enhancement by a drop of $HClO_4 \cdot H_2O$ (72% by weight) could be due solely to the H_2O. If this is true, the enhancement by partial decomposition is due to the H_2O produced.

5-3-3 Conductivity of Single Crystals

The effect of moisture (H_2O) on the low temperature conductivity of AP pellets is evident from the preceeding section. One should then expect that this effect might be less, or even not observed at all, when single crystals are used because of their relatively much smaller surface area. This is not necessarily true, however, since the single crystals which were used for the conductivity measurements were grown from aqueous solution. The inclusion of water is almost inevitable during crystallization from solution. This water inclusion will not be as easy to eliminate as that adsorbed on the surface in the case of pellets. One should then expect that the low temperature range might be extended to higher temperatures. Figure 34 shows that this region is considerably prolonged to as high as nearly 230°C. Annealing at any point in this region causes σ to drop (curves 2,3,4,5 in Fig. 35). The high temperature (intrinsic) region has been presumably masked by the low temperature conductivity and is not reached before decomposition occurs, beginning somewhere around 200°C (arrow A in Fig. 35). The effect of partial decomposition is as expected. The conductivity in the low temperature region is much enhanced and measurable decomposition sets in at lower temperature (ca. 140°C in curve 7, Fig. 35) on successive heating cycles. Again the conductivity along this curve does not correspond to a steady state since annealing at 117° and 127°C causes σ

to fall. However, if the sample is allowed to undergo the phase transition at 240°C, the low temperature region is then considerably reduced. The high temperature region now appears at about 110°C and terminates at about 165°C. The conductivity in the low temperature region is enhanced partly due to adsorbed product gases, but if the sample is subjected to thermal cycling to get rid of these species, a linear region with activation energy of about 0.6 eV then appears to extend from the high temperature region down to about 105°C (compare curves 2 and 3 in Fig. 34). If sufficient annealing were to be carried out, one would expect to get eventually a single straight line as in the case of pellets (Fig. 27). At the phase transition, rearrangement in the lattice most probably assists in the exclusion of H_2O.

Curves 2,3 in Fig. 34 and curve 3 in Fig. 36 corresponds to the conductivity of a partially decomposed AP. However, the reproducibility at high temperatures upon thermal cycling to the transition point (curves 3,4 in Fig. 36) or to 165°C (curves 2,3 in Fig. 34) indicates that (i) desorption of product gases (presumably NH_3 or H_2O) is nearly complete, and (ii) the conductivity at this region is not seriously affected by partial decomposition. The effect of partial decomposition can be visualized in two ways. (i) If decomposition is restricted only to the surface, the bulk of the crystal is unaffected and the high temperature is therefore most probably dominated by bulk

conduction. (ii) If partial decomposition is severe such that bulk reaction occurs, one should then expect the change in cell constant and disorganization of the crystal lattice to give rise to a complicated conductivity curve, as seen in the case of pellets (curve 5 in Fig. 26), although the adsorption of large amounts of product gases could equally well give rise to such irregularities. As in the case of pellets, Figure 36 rules out the possibility that the low temperature region is dominated by surface conductance.

Annealing experiments in the low temperature range of a single crystal at 89° and 114°C (arrows B and C in Fig. 35) show that σ decreases with time but that the change is rather small (Fig. 41), and that desorption involves diffusion as the rate-controlling process (as in the case of pellets).

5-3-4 Adsorption and Desorption Isotherms

The study of the kinetics of decomposition by following the change in σ with time is complicated by some technical problèms which have been explained in section 4-2-1 of Chapter 4. The kinetics of adsorption and desorption of NH_3 could be studied but the results (isotherms are given in Fig. 45 for PP and in Fig. 48 for PC) do not permit one to evaluate either the heat of adsorption or the activation energy for the rate process. Nevertheless, there are two important physical implications from this study: (i) adsorption of NH_3 does not involve a chemical reaction

between the adsorbed species and AP, since the initial value of σ of the untreated sample can be regained by sufficiently prolonged desorption; (ii) the rate of desorption is very much more rapid in pellets than that in crystals, and (iii) the rate process involved in desorption is dominated by the contribution from the surface desorption (log t law as in Fig. 44) for pellets, but is diffusion-controlled in single crystals ($t^{\frac{1}{2}}$ law in Fig. 47). These results explain why the loss of water from single crystals would be such a slow process and consequently why the low temperature region is so prolonged (curve 1 in Fig. 34).

5-3-5 Proposed Mechanism for Protonic Conduction

The work of Boldyrev[34] has revealed protonic conductivity in AP in the temperature range 20°C to 100°C. The present results indicate that the conductivity at higher temperature (>100°C) is probably also due to protonic conduction since the two regions are characterized by similar activation energies (e.g. curves 3,4 in Fig. 26). The thermal instability of AP above 150°C restricts the useful temperature range to about 180°C as the highest limit (the useful temperature range being raised by the rather long induction period for decomposition).

Two different types of conductivity behavior can be distinguished: (i) one with an apparent activation energy of zero eV; and (ii) one with an activation energy of 0.6 to 0.9 eV. The low temperature region is associated with

protonic conduction since Boldyrev[34] has confirmed this by electrolysis in the temperature range 25°-100°C. Migration of protons in solids is energetically favorable because of their small size. Protonic conduction had been found to operate in some solids that contain hydrogen bonds such as ammonium dihydrogen phosphate (ADP)[57,58], ice[59,60], borax[61], lithium sulfate monohydrate[62], potassium hydrogen fluoride[63], and some organic acids[64]. Upon electrolysis, all these show the evolution of only hydrogen at the cathode. During conductivity measurements, it was found that (i) in ADP[58], σ increased with time at constant temperature; (ii) in borax[59], the low temperature region (<30°C) showed irreproducible σ, and deviated from linearity of the conductivity plot in the high temperature region; (iii) an apparent zero-activation energy appeared in the case of ice[60]. AP is similar to NH_4Cl in that they both lack hydrogen bonding. The study of the conductivity of NH_4Cl[65,66] has led to a proposed mechanism which comprises a reversible proton transfer involving vacancies. Owing to the lack of information regarding the conducting species, this mechanism should be viewed as a tentative proposal.

The importance of the thermal instability of AP had not been realized by previous workers[27,33]; in addition the profound effects of adsorbed moisture and included water were generally ignored during the conductivity measurements in the low temperature range[32,34]. The wide scattering[27,33] appearing in the published conductivity curves is more than

that due to experimental errors. The results of this work have emphasized that σ is not independent of time either in the decomposition region or in the low temperature region with the presence of adsorbed or included water. Hence virtually any slope can arise from the plot of $\log \sigma T$ vs. $1/T$ depending on the conditions of measurement. These values differ greatly from one another and activation energies calculated from them should not, therefore, be taken too seriously. It is definitely not possible to deduce mechanisms for conduction from a conductivity curve, in which several linear protions were drawn[27], based on these non-steady values of σ. The disagreement among the results of previous workers is thus only to be expected.

The zero-activation energy region is found in the presence of adsorbed NH_3 or H_2O. When it occurs naturally it is possibly also due either to adsorbed or included water (Fig. 26,32,34) arising from sample preparation, or to NH_3 or H_2O formed by partial decomposition. The role of the adsorbed H_2O and NH_3 is probably therefore that of functionning as proton traps. Transfer of a proton to an NH_3 or H_2O molecule from a normal lattice NH_4^+ ion results in a proton hole. Conduction is then due to the jump of a proton from an NH_4^+ ion into the proton hole, leaving behind a vacancy occupied by the NH_3 molecule. Continuation of this process, eqn. 5-19, leads to the migration of $\boxed{NH_3}^+$ (proton holes) in the direction of the anode. Note that this process should

involve very little, virtually zero, activation energy since no change in lattice energy is involved. The initial step of forming the proton hole by transfer to an adsorbed or included H_2O molecule or to an adsorbed NH_3 molecule will require some activation energy since the proton trap is not an NH_3 molecule at a normal cation site inside the crystal. The whole process may be depicted schematically as follows:-

(i) formation of proton holes

$$NH_4^+(\ell) + \begin{matrix} NH_3(a)S \\ \text{or} \\ H_2O(a)S \end{matrix} \rightleftharpoons \boxed{NH_3}_+ + \begin{matrix} NH_4^+S \\ \text{or} \\ H_3O^+S \end{matrix} \qquad 5\text{-}18$$

where S is any unspecified site for adsorption and $\square_+$ denote a cation vacancy.

(ii) migration of proton holes

$$NH_4^+ + \boxed{NH_3}_+ \rightleftharpoons \boxed{NH_3}_+ + NH_4^+ \qquad 5\text{-}19$$

In the absence of the available proton traps formed by adsorbed NH_3 or H_2O the activation energy of 0.6 to 0.9 eV in the high temperature region corresponds to the formation of proton holes, equation 5-17

$$NH_4^+(\ell) + \square_+ \rightleftharpoons \boxed{NH_3}_+ + H^+(\ell) \qquad 5\text{-}17$$

This reaction is favoured at cation vacancies because of their virtual negative charge would facilitate proton transfer. Note that there is little change in lattice energy since a positive NH_4^+ ion is replaced by a proton.

The experimental results can be understood in terms of these mechanism. It is seen from Fig. 26 that as moisture is gradually annealed out by successive thermal cycles, zero-slope region becomes less pronounced and the activated process in the low temperature region becomes increasingly prominent. The appearance of a zero-slope region indicates that all the available proton traps are filled and the conductivity is governed by equation 5-19. The process has been depicted as taking place at cation vacancies but possibly dislocations might function as proton acceptors. At higher temperatures the conductivity due to the "intrinsic" mechanism (eqn. 5-17) gradually takes over as it exceeds that initiated by the adsorbed water. In this context "intrinsic" means conductivity due to defects (cation vacancies or dislocations) present in the crystal rather that due to adsorbed or included impurities. An accurate value for the activation energy associated with the intrinsic formation of proton holes is difficult to determine because of the onset of thermal decomposition (Fig. 26). The same picture applies to single crystals except that the low temperature region is much more prolonged (see Fig. 34, curve 1) and the intrinsic conductivity smaller until heated

through the phase transition. The former fact is obviously due to the greater difficulty in removing the included water. When this water is driven off by heating the crystal up to the transition temperature, the conduction process according to eqn. 5-17 then sets in (curve 3 in Fig. 34). The increase in the intrinsic conduction implies that proton traps, vacancies or dislocations, have been either introduced or dispersed by heating. Possibly the phase transition might yield an increase in dislocation content, since Bahl and Thomas[67] have shown dislocation multiplication occurs in $NaNO_3$ on approaching the λ point. If dislocations are involved in the intrinsic conduction process, the effect of the phase transition would then be to displace the conductivity curve to higher values without affecting the activation energy.

5-4 Conclusions

The study of the low temperature thermal decomposition of ammonium perchlorate (AP) has shown that the kinetics of the reaction as given by the decomposition curve $\alpha(t)$ can be described by a model which involves four consecutive steps: (i) instantaneous desorption of adsorbed species; (ii) a linear process; (iii) a modified exponential process; and (iv) an Avrami process. The fitting of this model to the experimental data was made possible through the use of computing techniques employing a non-linear least-squares program. The success resulting from using the exact form of

the Avrami equation over the major portion of the decomposition curve ($0.01<\alpha<1.00$) indicates the adequacy of the model based on the topochemical events associated with this equation.

The complications and uncertainties found previously[8,15,17,18] in choosing the right value for n, and the corresponding range of α, for the AE equation should not arise if the exact Avrami equation is used. The entire solid state reaction is interpreted in terms of a surface reaction which corresponds to α of $\sim 10^{-4}$ to 10^{-3} (Tables 11 to 14) and a bulk reaction which is responsible for the remaining part of the decomposition. This is represented diagramatically in Fig. 50. The surface reaction appears to involve cation vacancies, which is reflected in the fact that the reaction is retarded or accelerated by doping with divalent SO_4^{2-} ions and Ba^{2+} ions respectively. Reaction in the bulk is associated with dislocations and that both impurities enhance the reaction rate as indicated by the shortening of the time for complete decomposition. These interpretations correlate with the most recent and detailed work of Herley, Jacobs and Levy[14,52] on the photomicrographic observation of the decomposition nuclei. It is further concluded that the presence of gross visual crystal faults enhances the overall chemical reactivity; and that the concurrent occurrence of sublimation apparently does not influence the kinetics of decomposition, but reduces considerably the percentage decomposition of single crystals at elevated temperatures.

Although the laws leading to nucleation and nucleus growth for the surface and bulk reaction have been successfully sorted out, the chemical events involved cannot be ascertained owing to the lack of information as to the types of intermediates that are involved during the reaction. However, there is no doubt that the primary reaction involves a proton transfer[11,12,68] to form NH_3 and $HClO_4$ both adsorbed on the surface. The present research suggests that this transfer occurs in two-steps.

This proposed mechanism is partially supportedly by the electrical conductivity study from which it was concluded that protonic conduction occurs over the entire temperature range ($25°<T<170°C$) studied. The profound effects of adsorbed H_2O and NH_3 on the conductivity have also been observed. It is further concluded that adsorption of these species does not involve chemical reaction and that the conductivity in the temperature range in which decomposition occurs does not correspond to steady state values in that it is continuously influenced by the accumulation of gaseous products (probably H_2O) from the decomposition. This result points to the fact that the slope associated with the conductivity curve above the decomposition temperature should not be taken seriously. The results discussed in section 5-3 explain satisfactorily the discrepancies that occur in the results of previous workers. Because the mobility of proton in the lattice of AP has not been determined, it is not possible to estimate

the concentration of the existing defects (proton holes) involved in the conduction process. Further work is therefore suggested to determine the products of electrolysis in the high temperature range (>100°C) so as to confirm protonic conduction in this temperature range. Comparison of the conductivities of pure and doped samples, using both divalent cations and anions, will also reveal whether vacancy conduction is possible. Conductivity measurements on deuterated AP should help to confirm proton motion in the lattice.

TABLE 1

AE PARAMETERS AND α-RANGE FOR AP PELLETS

TEMP. °C	$10^3/T$ K^{-1}	log $\bar{k}_2$ $\bar{k}_2$ in min^{-1}	α_2-range	log $\bar{k}_3$ $\bar{k}_3$ in min^{-1}	α_3-range
219.3	2.030	-2.053	0.20-0.65	-2.101	0.00-0.55
222.1	2.019	-1.956	0.25-0.73	-2.015	0.00-0.50
225.4	2.006	-1.921	0.20-0.77	-1.985	0.00-0.60
227.5	1.997	-1.864	0.15-0.85	-1.971	0.00-0.80
230.0	1.987	-1.718	0.25-0.77	-1.802	0.00-0.71
235.3	1.967	-1.625	0.10-0.83	-1.691	0.00-0.80
237.6	1.958	-1.605	0.20-0.82	-1.677	0.03-0.70
238.4	1.955	-1.523	0.20-0.80	-1.602	0.04-0.70
240.2	1.948	-1.495	0.08-0.80	-1.513	0.00-0.50
241.3	1.944	-1.560	0.02-0.76	-1.497	0.00-0.24
243.6	1.935	-1.570	0.01-0.77	-1.418	0.00-0.06
246.3	1.925	-1.558	0.02-0.70	-1.421	0.00-0.05
248.7	1.916	-1.541	0.05-0.65	-1.538	0.02-0.45
250.0	1.911	-1.533	0.02-0.70	-1.514	0.00-0.40
251.2	1.907	-1.423	0.04-0.70	-1.452	0.01-0.50
255.2	1.893	-1.405	0.02-0.55	-1.374	0.00-0.30
259.7	1.877	-1.301	0.02-0.70	-1.239	0.02-0.35
263.7	1.863	-1.249	0.01-0.63	-1.119	0.00-0.33
269.4	1.843	-1.149	0.02-0.70	-1.119	0.00-0.50

TABLE 2

LEAST-SQUARES KINETIC PARAMETERS FOR ORTHORHOMBIC AP PELLETS

RUN	TEMP.	MASS	LINEAR			EXPONENTIAL			AVRAMI			
	°C	mg	$10^4 P_o$	$10^5 k_L$	t_L	$10^2 C_3$	$10 k_3$	t_E	$10^2 P_A$	$10^2 C_1$	$10\ k_1$	t_A
			torr	torr/min	min	torr	min^{-1}	min	torr		min^{-1}	min
PP007	219.3	40.8	0.00	3.14	11.5	10.77	0.299	40.1	70.96	3.72	0.132	37.3
PP031	222.1	13.0	3.23	1.06	12.9	2.36	0.364	44.3	20.97	2.99	0.170	40.5
PP012	222.1	32.2	0.40	0.60	9.2	5.38	0.364	37.5	56.23	2.85	0.167	31.1
PP004	222.1	40.7	0.00	0.12	9.6	7.44	0.362	41.8	67.38	3.14	0.183	36.9
PP002	222.1	44.7	0.00	3.37	10.0	8.22	0.364	42.2	75.52	3.88	0.168	38.6
PP011	222.1	61.4	0.00	1.66	15.7	6.37	0.366	55.5	113.36	4.97	0.138	49.1
PP026	225.4	38.9	0.00	0.76	14.6	3.27	0.481	46.4	71.44	2.22	0.245	42.7
PP025	227.5	38.0	0.11	1.13	14.6	2.96	0.527	45.9	68.52	2.57	0.255	42.7
PP005	230.0	42.4	0.00	2.35	8.2	8.38	0.625	25.0	76.66	5.47	0.222	23.3
PP001	232.0	40.2	0.05	3.39	5.0	9.05	0.714	21.8	65.45	6.91	0.248	19.3
PP027	232.3	46.3	0.03	1.29	12.4	2.27	0.729	40.3	84.74	2.65	0.314	36.4
PP006	235.3	39.3	0.00	2.31	6.1	4.36	0.899	24.4	60.89	4.81	0.351	22.3
PP008	235.3	42.2	0.00	1.41	7.3	4.88	0.888	25.3	71.13	4.94	0.351	23.1
PP022	237.6	68.9	0.92	1.45	10.2	1.54	1.030	30.1	71.63	3.36	0.393	27.6
PP023	238.5	40.6	0.00	3.52	9.6	2.25	1.310	23.1	78.54	4.33	0.426	23.1

TABLE 3

LEAST-SQUARES KINETIC PARAMETERS FOR CUBIC AP PELLETS

RUN	TEMP.	MASS	LINEAR			EXPONENTIAL			AVRAMI			
	°C	mg	$10^4 P_o$	$10^5 k_L$	t_L	$10^2 C_3$	$10 k_3$	t_E	$10^2 P_A$	$10^2 C_1$	$10\ k_1$	t_A
			torr	torr/min	min	torr	min^{-1}	min	torr		min^{-1}	min
PP009	240.2	43.8	0.01	3.04	4.8	4.60	0.121	15.6	80.44	3.88	0.469	13.1
PP013	241.3	45.3	0.15	2.42	4.9	1.93	0.131	12.0	88.38	2.05	0.517	9.7
PP010	243.7	44.8	0.48	1.36	4.7	6.86	0.158	12.3	78.01	2.04	0.607	11.3
PP014	246.3	40.5	0.57	0.00	4.8	3.11	0.184	12.8	73.20	1.51	0.737	11.8
PP024	248.7	38.7	1.19	2.72	6.4	1.22	0.187	13.9	81.16	1.13	0.792	13.9
PP015	250.0	41.0	0.02	1.51	5.1	1.69	0.234	10.9	84.39	1.20	0.836	10.9
PP028	251.2	39.0	0.00	1.14	5.1	0.35	0.244	14.9	79.73	1.25	0.843	13.9
PP021	252.6	42.9	0.17	2.00	6.1	0.44	0.268	15.6	90.55	1.43	0.969	14.9
PP016	255.2	44.0	3.38	7.34	4.7	0.78	0.361	9.0	97.04	1.14	0.998	8.2
PP020	259.7	46.8	2.18	0.00	3.7	0.06	0.393	13.4	97.99	1.53	1.170	13.4
PP029	261.5	39.8	0.39	0.07	4.3	0.26	0.479	10.4	80.95	1.08	1.567	10.2
PP017	263.7	38.0	0.90	0.00	2.4	0.21	0.506	6.0	84.00	1.19	1.477	5.9
PP030	266.2	36.5	0.00	3.84	4.5	0.21	0.579	9.8	70.15	1.15	1.779	9.8
PP018	269.4	39.6	0.26	2.85	3.9	0.76	0.628	5.9	85.60	1.09	1.923	5.8
PP019	269.4	38.8	0.40	0.00	1.2	0.05	0.620	6.1	84.81	1.36	1.923	6.1

TABLE 4

LEAST-SQUARES KINETIC PARAMETERS FOR CUBIC AP SINGLE CRYSTALS (BNL)

RUN	TEMP.	MASS	LINEAR			EXPONENTIAL			AVRAMI			
	°C	mg	$10^4 P_o$	$10^5 k_L$	t_L	$10^2 C_3$	$10 k_3$	t_E	$10^2 P_A$	$10^2 C_1$	$10^3 k_1$	t_A
			torr	torr/min	min	torr	min^{-1}	min	torr		min^{-1}	min
PC003	250.0	11.4	0.14	0.91	4.1	0.543	0.145	71.3	11.91	28.6	1.185	51.3
PC004	255.7	13.0	0.23	4.13	2.5	1.850	0.183	12.1	12.28	79.0	1.118	9.9
PC005	259.8	12.5	0.37	1.03	15.4	0.808	0.304	24.4	10.62	47.4	1.580	23.7
PC006	263.7	11.8	0.29	6.17	30.0	0.449	0.315	82.1	9.60	33.7	1.753	69.7
PC007	266.2	11.4	0.16	5.51	0.5	1.730	0.497	1.2	4.74	39.1	1.886	0.8
PC008	269.4	10.5	0.18	1.69	1.7	0.207	0.650	7.6	7.90	52.4	2.258	6.6
PC009	271.9	11.6	0.56	0.57	2.4	0.075	0.861	41.9	7.67	37.1	2.348	28.6
PC010	274.3	10.3	0.10	1.93	2.7	0.014	0.899	46.6	6.56	51.2	2.410	23.8
PC011	276.9	10.6	0.00	3.41	3.0	0.120	1.170	16.2	2.20	199.5	2.782	6.6
PC012	276.9	11.7	1.40	0.97	21.7	0.596	1.190	31.0	9.54	66.4	2.673	21.8
PC013	276.9	13.5	0.34	1.13	21.4	0.466	1.110	31.6	2.03	191.8	2.896	22.1
PC014	276.9	12.4	0.77	1.63	20.0	0.323	1.100	32.9	9.50	54.2	2.797	22.1
PC015	276.9	24.0	0.12	3.67	3.6	0.233	1.100	18.2	17.09	67.5	2.888	15.7
PC016	280.4	10.3	0.39	0.47	17.7	0.197	0.997	36.1	3.09	100.0	3.168	32.3
PC017	280.4	19.6	0.70	1.66	15.8	0.105	1.200	32.9	5.33	116.0	3.150	21.3

TABLE 5

LEAST-SQUARES KINETIC PARAMETERS FOR ORTHORHOMBIC AP SINGLE CRYSTALS (PC)

RUN	TEMP.	MASS	LINEAR			EXPONENTIAL			AVRAMI			
	°C	mg	$10^4 P_o$	$10^5 k_L$	t_L	$10^3 C_3$	$10 k_3$	t_E	$10^2 P_A$	$10^2 C_1$	$10^2 k_1$	t_A
			torr	torr/min	min	torr	min^{-1}	min	torr		min^{-1}	min
PC018	222.1	96.7	0.44	0.416	46.9	0.76	0.394	114.3	202.6	—	—	—
PC019	222.1	75.1	0.20	0.505	42.6	0.40	0.436	120.2	203.5	—	—	—
PC037	222.1	51.3	0.04	0.410	33.0	0.40	0.436	102.7	133.5	1.70	0.341	94.1
PC032	227.7	81.2	0.03	0.414	37.5	0.55	0.493	110.1	219.8	0.73	0.559	102.3
PC033	230.3	80.1	0.29	0.558	36.2	0.31	0.619	96.9	214.1	1.29	0.420	90.6
PC034	232.5	59.8	0.28	0.535	18.0	0.23	0.748	68.2	169.6	0.58	0.813	62.8
PC035	235.3	49.3	0.27	0.551	15.2	0.51	0.721	66.0	145.8	0.64	0.932	57.1

TABLE 6

LEAST-SQUARES KINETIC PARAMETERS FOR CUBIC AP SINGLE CRYSTALS (PC)

RUN	TEMP.	MASS	LINEAR			EXPONENTIAL			AVRAMI			
	°C	mg	$10^4 P_o$	$10^5 k_L$	t_L	$10^2 C_3$	$10 k_3$	t_E	$10^2 P_A$	$10^2 C_1$	$10^3 k_1$	t_A
			torr	torr/min	min	torr	min^{-1}	min	torr		min^{-1}	min
PC030	240.2	84.5	0.03	0.23	18.3	1.42	0.244	126.3	227.5	1.81	0.494	33.2
PC031	243.9	80.9	0.30	0.29	10.6	0.03	1.000	49.8	166.4	66.64	0.391	27.2
PC022	264.1	51.0	0.22	0.38	4.2	3.14	0.074	32.8	24.4	30.22	1.032	32.8
PC023	272.5	35.9	0.11	0.70	6.3	0.93	0.179	65.3	14.3	37.60	1.326	22.8
PC024	277.5	40.7	0.24	0.42	3.9	8.59	0.163	37.3	30.5	40.49	1.718	24.0
PC025	280.0	30.1	0.92	2.39	2.4	0.49	0.267	56.4	9.9	73.29	1.661	18.2
PC026	282.2	39.0	0.00	1.66	4.3	1.95	0.244	35.3	10.8	61.63	2.072	21.2
PC027	285.0	55.3	0.17	0.07	2.2	1.26	0.275	43.7	11.9	56.85	2.170	16.9
PC028	287.9	40.5	0.23	0.01	1.4	0.60	0.357	43.7	13.7	48.56	2.509	14.8
PC029	290.7	51.1	0.12	1.02	1.6	1.34	0.366	33.3	12.7	81.23	2.615	18.8

TABLE 7

LEAST-SQUARES KINETIC PARAMETERS FOR ORTHORHOMBIC AP SINGLE CRYSTALS DOPED WITH Ba^{2+}

RUN	TEMP.	MASS	LINEAR			EXPONENTIAL			AVRAMI			
	°C	mg	$10^4 P_o$	$10^5 k_L$	t_L	$10^2 C_3$	$10^2 k_3$	t_E	$10^2 P_A$	$10^2 C_1$	$10^2 k_1$	t_A
			torr	torr/min	min	torr	min^{-1}	min	torr		min^{-1}	min
APB11	222.1	4.1	0.09	0.376	29.6	2.52	0.304	123.2	11.65	31.70	0.102	106.6
APB12	227.7	4.1	0.24	0.637	19.9	2.29	0.404	71.1	11.99	39.54	0.117	68.9
APB13	230.3	4.3	0.38	0.923	9.6	3.24	0.555	62.1	10.37	34.84	0.134	52.8
APB14	232.5	3.2	0.07	0.327	22.9	1.95	0.687	71.9	7.79	35.77	0.141	48.9
APB15	235.3	3.4	0.24	0.373	20.0	2.09	0.871	66.8	9.40	45.75	0.159	41.8

TABLE 8

LEAST-SQUARES KINETIC PARAMETERS FOR CUBIC AP SINGLE CRYSTALS DOPED WITH Ba^{2+}

RUN	TEMP.	MASS	LINEAR			EXPONENTIAL			AVRAMI			
	°C	mg	10^4P_o	10^5k_L	t_L	10^2C_3	$10k_3$	t_E	10^2P_A	10^2C_1	10^2k_1	t_A
			torr	torr/min	min	torr	min^{-1}	min	torr		min^{-1}	min
APB16	240.2	4.3	0.24	0.34	26.3	8.85	0.079	88.9	10.33	36.23	0.164	26.9
APB17	243.9	3.2	0.18	0.40	16.4	19.91	0.050	65.9	4.49	7.94	0.212	23.1
APB18	250.0	5.0	0.00	1.98	2.6	2.00	0.064	47.9	6.48	7.05	0.348	42.5
APB19	255.7	3.4	0.00	0.75	4.1	3.16	0.076	24.4	5.04	4.82	0.508	20.3
APB20	259.7	3.2	0.20	0.66	4.8	4.32	0.096	40.8	3.38	4.05	0.753	30.8
APB10	266.2	5.3	0.04	0.61	1.8	7.18	0.126	4.9	6.45	4.84	0.899	0.9
APB09	269.4	6.9	0.01	0.71	1.5	4.11	0.197	8.7	8.54	4.67	1.058	7.6
APB08	274.3	5.1	0.11	0.28	2.2	1.65	0.229	9.1	4.95	4.02	1.376	8.5
APB07	276.9	5.5	0.00	1.34	6.2	33.72	0.200	7.4	4.47	3.19	1.450	6.7
APB06	280.4	4.3	0.09	0.69	4.9	2.95	0.217	30.3	1.83	6.90	1.616	27.2
APB05	282.2	5.2	0.12	1.50	4.7	8.88	0.229	6.9	3.55	3.23	1.674	4.9
APB04	285.0	6.6	0.35	1.33	2.7	20.68	0.311	3.1	4.15	2.21	1.923	2.7
APB03	287.9	7.9	0.45	45.60	1.0	0.38	0.467	27.0	6.24	4.36	2.000	4.4
APB02	290.7	6.6	0.15	4.17	0.3	0.0004	0.476	207.4	8.16	6.69	2.304	2.3
APB01	290.7	7.4	0.20	0.35	0.0	1.72	0.553	15.9	4.29	5.75	2.300	12.3

TABLE 9

LEAST-SQUARES KINETIC PARAMETERS FOR ORTHORHOMBIC AP SINGLE CRYSTALS DOPED WITH SO_4^{2-}

RUN	TEMP.	MASS	LINEAR			EXPONENTIAL			AVRAMI			
	°C	mg	10^4P_o	10^5k_L	t_L	10^2C_3	$10k_3$	t_E	10^2P_A	10^2C_1	10^2k_1	t_A
			torr	torr/min	min	torr	min^{-1}	min	torr		min^{-1}	min
APS01	222.1	60.9	0.31	0.724	42.5	0.40	0.173	149.6	168.0	14.84	0.791	132.2
APS02	227.7	81.2	0.25	0.566	53.3	0.31	0.214	117.2	45.4	23.53	0.975	104.7
APS03	230.3	13.6	0.28	0.405	38.4	0.12	0.245	92.3	38.2	15.05	1.190	79.3
APS04	232.5	13.1	0.32	0.410	44.5	0.23	0.272	97.6	36.6	24.34	1.259	85.7
APS05	235.3	9.1	0.32	0.326	34.2	0.13	0.304	79.8	24.8	25.94	1.396	69.7

TABLE 10

LEAST-SQUARES KINETIC PARAMETERS FOR CUBIC AP SINGLE CRYSTALS DOPED WITH SO_4^{2-}

RUN	TEMP.	MASS	LINEAR			EXPONENTIAL			AVRAMI			
	°C	mg	10^4P_o	10^5k_L	t_L	10^2C_3	$10k_3$	t_E	10^2P_A	10^2C_1	$10\ k_1$	t_A
			torr	torr/min	min	torr	min^{-1}	min	torr		min^{-1}	min
APS06	240.2	8.2	0.04	0.25	22.0	0.10	0.453	45.3	22.86	31.60	0.017	40.2
APS07	244.0	15.3	0.11	0.28	18.3	9.01	0.028	170.6	20.69	7.27	0.016	138.2
APS08	244.0	11.0	0.13	0.79	35.2	6.75	0.025	307.2	10.51	7.23	0.018	273.5
APS09	250.0	12.2	0.68	0.13	32.1	6.68	0.047	121.8	9.92	4.96	0.028	114.0
APS10	255.7	9.1	0.06	0.47	13.1	1.80	0.060	60.8	5.58	3.57	0.054	52.8
APS11	259.7	10.6	0.15	0.69	24.5	2.78	0.067	88.4	5.70	1.19	0.074	64.6
APS12	266.2	6.0	0.11	0.51	10.5	2.78	0.100	14.3	1.94	2.67	0.096	12.9
APS13	269.4	6.8	0.03	0.52	9.7	1.03	0.120	43.4	2.41	2.97	0.100	28.4
APS14	274.3	7.8	0.10	0.41	11.7	1.71	0.110	50.3	1.88	1.67	0.150	38.8
APS15	276.9	6.9	0.00	2.33	14.5	8.66	0.168	21.5	2.54	2.19	0.149	19.1
APS16	280.4	7.2	0.00	2.01	2.9	0.53	0.186	41.5	1.77	1.16	0.200	24.9
APS17	282.2	7.2	0.00	1.20	3.7	0.48	0.219	38.6	1.74	1.67	0.200	18.4
APS18	285.0	7.1	0.32	2.51	7.1	1.85	0.177	29.7	1.38	1.76	0.236	22.5
APS19	287.9	7.5	0.46	2.57	7.2	14.48	0.232	8.2	1.43	1.13	0.250	7.8
APS20	290.7	7.7	0.00	2.12	3.0	0.64	0.252	28.8	1.08	1.28	0.270	14.4

TABLE 11

RATE CONSTANTS AND EXTENT OF DECOMPOSITION FOR ORTHORHOMBIC AP PELLETS

RUN	$10^3/T$	$10^2 PF/M$	$\ell n\ t_L$	$\ell n\ k_3$	$\ell n\ C_1^{1/3} k_1$	$\ell n\ k_1$	$10^3 \alpha_{LT}$	$10 \alpha_{ET}$	$10 \alpha_{AS}$
PP007	2.031	1.843	2.446	-3.508	-3.888	-4.326	0.482	0.713	0.566
PP031	2.019	1.748	2.554	-3.314	-3.709	-4.075	2.020	1.050	0.774
PP012	2.019	1.816	2.222	-3.313	-3.743	-4.092	0.162	0.710	0.388
PP004	2.019	1.783	2.262	-3.319	-3.619	-3.999	0.160	1.071	0.716
PP002	2.019	1.836	2.306	-3.313	-3.634	-4.086	0.412	1.061	0.800
PP011	2.019	1.968	2.754	-3.308	-3.751	-4.287	0.216	0.968	0.622
PP026	2.006	1.964	2.678	-3.035	-3.443	-3.710	0.145	0.900	0.653
PP025	1.998	1.953	2.683	-2.943	-3.354	-3.668	0.237	1.021	0.768
PP005	1.987	1.932	2.107	-2.773	-3.242	-3.808	0.235	0.831	0.642
PP001	1.979	1.799	1.610	-2.639	-3.052	-3.096	0.241	1.417	0.954
PP027	1.978	1.977	2.516	-2.619	-3.136	-3.461	0.178	1.140	0.745
PP006	1.967	1.754	1.808	-2.409	-2.826	-3.349	0.204	1.597	1.168
PP008	1.967	1.878	1.983	-2.421	-2.817	-3.349	0.129	1.462	1.025
PP022	1.958	1.112	2.322	-2.273	-2.832	-3.236	0.313	0.954	0.651
PP023	1.955	2.107	2.263	-2.033	-2.669	-3.157	0.395	0.820	0.819

TABLE 12

RATE CONSTANTS AND EXTENT OF DECOMPOSITION FOR CUBIC AP PELLETS

RUN	$10^3/T$	$10^2 PF/M$	$\ell n\ t_L$	$\ell n\ k_3$	$\ell n\ C_1^{1/3} k_1$	$\ell n\ k_1$	$10^3 \alpha_{LT}$	$10 \alpha_{ET}$	$10 \alpha_{AS}$
PP009	1.948	1.913	1.565	-2.112	-2.608	-3.060	0.175	0.761	0.399
PP013	1.944	1.961	1.604	-2.031	-2.723	-2.963	0.152	0.130	0.052
PP010	1.935	1.865	1.545	-1.845	-2.564	-2.801	0.134	0.935	0.655
PP014	1.925	1.908	1.567	-1.693	-2.470	-2.607	0.073	0.762	0.531
PP024	1.916	2.149	1.859	-1.677	-2.493	-2.536	0.352	0.245	0.245
PP015	1.912	2.123	1.625	-1.452	-2.421	-2.482	0.089	0.306	0.306
PP028	1.907	2.093	1.623	-1.411	-2.399	-2.474	0.071	0.333	0.234
PP021	1.902	2.184	1.811	-1.317	-2.216	-2.335	0.149	0.436	0.337
PP016	1.893	2.229	1.545	-1.018	-2.261	-2.304	0.695	0.180	0.108
PP020	1.877	2.145	1.319	-0.934	-2.004	-2.146	0.217	0.241	0.241
PP029	1.870	2.114	1.476	-0.737	-1.828	-1.853	0.503	0.416	0.380
PP017	1.863	2.227	0.881	-0.681	-1.855	-1.913	0.106	0.083	0.075
PP030	1.854	2.021	1.512	-0.547	-1.681	-1.727	0.236	0.492	0.492
PP018	1.843	2.184	1.370	-0.465	-1.620	-1.649	0.159	0.108	0.103
PP019	1.843	2.207	0.190	-0.478	-1.547	-1.649	0.046	0.097	0.096

TABLE 13

RATE CONSTANTS AND EXTENT OF DECOMPOSITION FOR CUBIC AP SINGLE CRYSTALS (BNL)

RUN	$10^3/T$	$10^2 PF/M$	$\ell n\ t_L$	$\ell n\ k_3$	$\ell n\ C_1^{1/3} k_1$	$\ell n\ k_1$	$10^3 \alpha_{LT}$	$10 \alpha_{ET}$	$10 \alpha_{AS}$
PC001	2.019	2.509	4.025	-3.680	-5.892	-7.148	0.009	0.016	0.011
PC002	2.019	2.806	3.904	-4.433	-5.992	-7.286	0.007	0.221	0.140
PC003	1.911	1.059	1.431	-4.235	-5.620	-6.738	0.004	0.305	0.137
PC004	1.891	0.947	0.922	-4.001	-5.340	-6.796	0.010	0.035	0.025
PC005	1.876	0.854	2.734	-3.493	-5.164	-6.450	0.018	0.050	0.045
PC006	1.863	0.877	3.403	-3.459	-5.174	-6.346	0.182	1.270	0.718
PC007	1.854	0.416	-0.597	-3.002	-5.051	-6.273	0.010	0.012	0.010
PC008	1.843	0.754	0.552	-2.733	-4.773	-6.093	0.006	0.028	0.020
PC009	1.834	0.702	0.909	-2.453	-4.850	-6.054	0.009	2.337	0.581
PC010	1.827	0.643	0.999	-2.409	-4.716	-6.028	0.009	0.967	0.086
PC011	1.818	0.210	1.114	-2.144	-4.119	-5.884	0.047	1.194	0.102
PC012	1.818	0.818	3.075	-2.129	-4.525	-5.924	0.037	0.617	0.037
PC013	1.818	0.153	3.062	-2.199	-4.092	-5.844	0.134	2.319	0.143
PC014	1.818	0.770	2.998	-2.206	-4.548	-5.879	0.042	0.625	0.052
PC015	1.818	0.727	1.287	-2.207	-4.443	-5.847	0.008	0.325	0.201
PC016	1.807	0.336	2.878	-2.306	-4.219	-5.755	0.035	1.977	1.063
PC017	1.807	0.275	2.763	-2.120	-4.176	-5.760	0.062	0.977	0.114

TABLE 14

RATE CONSTANTS AND EXTENT OF DECOMPOSITION FOR AP SINGLE CRYSTALS (PC)

RUN	$10^3/T$	$10^2 PF/M$	$\ell n\ t_L$	$\ell n\ k_3$	$\ell n\ C_1^{1/3} k_1$	$\ell n\ k_1$	$10^3 \alpha_{LT}$	$10 \alpha_{ET}$	$10^2 \alpha_{AS}$
PC018	2.019	2.101	3.849	-3.233	———	———	0.118	0.041	0.284
PC019	2.019	2.718	3.751	-3.132	———	———	0.115	0.051	0.319
PC037	2.019	2.611	3.496	-3.132	-5.504	-5.680	0.104	0.051	0.329
PC032	1.997	2.720	3.623	-3.010	-5.291	-5.187	0.072	0.078	0.508
PC033	1.986	2.683	3.589	-2.783	-5.387	-5.471	0.107	0.056	0.365
PC034	1.978	2.845	2.888	-2.593	-4.996	-4.812	0.073	0.052	0.335
PC035	1.967	2.974	2.722	-2.630	-4.824	-4.675	0.075	0.120	0.579
PC030	1.948	2.693	2.907	-3.713	-5.113	-5.310	0.031	0.646	0.050
PC031	1.934	2.059	2.358	-2.303	-6.447	-7.847	0.020	0.086	0.051
PC022	1.861	0.479	1.449	-4.909	-5.740	-6.876	0.155	0.032	0.321
PC023	1.833	0.399	1.845	-4.023	-5.416	-6.625	0.385	0.537	0.350
PC024	1.816	0.763	1.376	-4.117	-5.133	-6.366	0.131	0.495	1.666
PC025	1.808	0.332	0.889	-3.623	-4.969	-6.400	1.499	0.895	0.656
PC026	1.801	0.283	1.451	-3.711	-4.806	-6.179	0.643	0.674	1.817
PC027	1.792	0.217	0.810	-3.593	-4.786	-6.133	0.152	1.043	0.994
PC028	1.782	0.341	0.342	-3.334	-4.694	-5.988	0.169	0.883	0.610
PC029	1.773	0.255	0.504	-3.307	-4.481	-5.946	0.220	1.063	2.550

TABLE 15

RATE CONSTANTS AND EXTENT OF DECOMPOSITION FOR AP SINGLE CRYSTALS DOPED WITH SO_4^{2-}

RUN	$10^3/T$	$10^2 PF/M$	$\ell n\ t_L$	$\ell n\ k_3$	$\ell n\ C_1^{1/3} k_1$	$\ell n\ k_1$	$10^3 \alpha_{LT}$	$10 \alpha_{ET}$	$10^2 \alpha_{AS}$
APS01	2.019	2.773	3.749	-4.057	-6.244	-7.143	0.200	0.085	0.530
APS02	1.997	0.562	3.975	-3.845	-5.881	-6.933	0.714	0.113	0.683
APS03	1.986	2.816	3.647	-3.710	-5.830	-6.734	0.479	0.050	0.279
APS04	1.977	2.813	3.795	-3.603	-5.613	-6.677	0.582	0.120	0.662
APS05	1.967	2.741	3.532	-3.494	-5.490	-6.574	0.573	0.086	0.490
APS06	1.948	2.793	3.093	-3.094	-5.227	-6.378	0.258	0.037	0.217
APS07	1.934	1.389	2.905	-5.878	-5.770	-6.431	0.289	0.449	2.707
APS08	1.934	1.090	3.562	-5.997	-5.676	-6.335	2.436	1.656	12.390
APS09	1.912	0.863	3.471	-5.358	-5.330	-5.864	4.553	0.698	5.822
APS10	1.891	0.620	2.573	-5.124	-4.804	-5.228	1.189	0.154	1.086
APS11	1.877	0.549	3.200	-5.010	-4.847	-4.907	3.183	0.533	2.185
APS12	1.854	0.326	2.354	-4.608	-4.323	-4.650	3.287	0.043	0.367
APS13	1.843	0.339	2.272	-4.425	-4.243	-4.606	2.165	0.417	1.358
APS14	1.827	0.252	2.465	-4.513	-4.028	-4.198	2.965	0.931	4.534
APS15	1.818	0.376	2.671	-4.086	-3.940	-4.202	12.970	0.376	2.329
APS16	1.806	0.255	1.052	-3.984	-3.861	-3.910	3.139	0.997	3.120
APS17	1.801	0.247	1.295	-3.819	-3.741	-3.912	2.464	1.054	1.813
APS18	1.792	0.208	1.958	-4.032	-3.558	-3.747	14.260	1.299	6.555
APS19	1.782	0.194	1.975	-3.765	-3.649	-3.688	15.920	0.188	1.679
APS20	1.773	0.145	1.104	-3.683	-3.529	-3.612	5.714	1.566	3.177

TABLE 16

RATE CONSTANTS AND EXTENT OF DECOMPOSITION FOR AP SINGLE CRYSTALS DOPED WITH Ba^{2+}

RUN	$10^3/T$	$10^2 PF/M$	$\ell n\ t_L$	$\ell n\ k_3$	$\ell n\ C_1^{1/3} k_1$	$\ell n\ k_1$	$10^3 \alpha_{LT}$	$10 \alpha_{ET}$	$10^2 \alpha_{AS}$
APB11	2.019	2.863	3.388	-5.797	-5.737	-6.890	1.028	0.106	0.739
APB12	1.997	2.941	2.990	-5.511	-5.529	-6.755	1.247	0.056	0.525
APB13	1.986	2.439	2.264	-5.193	-5.431	-6.615	1.205	0.157	1.084
APB14	1.977	2.449	3.134	-4.980	-5.221	-6.561	1.050	0.169	0.527
APB15	1.967	2.780	2.996	-4.744	-5.170	-6.445	1.043	0.222	0.516
APB16	1.948	2.404	3.271	-4.837	-5.211	-6.408	1.091	1.261	0.110
APB17	1.934	1.408	2.799	-5.298	-5.464	-6.155	1.866	1.488	0.433
APB18	1.912	1.311	0.969	-5.053	-5.008	-5.659	0.795	0.149	1.161
APB19	1.891	1.490	1.420	-4.878	-4.758	-5.282	0.615	0.085	0.554
APB20	1.877	1.104	1.579	-4.649	-4.423	-4.889	1.458	0.827	4.244
APB10	1.854	1.218	0.600	-4.373	-4.186	-4.711	0.234	0.011	0.031
APB09	1.843	1.242	0.417	-3.925	-4.035	-4.549	0.137	0.053	0.372
APB08	1.827	0.975	0.803	-3.778	-3.822	-4.286	0.347	0.047	0.387
APB07	1.818	0.816	1.831	-3.912	-3.846	-4.234	1.866	0.037	0.215
APB06	1.806	0.523	1.586	-3.828	-3.481	-4.125	1.876	2.449	1.841
APB05	1.801	0.685	1.548	-3.776	-3.698	-4.090	2.304	0.053	0.233
APB04	1.792	0.629	0.984	-3.470	-3.687	-3.951	1.712	0.020	0.171
APB03	1.782	0.796	0.026	-3.064	-3.421	-3.912	8.144	0.784	0.895
APB02	1.773	1.237	-1.246	-3.046	-3.137	-3.770	0.331	9.944	0.033
APB01	1.773	0.648	——	-2.895	-3.189	-3.772	0.423	1.907	1.057

TABLE 17

ARRHENIUS PARAMETERS FOR THE LINEAR PROCESS

SAMPLE	E_L, kcal $mole^{-1}$	log (A_L/min^{-1})
PP	18.9 ± 2.3	6.1 ± 0.8
PC	28.1 ± 2.1	9.1 ± 0.8
BNL	———	———
APB	26.5 ± 4.6	8.4 ± 1.7
APS	23.9 ± 2.8	7.3 ± 1.0

TABLE 18

ARRHENIUS PARAMETERS FOR THE NUCLEATION, GROWTH AND BRANCHING PROCESSES

(THE UNITS OF A ARE MIN^{-1})

SAMPLE	CRYSTAL FORM*	E_1	$\log A_1$	E_2	$\log A_2$	E_3	$\log A_3$
		kcal $mole^{-1}$		kcal $mole^{-1}$		kcal $mole^{-1}$	
PP	o	28.1 ± 2.4	10.6 ± 1.0	30.8 ± 1.2	12.0 ± 0.5	35.3 ± 1.0	14.1 ± 0.4
PC	o	37.0 ±14.4	13.9 ± 6.3	24.9 ± 9.1	8.6 ± 4.0	22.1 ± 5.5	8.4 ± 2.4
BNL	o						
APB	o	17.0 ± 1.7	4.5 ± 0.8	22.6 ± 3.1	7.5 ± 1.3	41.0 ± 4.9	15.5 ± 2.1
APS	o	22.3 ± 2.2	6.7 ± 1.0	28.5 ± 2.7	9.9 ± 1.2	21.7 ± 1.0	7.8 ± 0.4
PP	c	24.6 ± 1.3	9.2 ± 0.6	23.7 ± 1.4	8.9 ± 0.6	31.1 ± 1.6	12.4 ± 0.7
PC	c	22.1 ± 1.5	6.0 ± 0.6	28.5 ± 1.6	9.1 ± 0.6	35.0 ± 4.6	12.2 ± 1.8
BNL	c	20.4 ± 1.1	5.6 ± 0.4	27.5 ± 2.8	9.0 ± 1.2	43.7 ± 2.4	16.4 ± 1.0
APB	c	25.4 ± 1.2	8.2 ± 0.5	24.5 ± 1.5	8.1 ± 0.6	29.3 ± 2.2	10.0 ± 0.9
APS	c	30.5 ± 1.7	10.3 ± 0.7	25.3 ± 1.5	8.5 ± 0.6	24.8 ± 1.6	8.0 ± 0.7

* o orthorhombic

c cubic

TABLE 19

ACTIVATION ENERGIES FOR THE FORMATION OF PROTON HOLE CALCULATED FROM THE CONDUCTIVITY CURVES

SAMPLE	FIGURE	CURVE	TEMPERATURE RANGE	ACTIVATION ENERGY
pellet	26		150° - 200°C	0.96 eV
	27		90° - 170°C	0.81 eV
single crystal	34	1	60° - 100°C	0.56 eV
		2	165° - 200°C	0.54 eV
	36	2	100° - 125°C	0.53 eV
		3	165° - 200°C	0.75 eV

FIG. 1

CRYSTAL GROWTH TANK

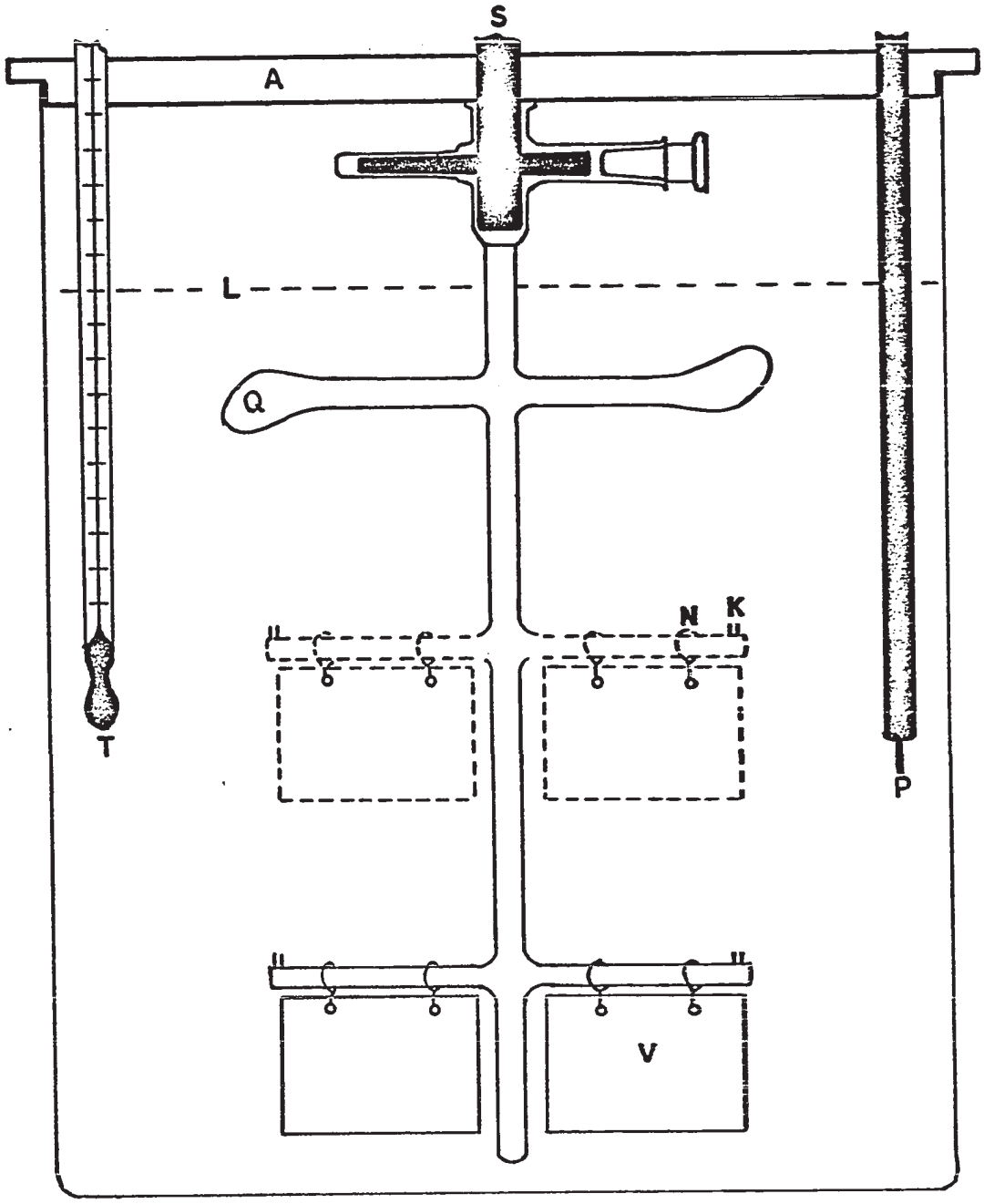

LEGEND FOR FIG. 1

A	plexi glass lid
S	rotating shaft
L	solution level
T	thermometer
V	glass vane
P	probe
N	nylon thread
K	seat for seed
Q	paddle for stirring

FIG. 2

REVERSIBLE ROTATING MECHANISM

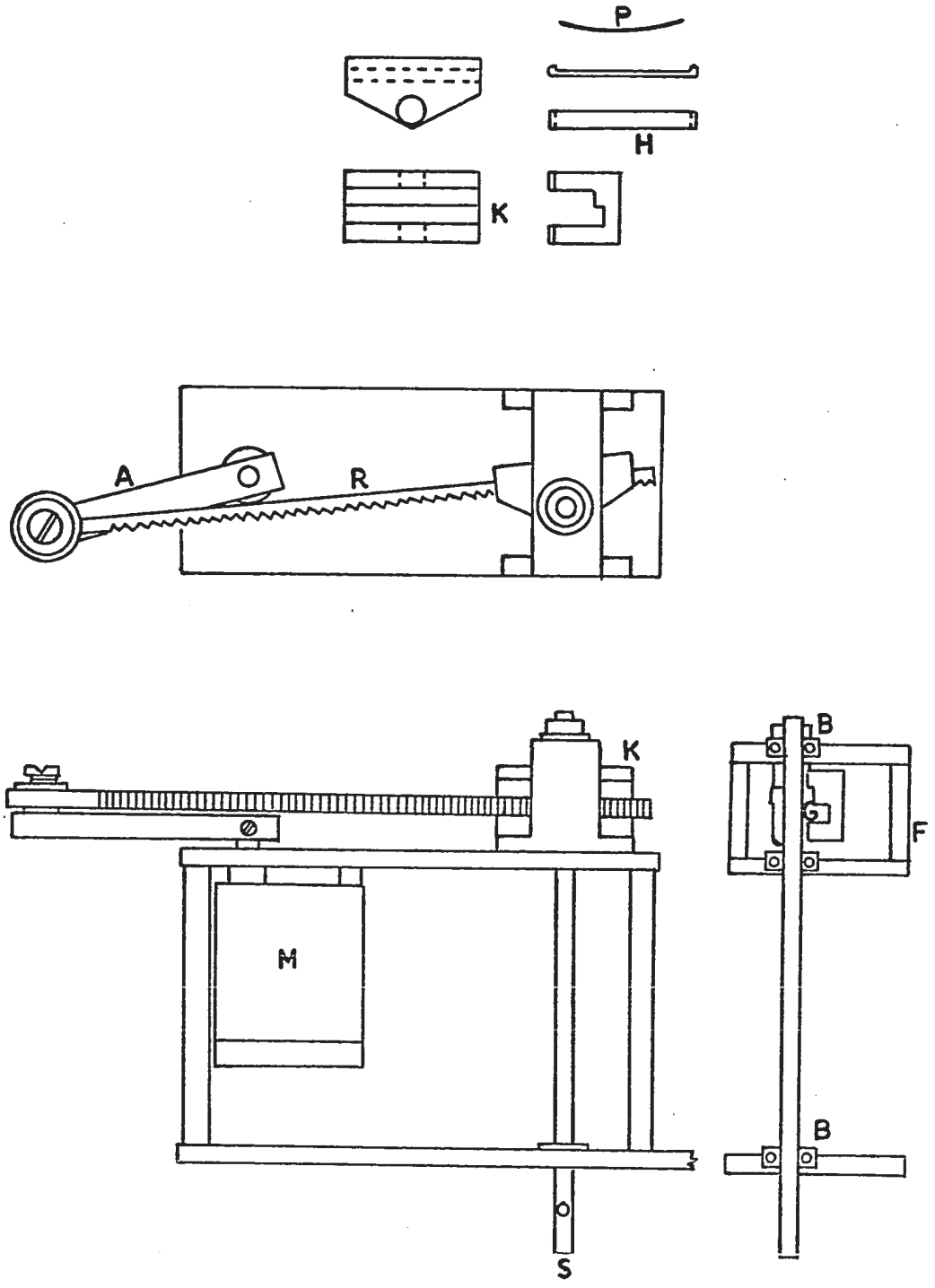

LEGEND FOR FIG. 2

A	driver arm
B	ball bearings
R	gear rack
M	gear reduction motor
S	rotating shaft
H	shoe
K	knuckle
F	frame
P	phosphor bronze spring
G	pinion gear

FIG. 3

DECOMPOSITION LINE

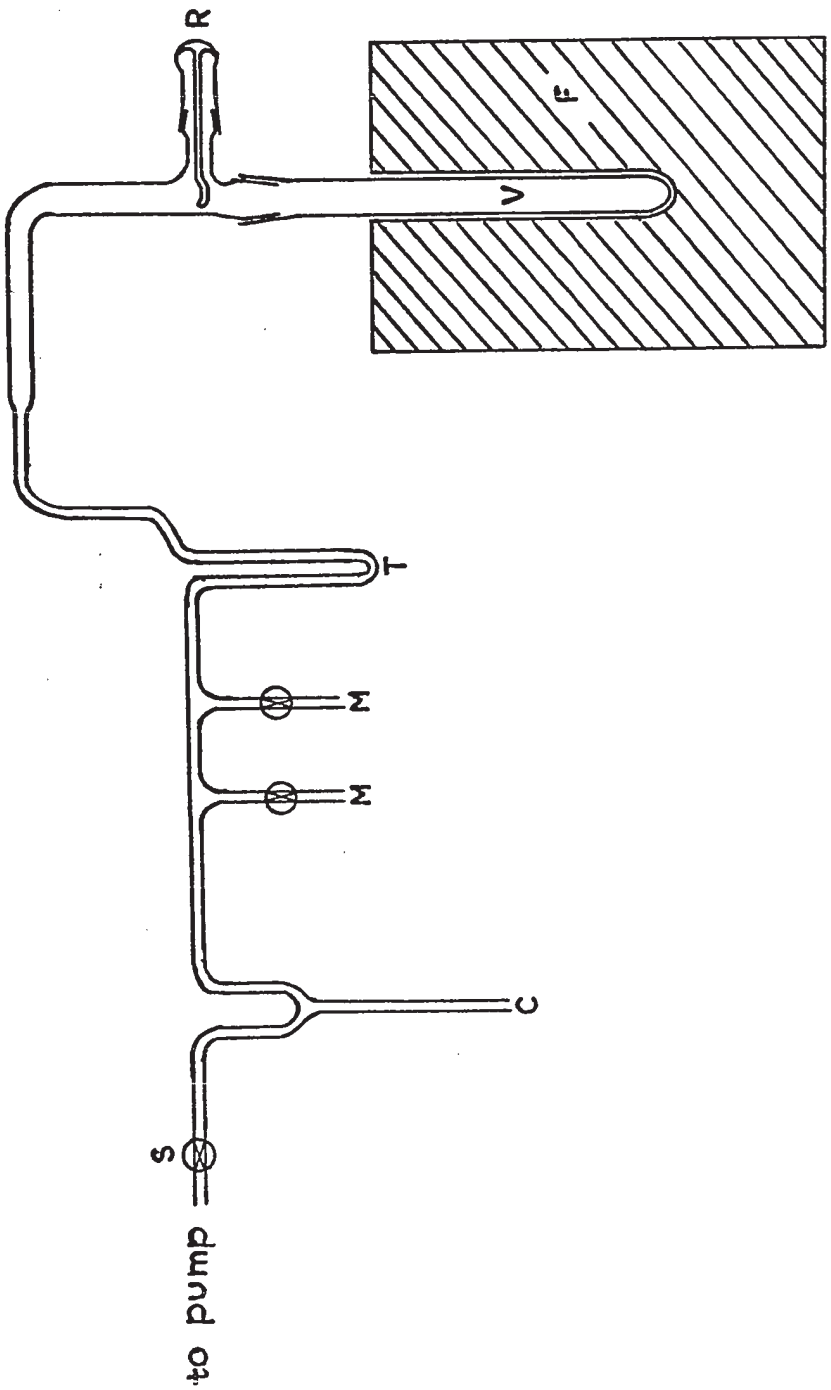

LEGEND FOR FIG. 3

C	mercury cut-off
M	McLeod gauge
T	U-trap
S	stockcock
V	reaction vessel
F	furnace
R	rotatable spoon

FIG. 4

CRYSTAL HOLDER

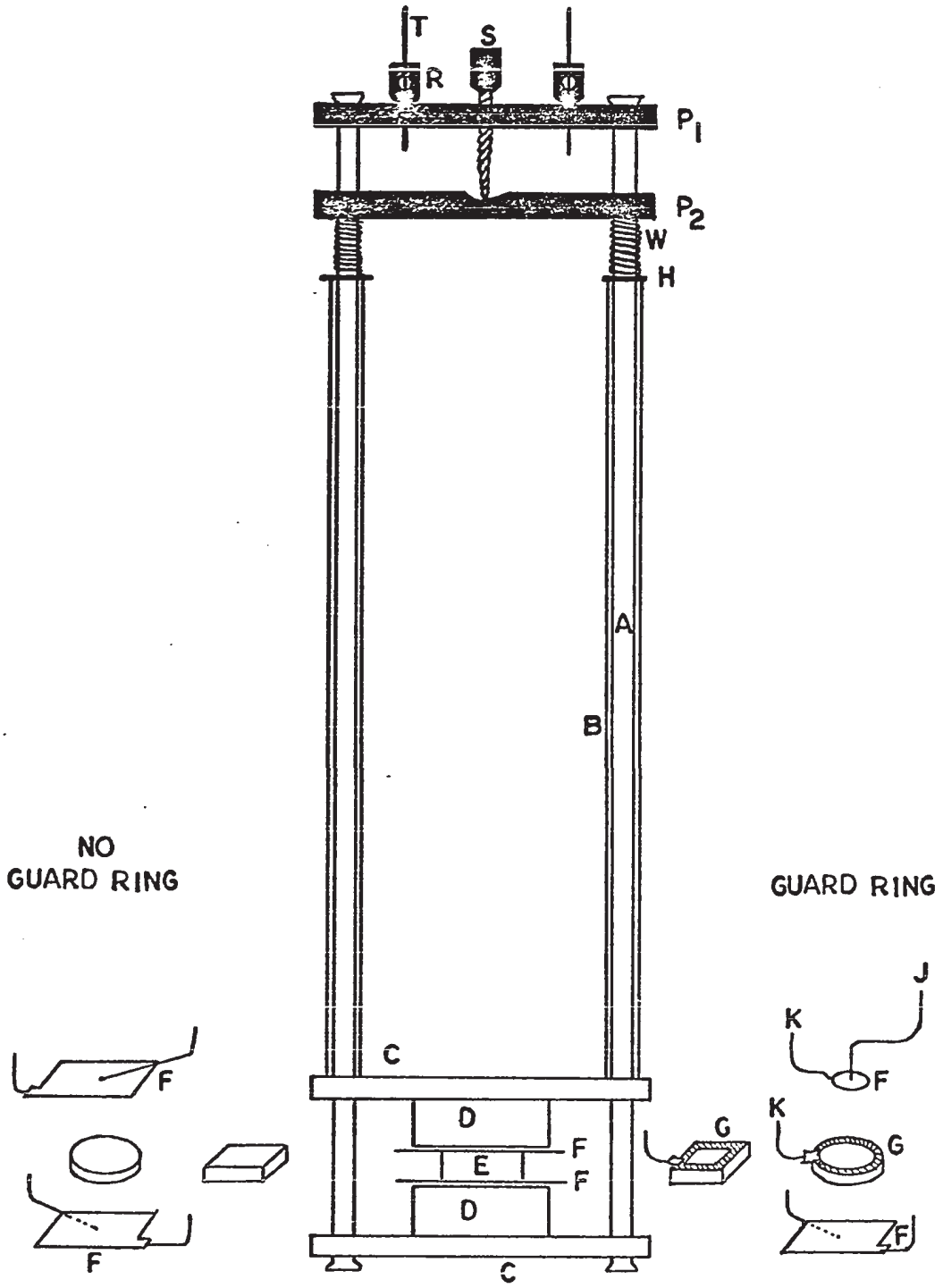

LEGEND FOR FIG. 4

T	tungsten rod
S	screw
R	socket for tungsten rod
P_1,P_2	metal plates
W	tungsten spring
H	washer
A	silica rod
B	silica tubing
C	silica plate
D	alumina discs
E	sample
F	electrode
J	Pt+13%Rh wire
K	Pt wire
G	dag ring

FIG. 5

CONDUCTIVITY CELL

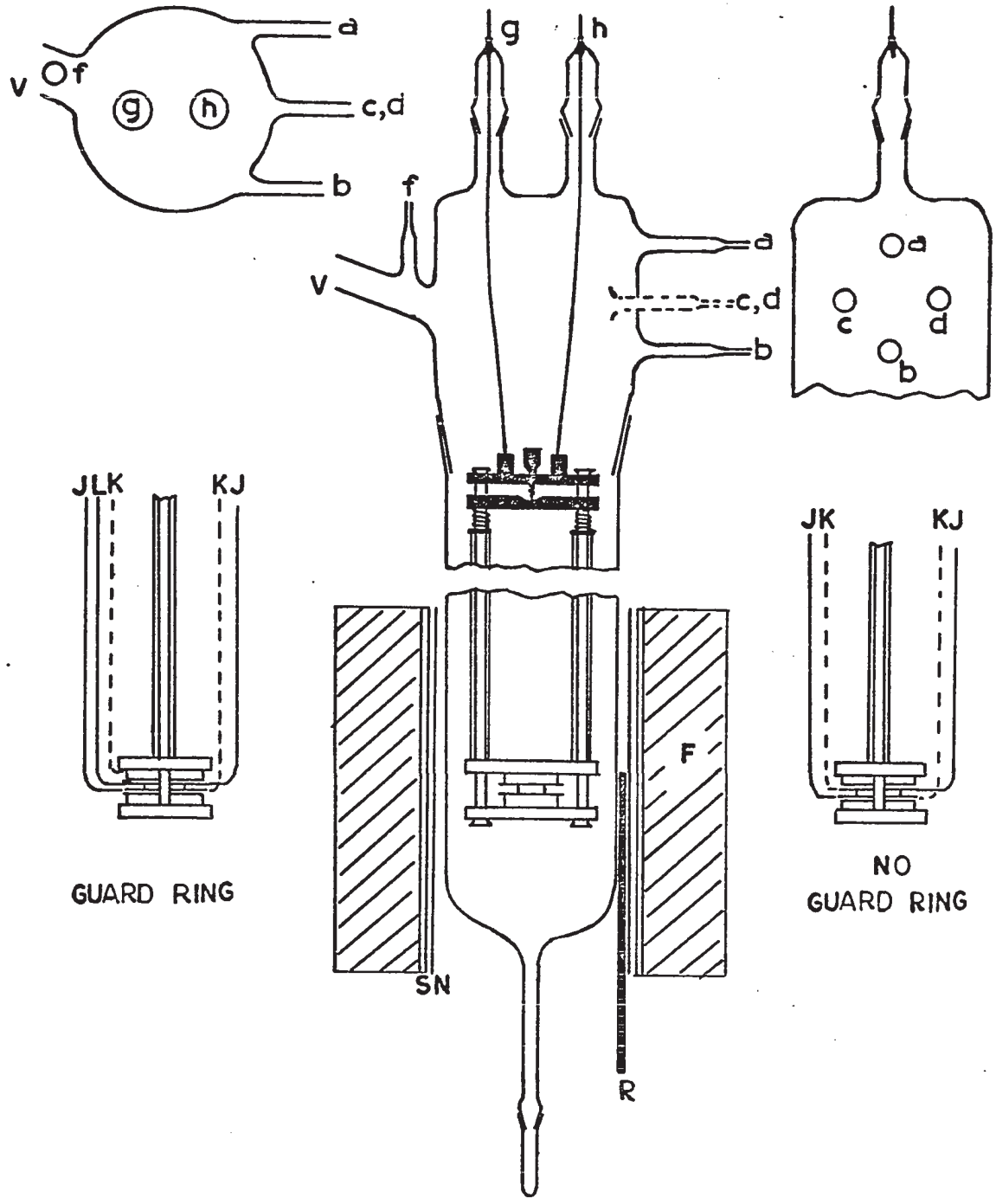

LEGEND FOR FIG. 5

a, b, c, d	thermocouple leads
f	ground lead
g, h	tungsten seals
V	to vacuum line
J	Pt+13%Rh wire
K	Pt wire
L	Pt wire for ground lead
N	nickel shield
S	silica tube
F	furnace
R	Pt resistance sensor

FIG. 6

VACUUM LINE FOR CONDUCTIVITY MEASUREMENT

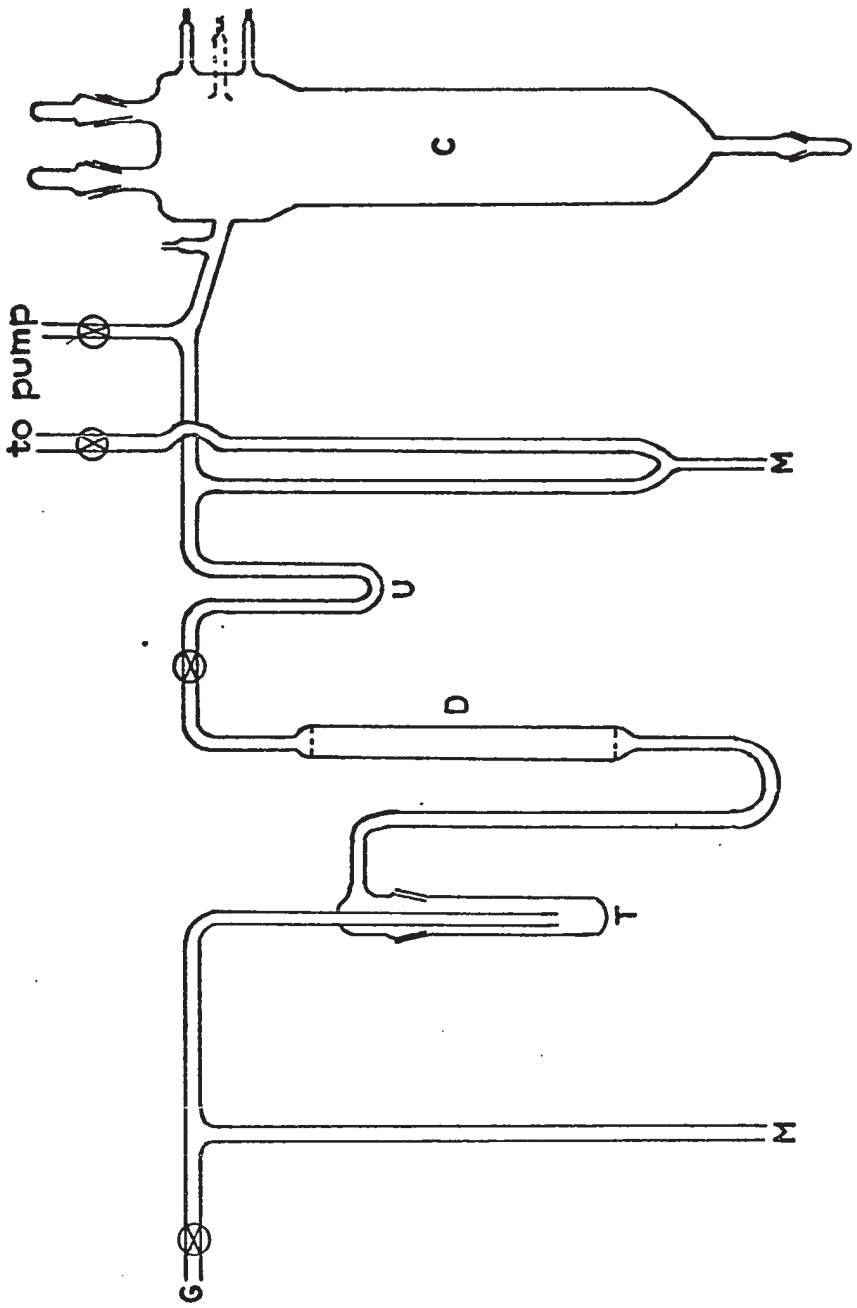

LEGEND FOR FIG. 6

G	gas inlet
M	manometer
T	trap
U	U-trap
D	P_2O_5 column
C	conductivity cell

FIG. 7

α(t) PLOT FOR AP PELLETS AT 222° C

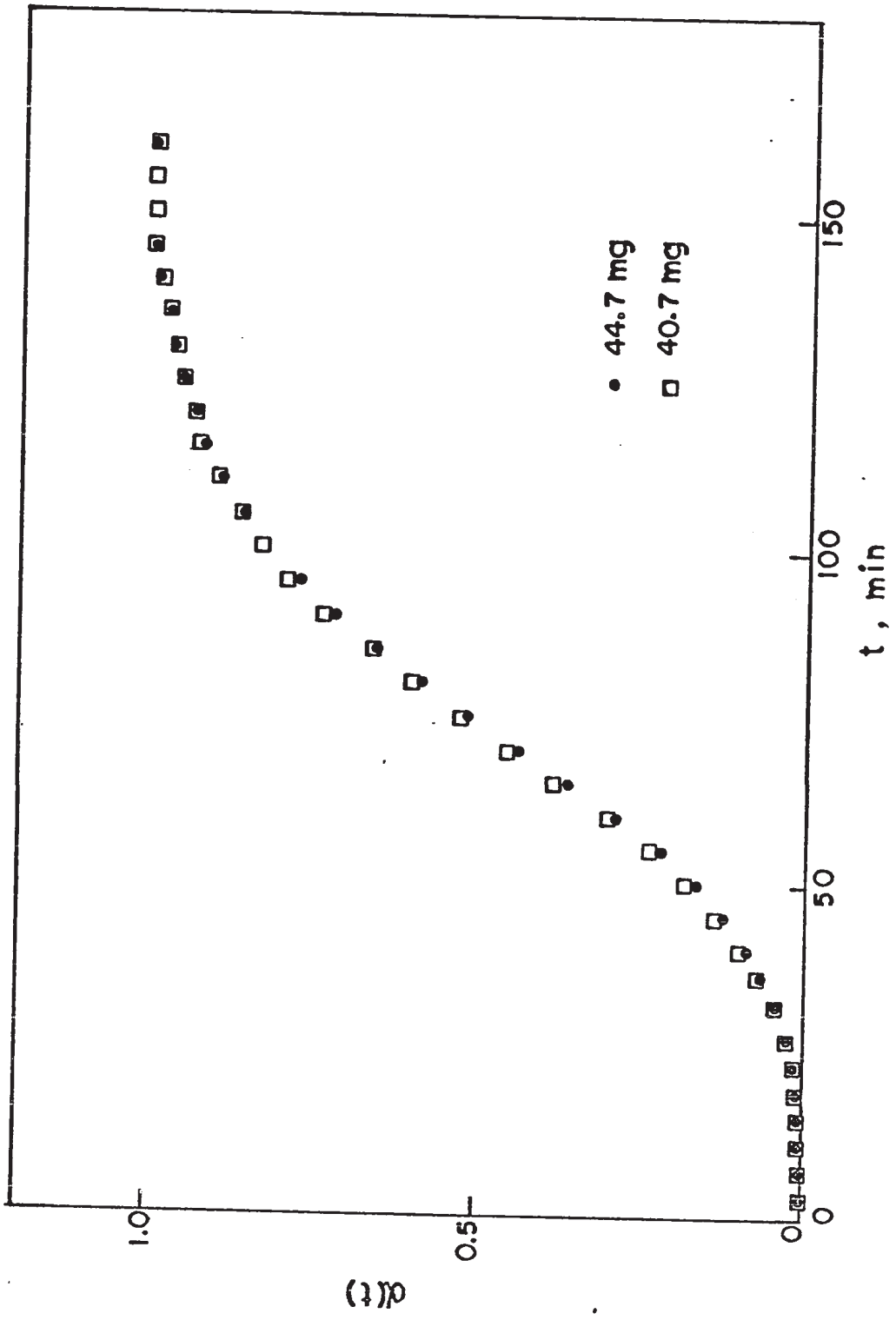

FIG. 8

DECOMPOSITION OF AP PELLETS AT 222°C:
VARIATION IN MASS

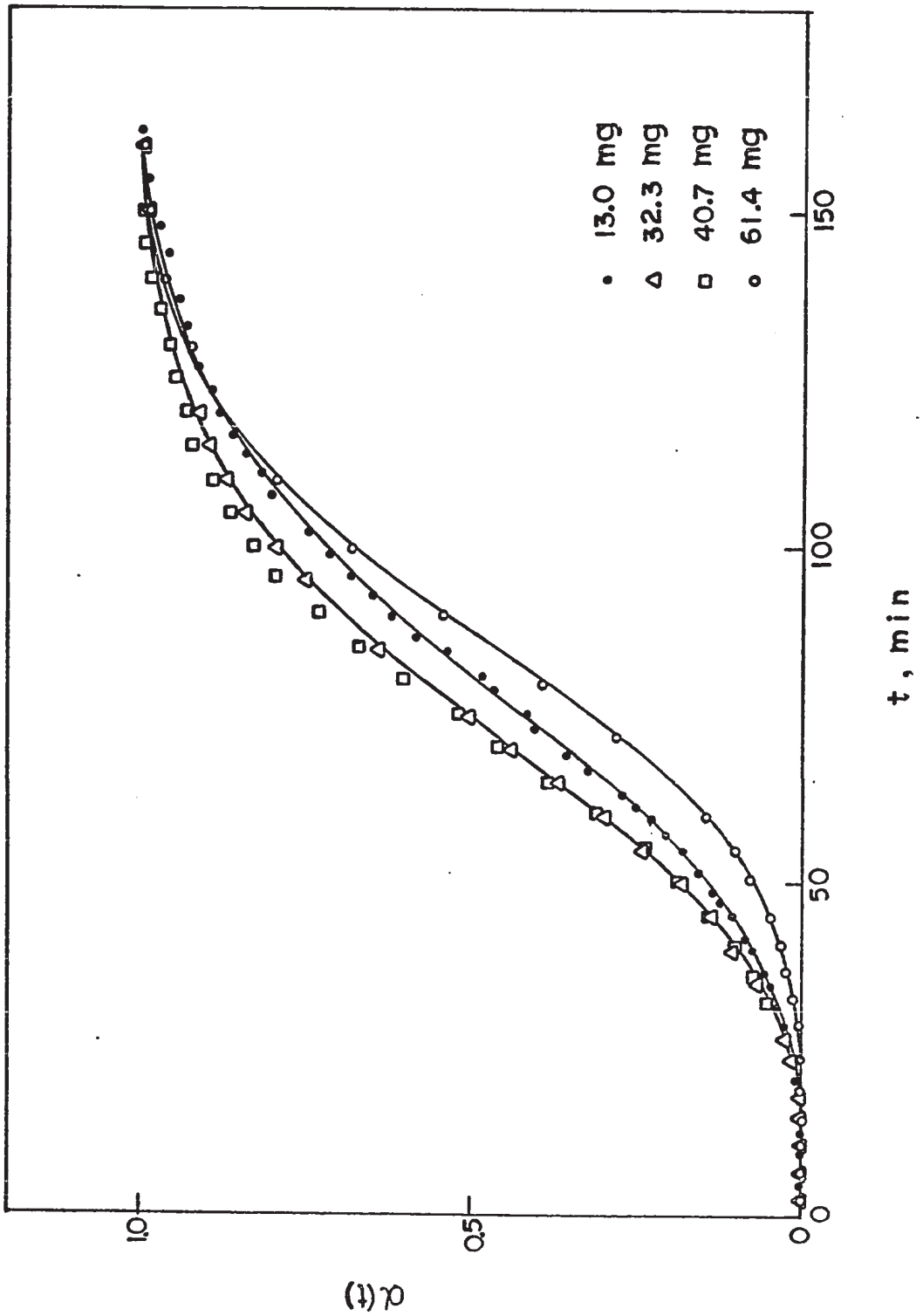

FIG. 9

TEST OF AE KINETICS

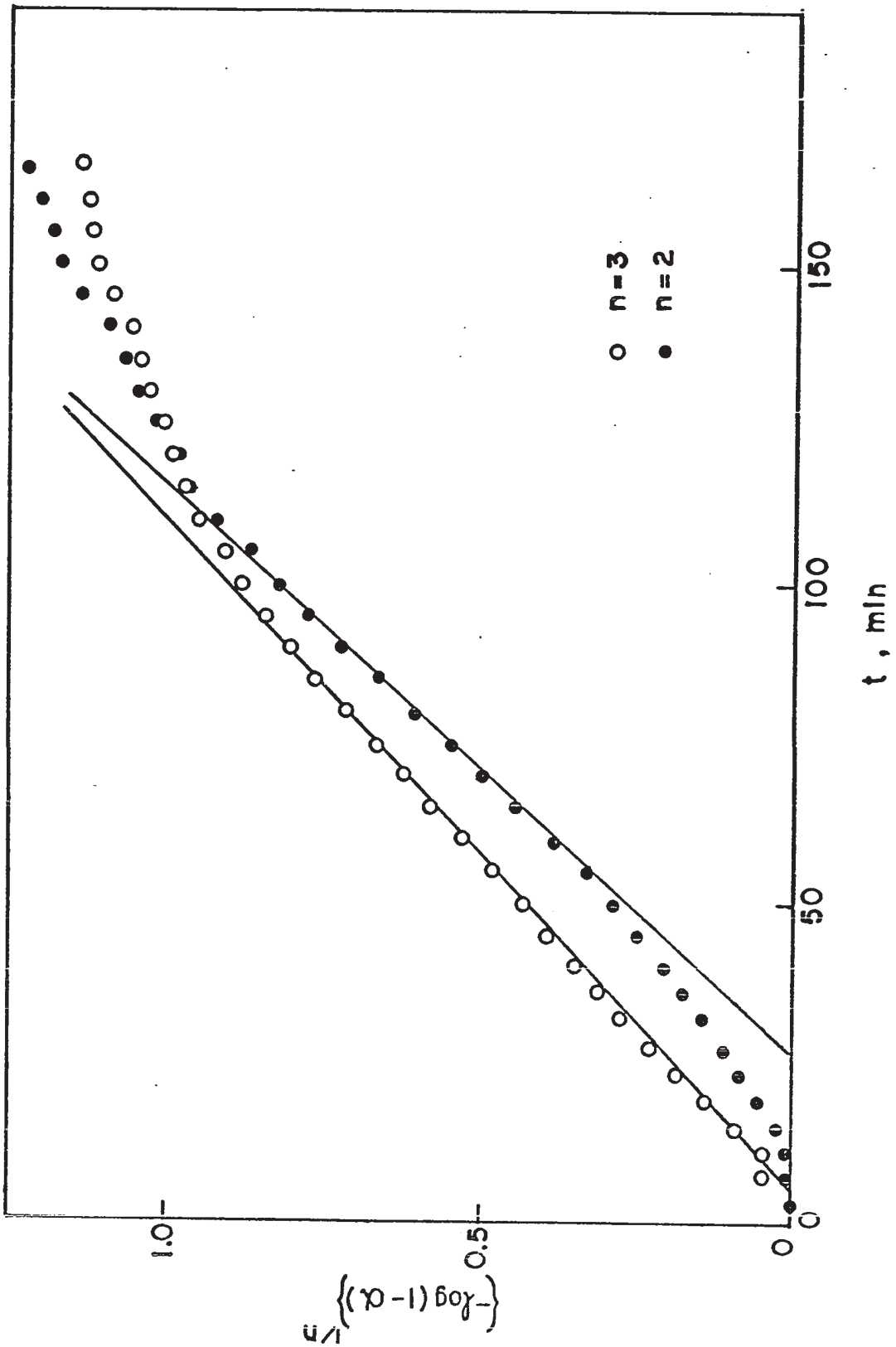

FIG. 10

ARRHENIUS PLOT OF AE RATE CONSTANTS

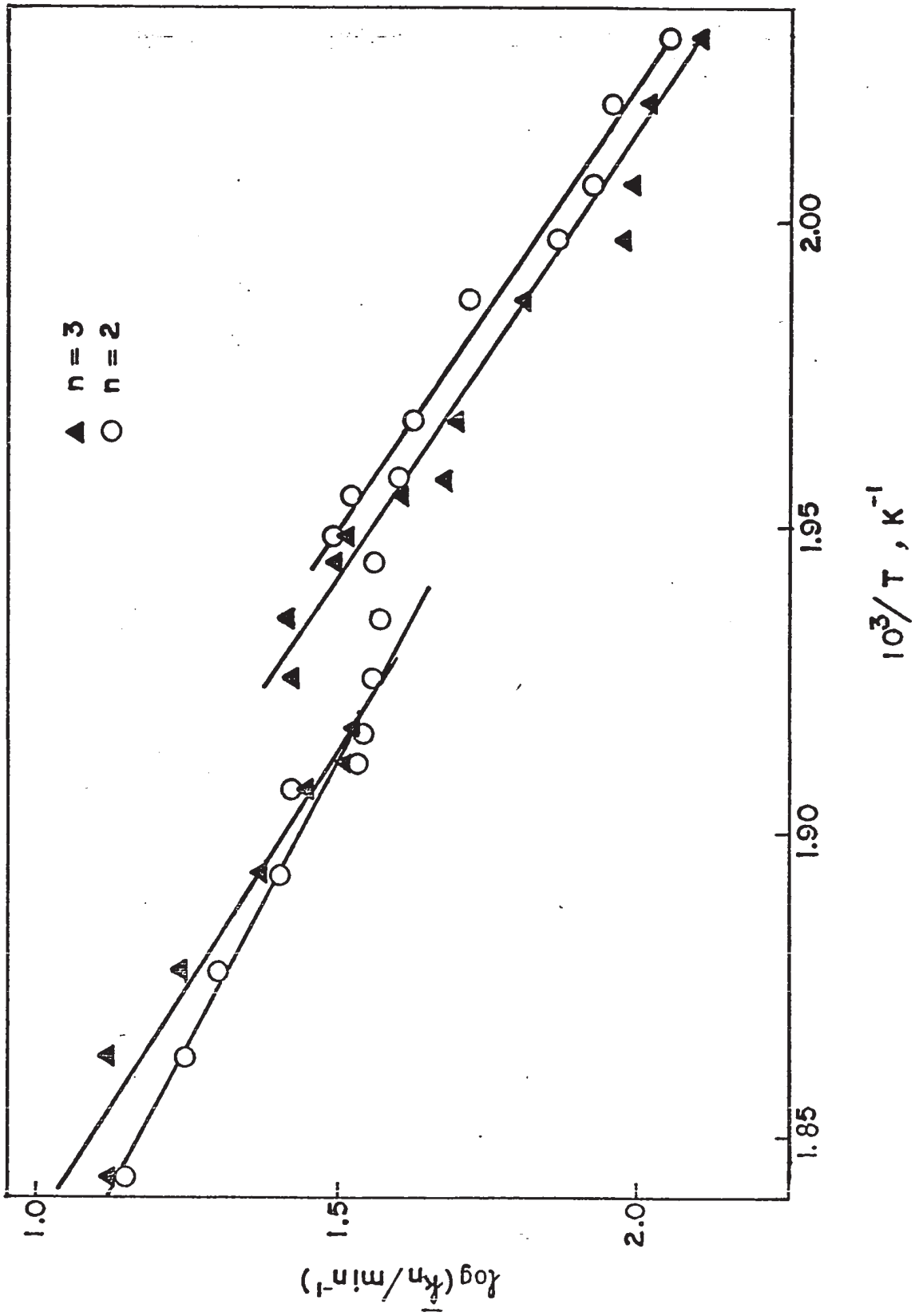

FIG. 11

PLOT OF $\ell n\ P$ VS. t DURING THE INDUCTION PERIOD FOR DECOMPOSITION OF A PURE AP CRYSTAL (BNL)

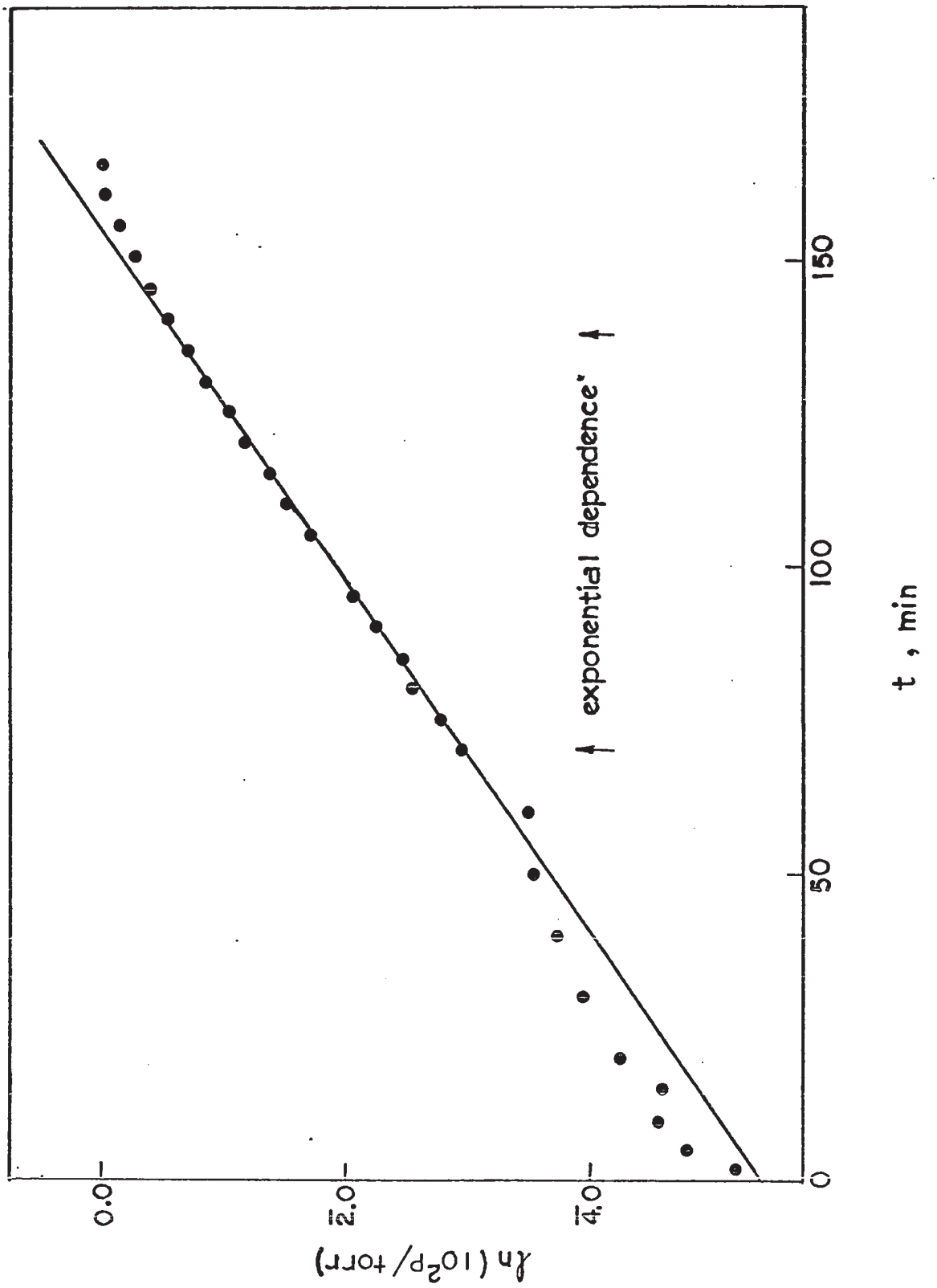

FIG. 12

PLOT OF FRACTIONAL DECOMPOSITION $\alpha(t)$
DURING INDUCTION PERIOD

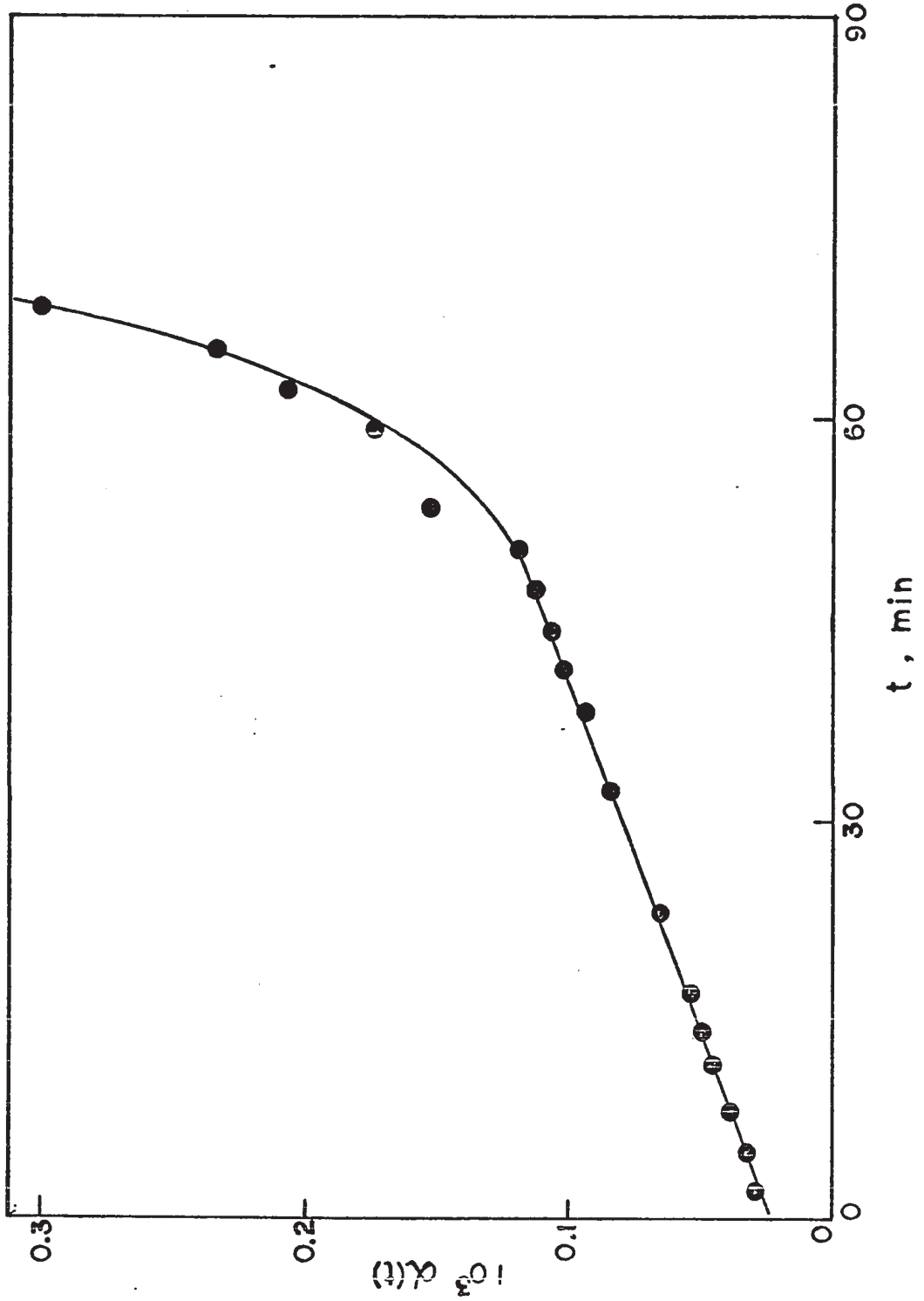

FIG. 13

$\alpha(t)$ PLOTS AT 230°C

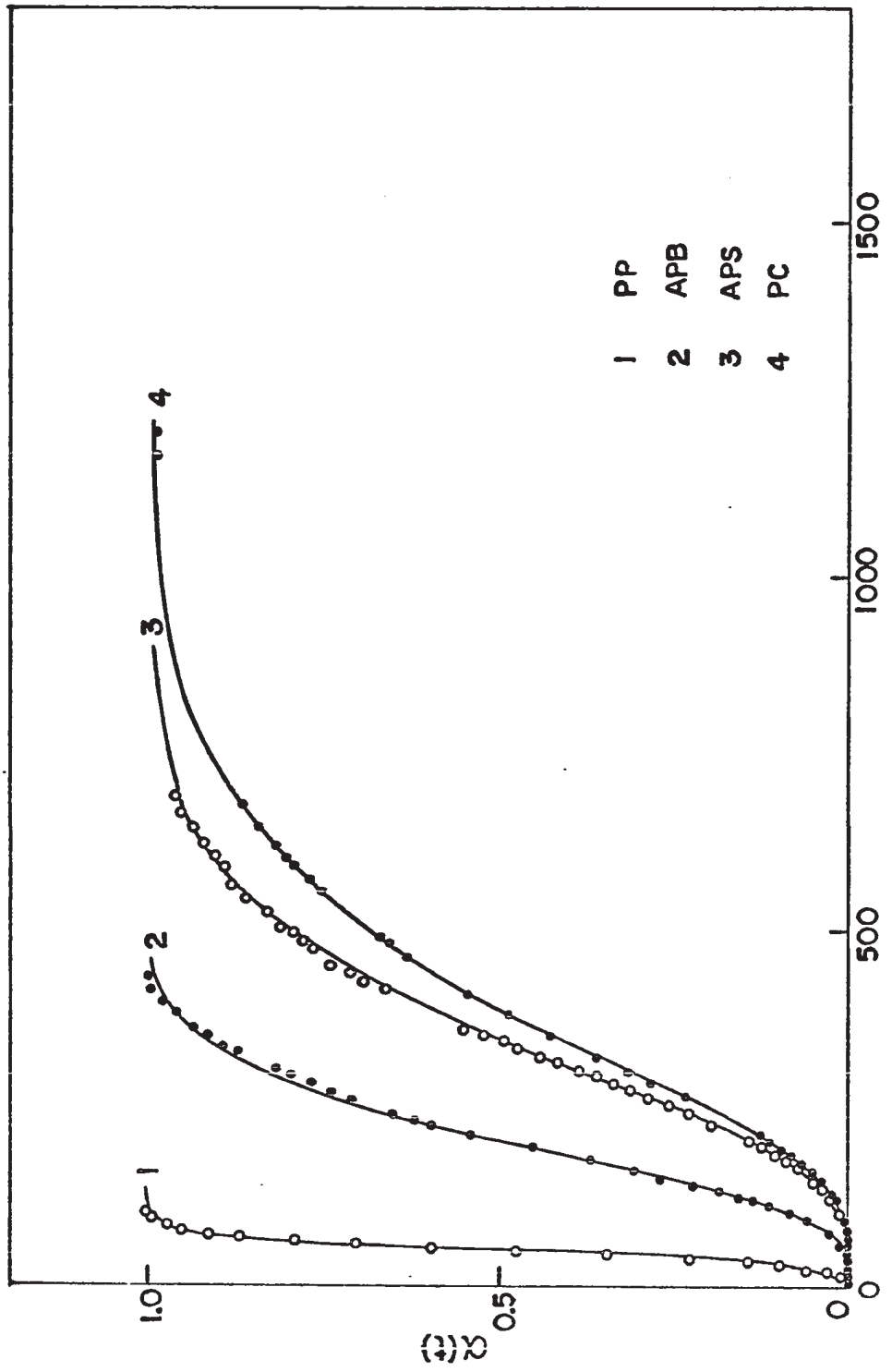

FIG. 14

LEAST-SQUARES FITTING DURING AVRAMI PROCESS
FOR A SINGLE CRYSTAL OF AP

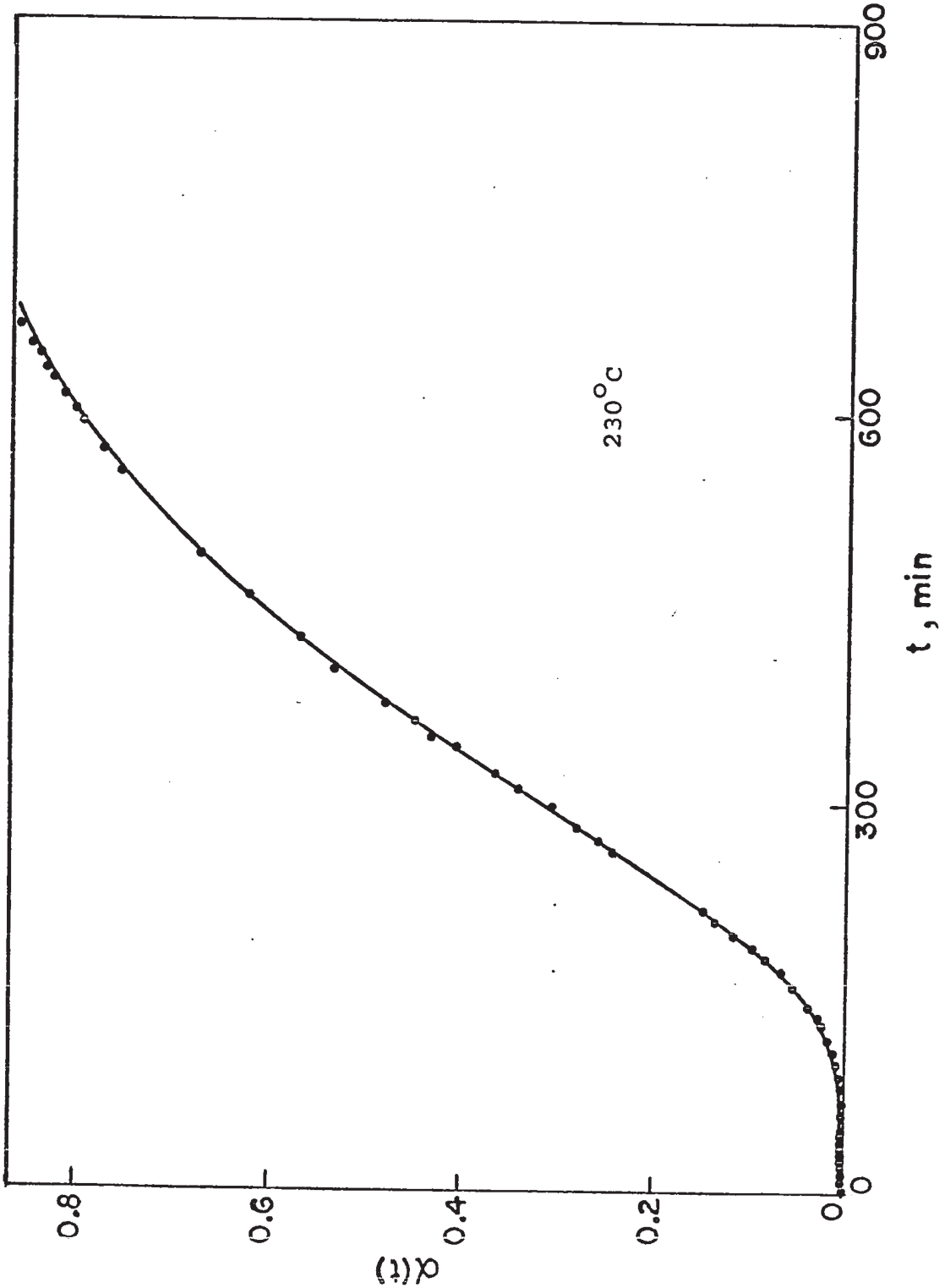

FIG. 15

LEAST-SQUARES FIT OVER THE INDUCTION PERIOD IN FIG. 14

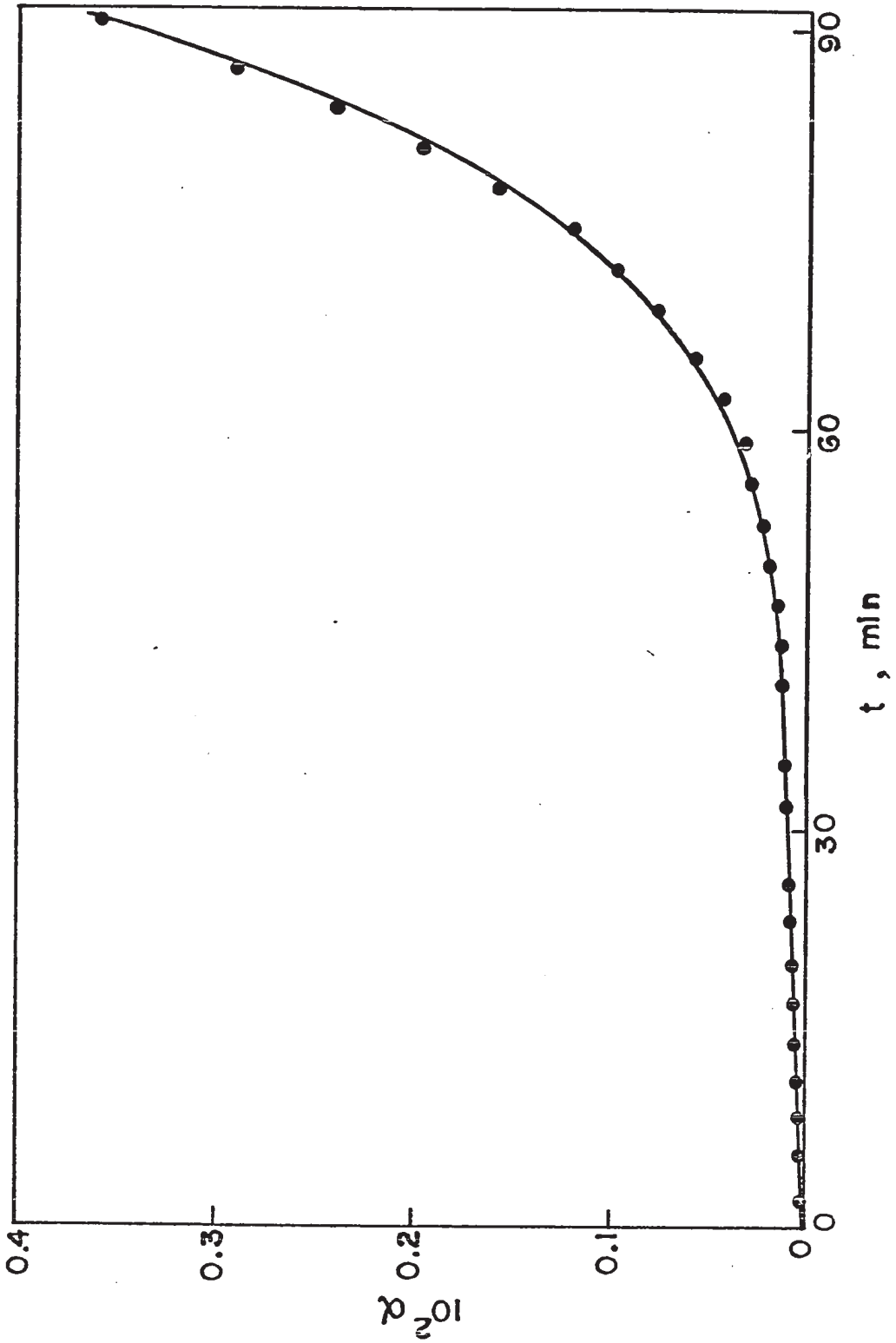

FIG 16

LEAST-SQUARE FIT OVER THE BEGINNING PART OF THE INDUCTION PERIOD IN FIG. 15 ON A LARGER SCALE

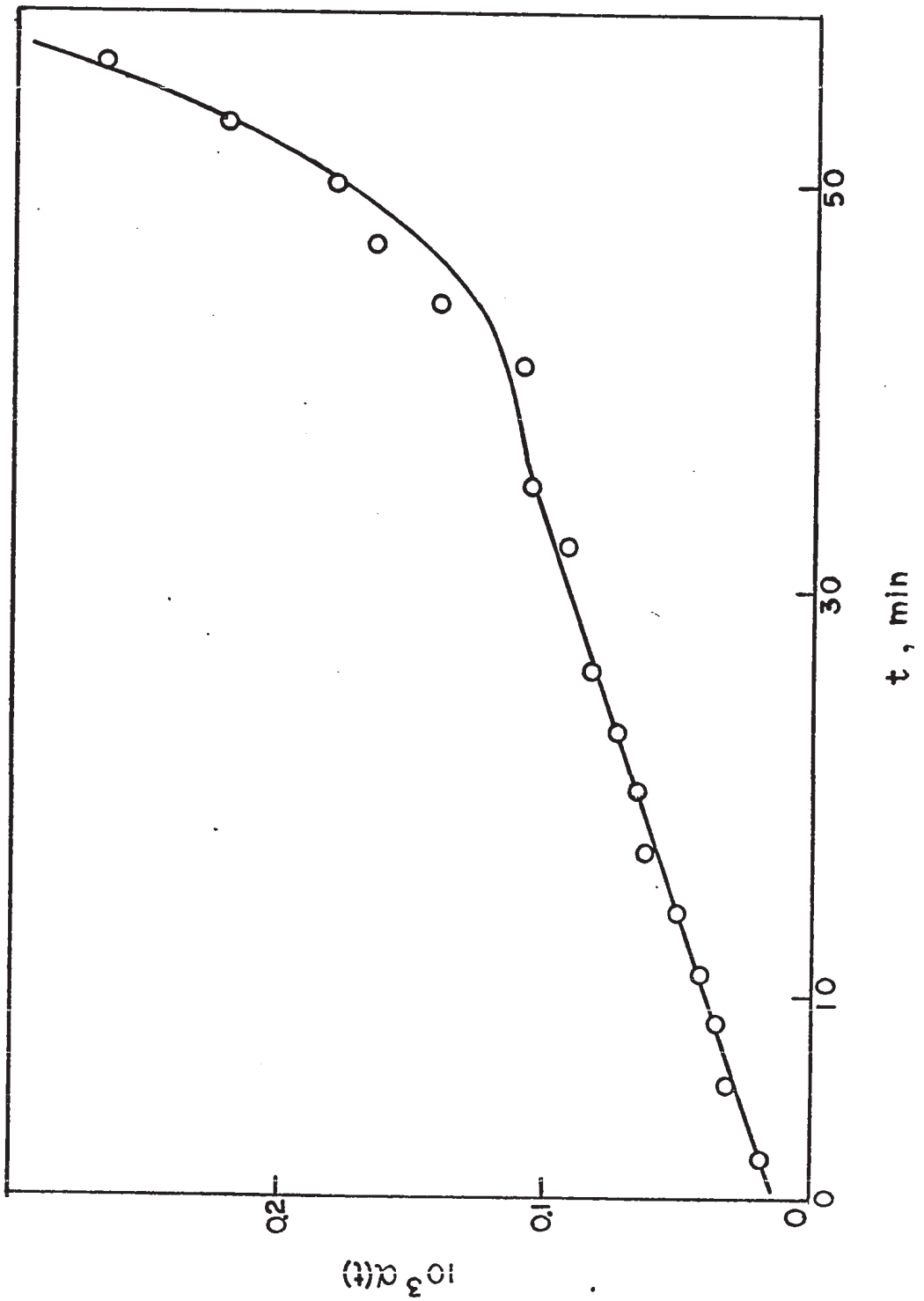

FIG. 17

ARRHENIUS PLOT FOR THE DURATION OF THE LINEAR PROCESS IN AP PELLETS

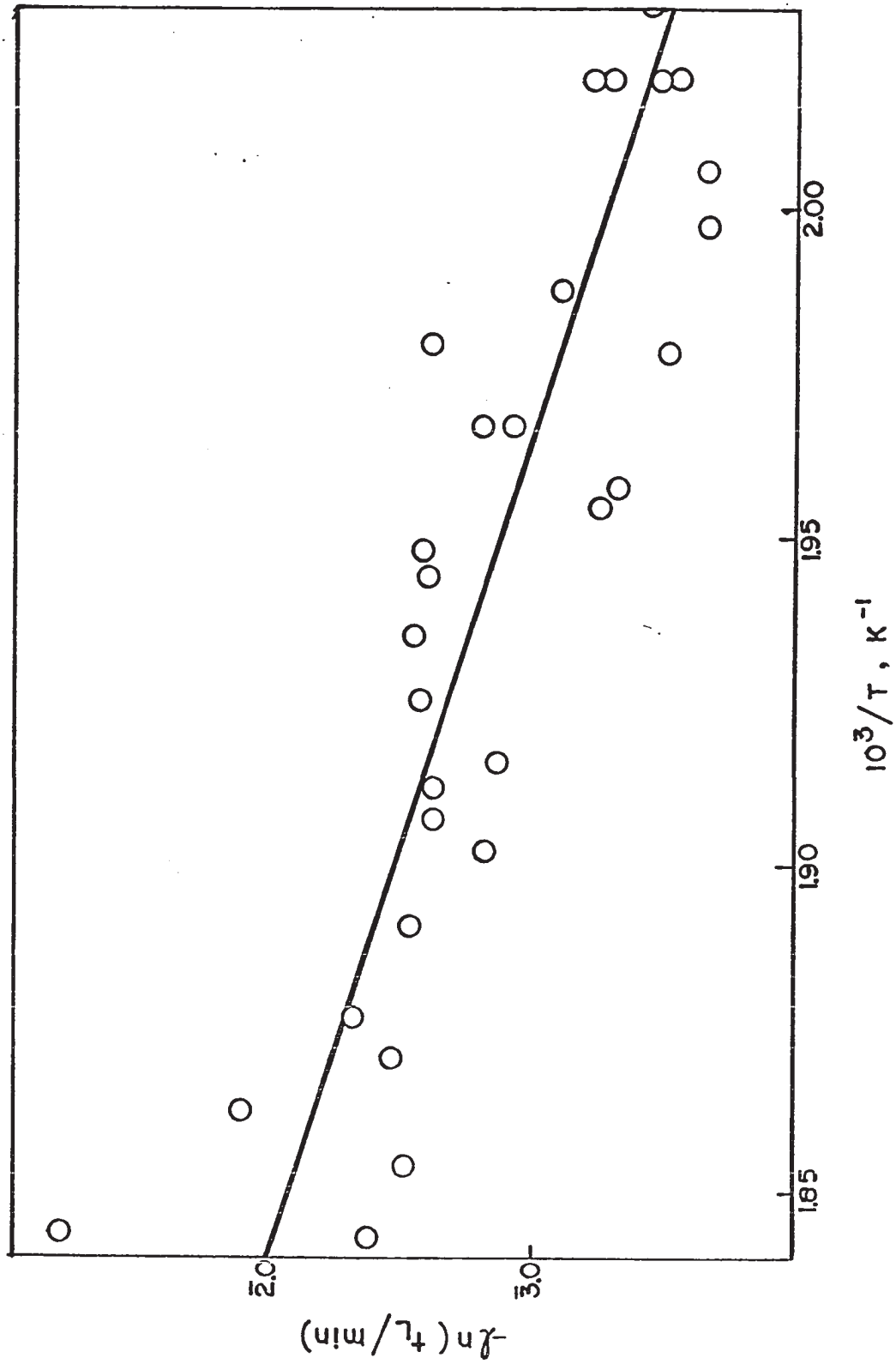

FIG. 18

ARRHENIUS PLOT FOR THE DURATION OF THE LINEAR PROCESS IN PURE CRYSTALS OF AP

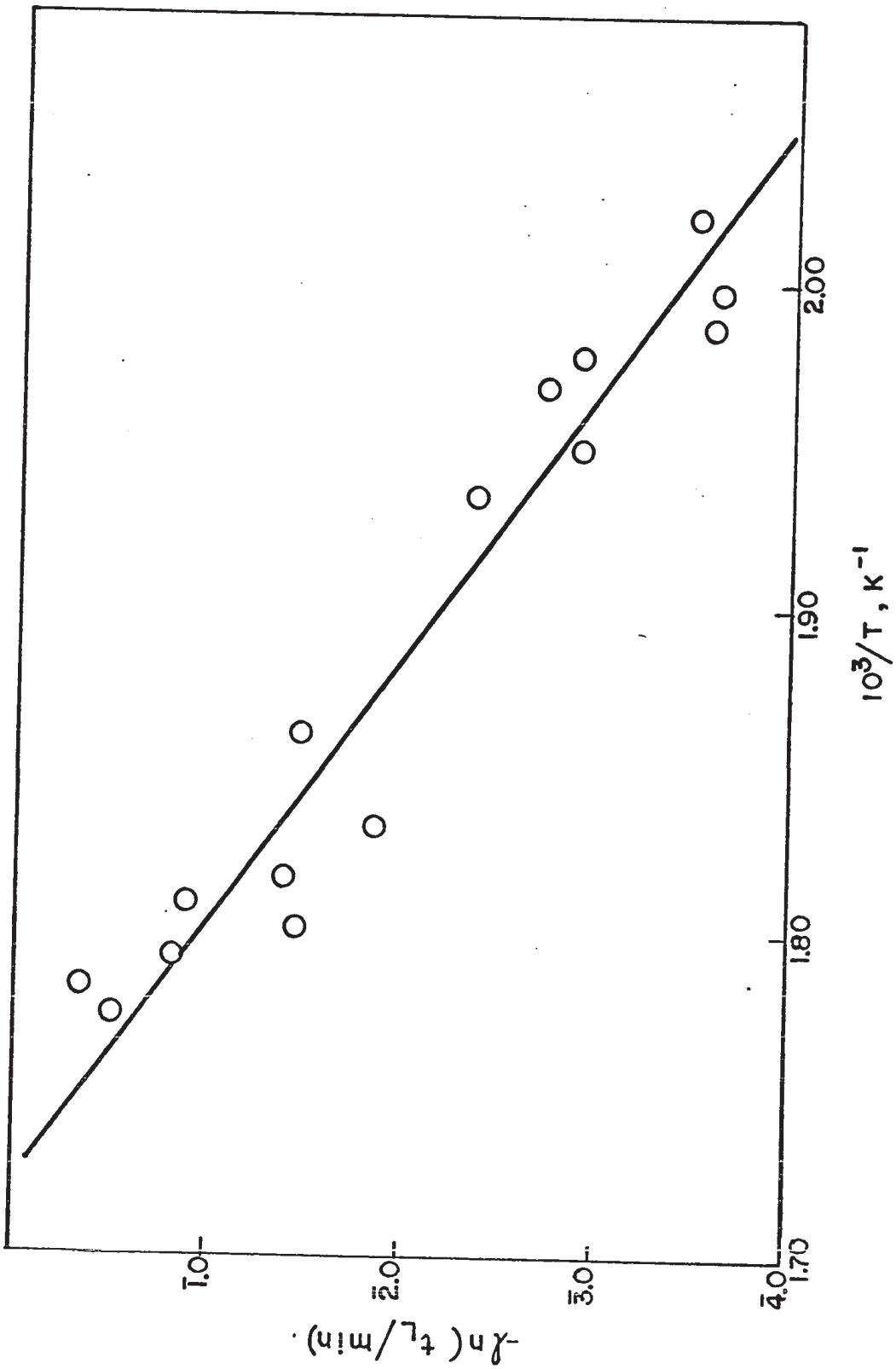

FIG. 19

ARRHENIUS PLOT FOR THE DURATION OF THE LINEAR PROCESS IN Ba^{2+}-DOPED AP CRYSTALS

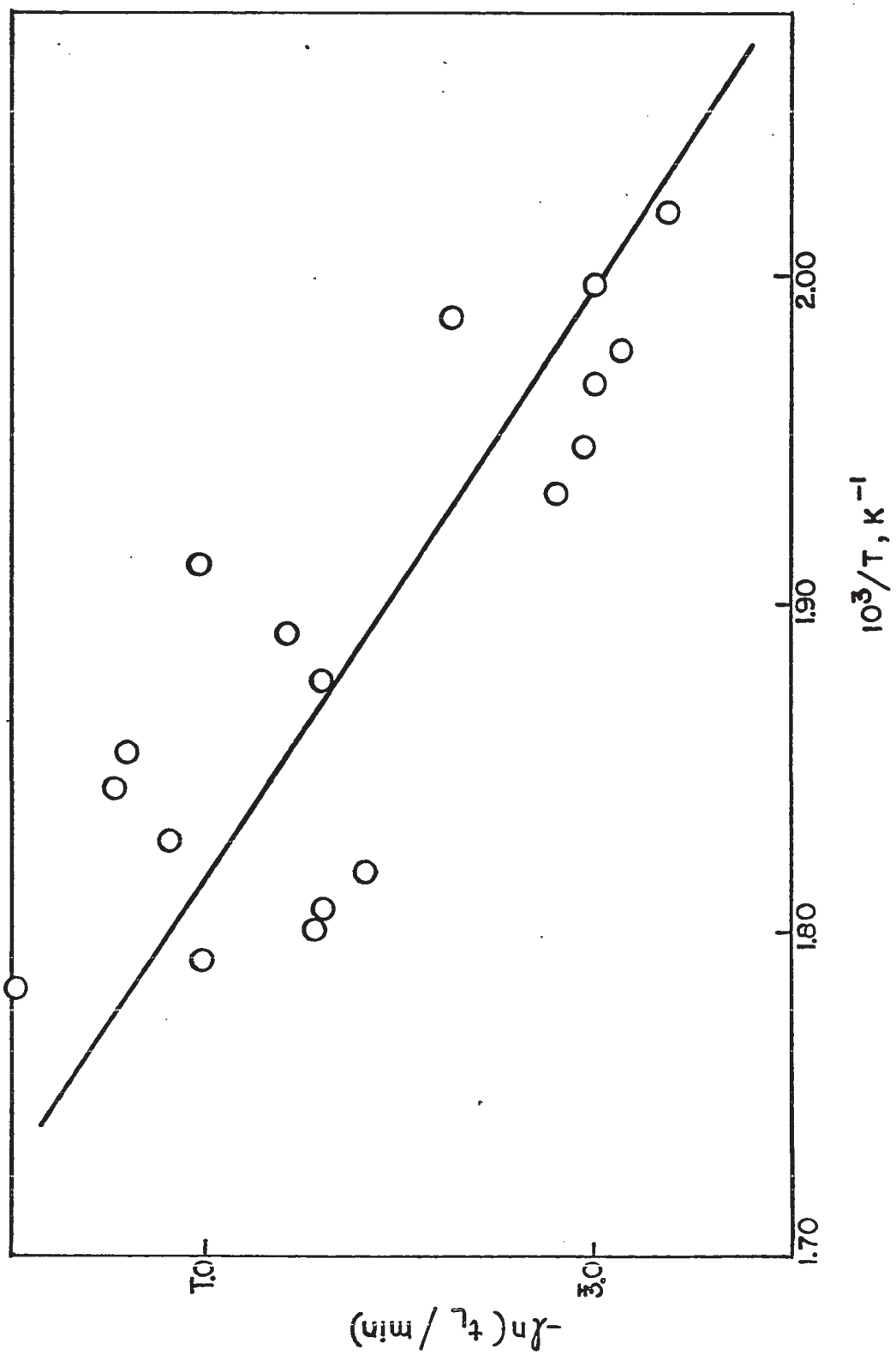

FIG. 20

ARRHENIUS PLOT FOR THE DURATION OF THE LINEAR PROCESS IN SO_4^{2-}-DOPED AP CRYSTALS

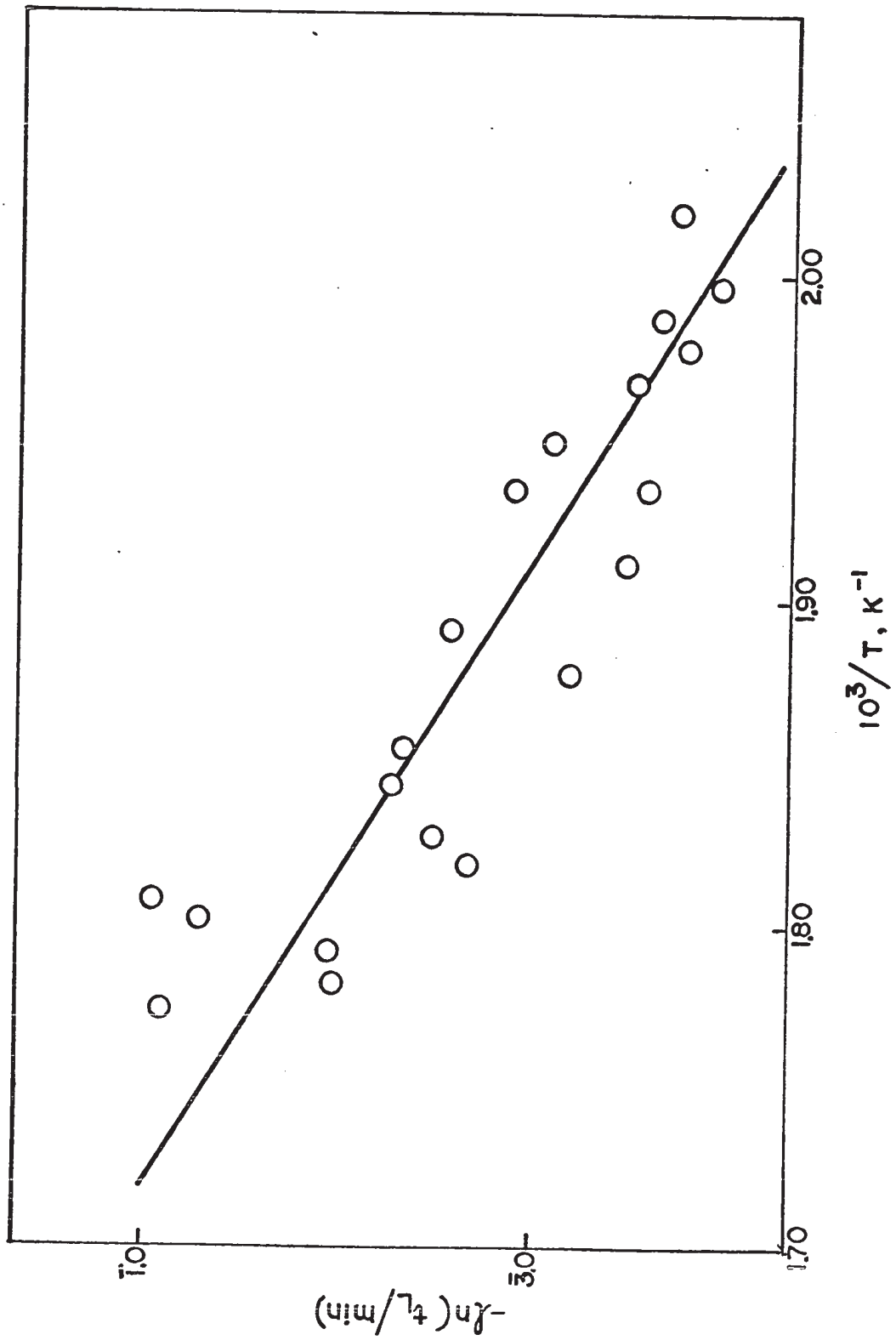

FIG. 21

ARRHENIUS PLOTS FOR THE RATE CONSTANTS FOR AP PELLETS

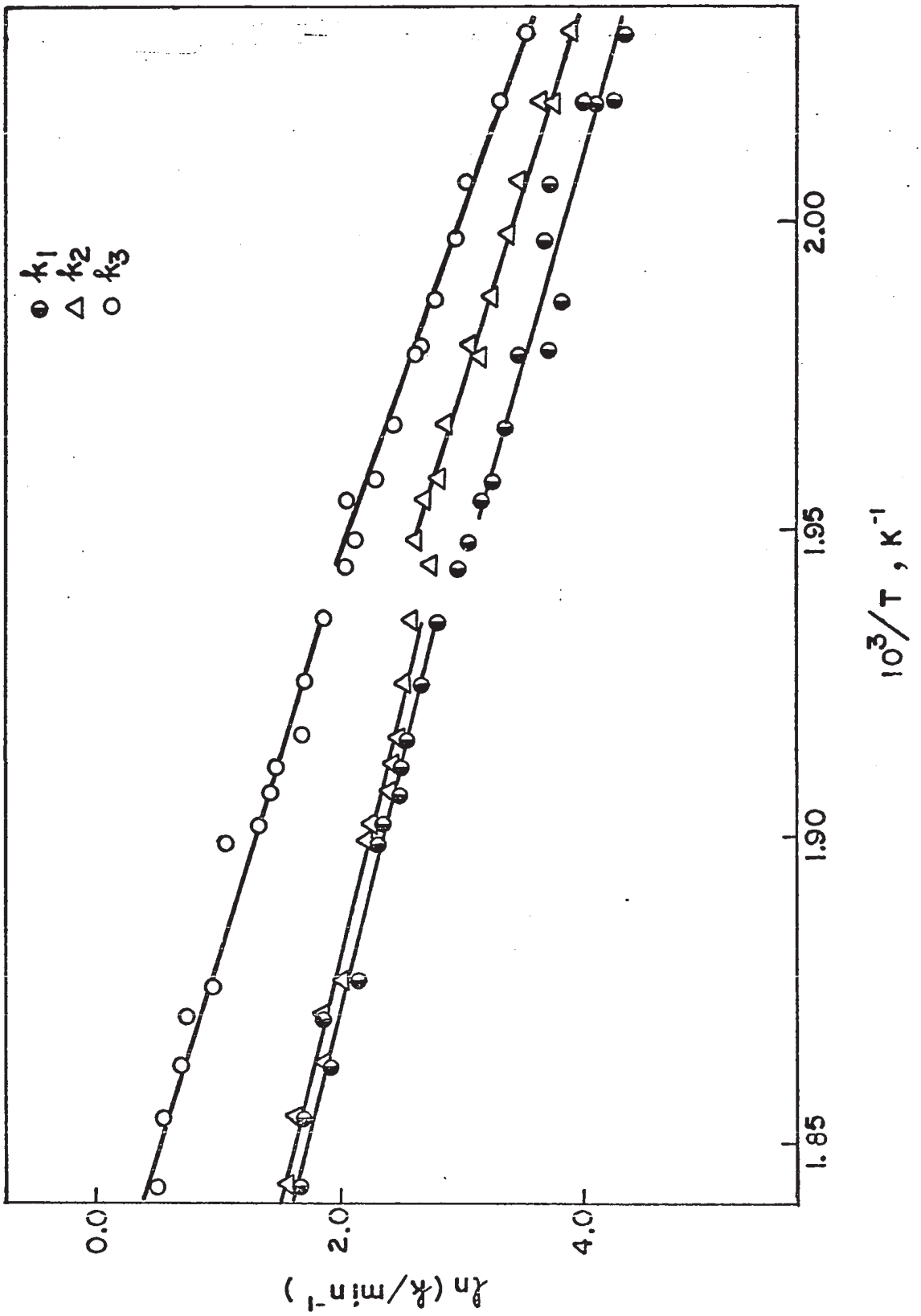

FIG. 22

ARRHENIUS PLOT FOR THE RATE CONSTANTS FOR BNL CRYSTALS

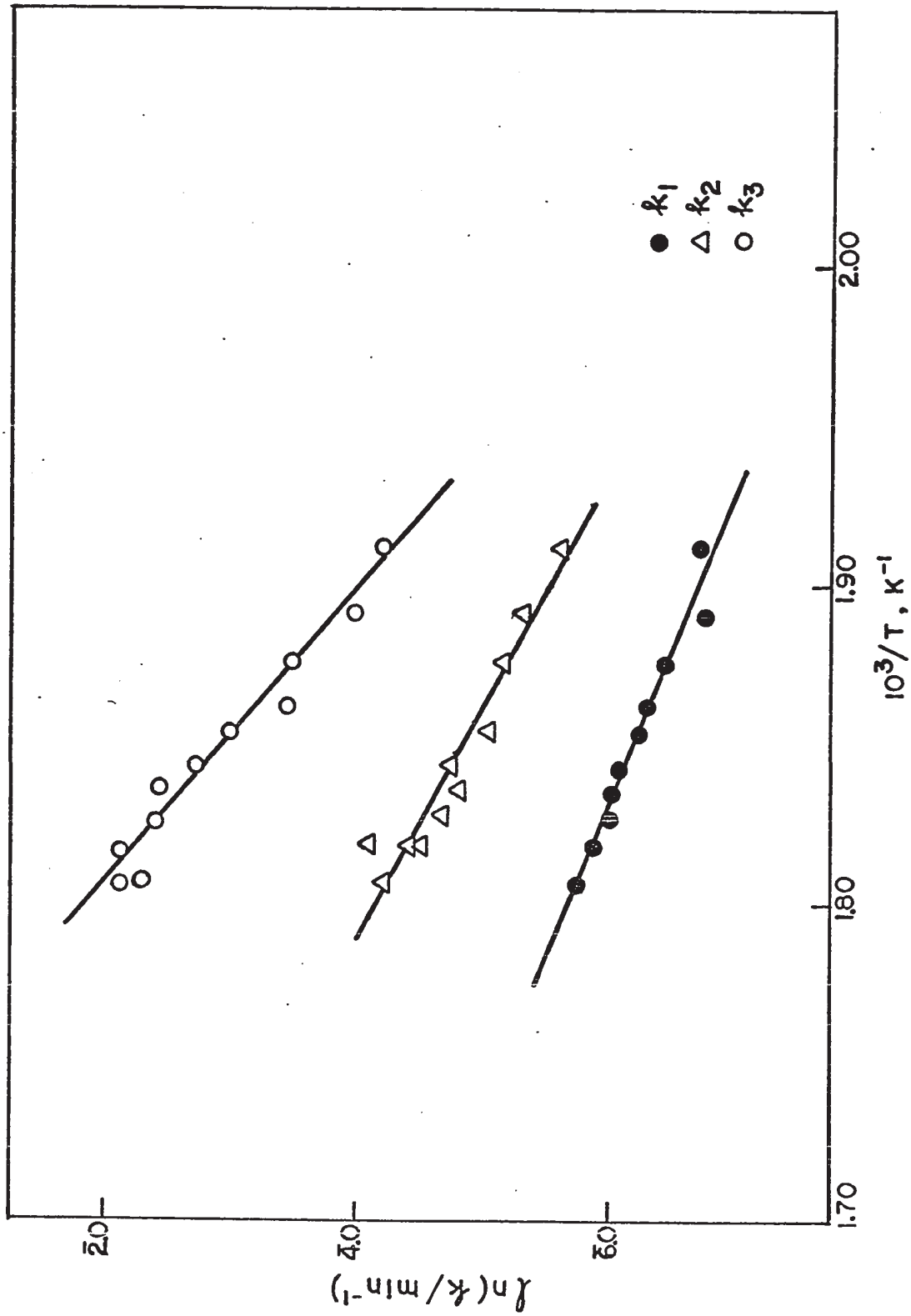

FIG. 23

ARRHENIUS PLOT FOR THE RATE CONSTANTS FOR CRYSTALS OF PURE AP

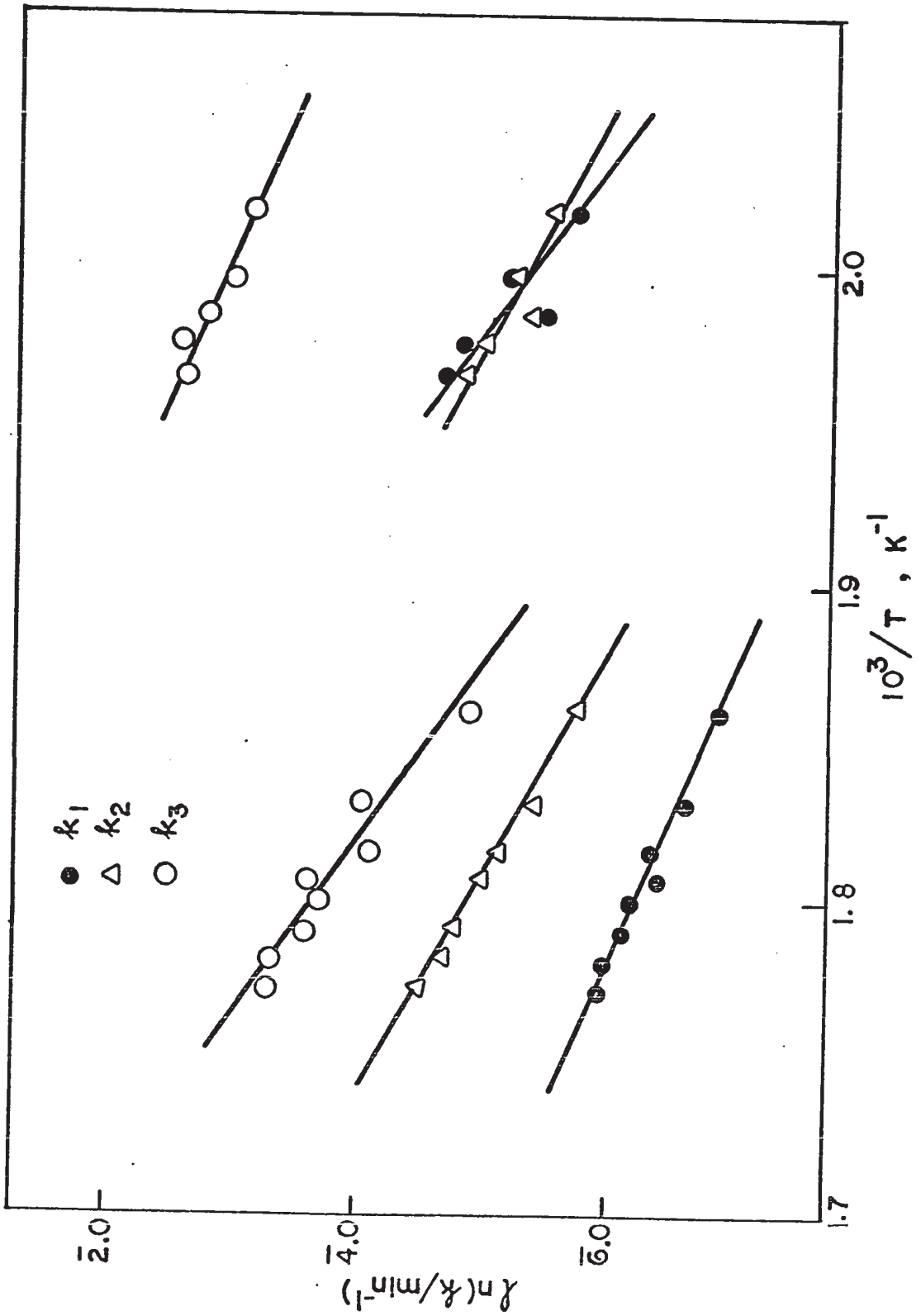

FIG. 24

ARRHENIUS PLOT FOR RATE CONSTANTS FOR CRYSTALS OF Ba^{2+}-DOPED AP

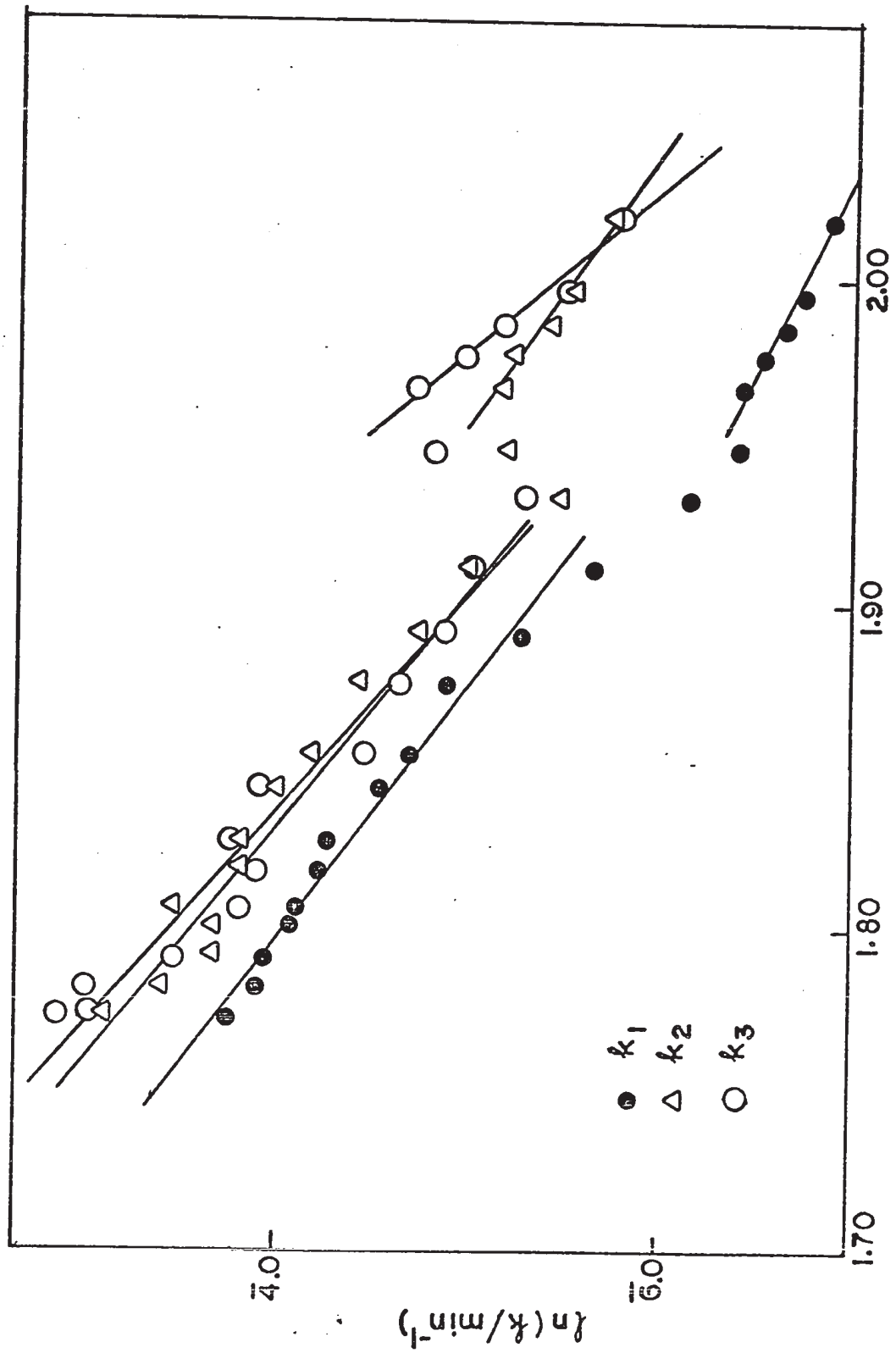

FIG. 25

ARRHENIUS PLOT FOR RATE CONSTANTS FOR SO_4^{2-} - DOPED AP CRYSTALS

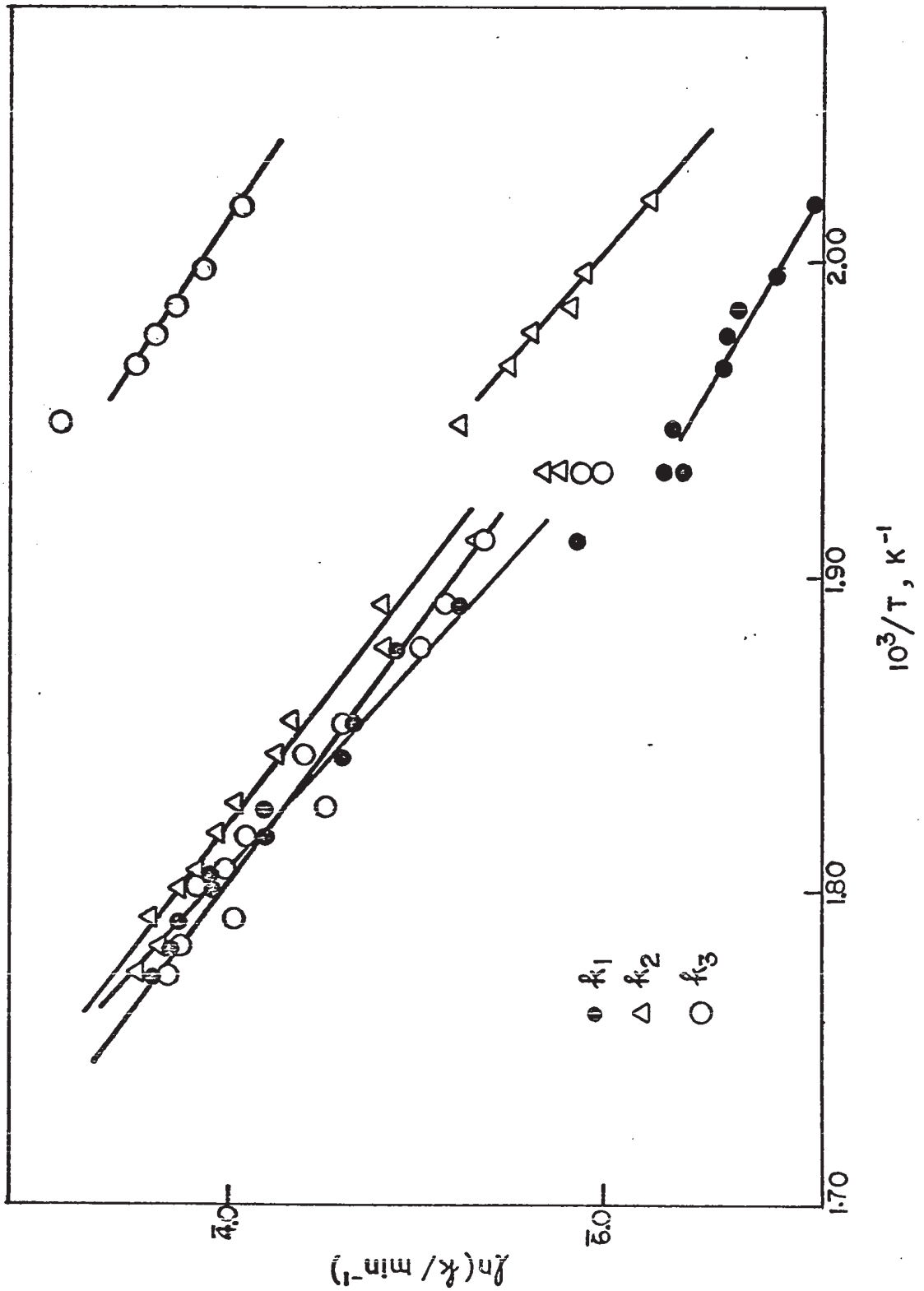

FIG. 26

CONDUCTIVITY OF AN AP PELLET :
SUCCESSIVE RUNS WERE IN THE ORDER 1,2,3,4,5

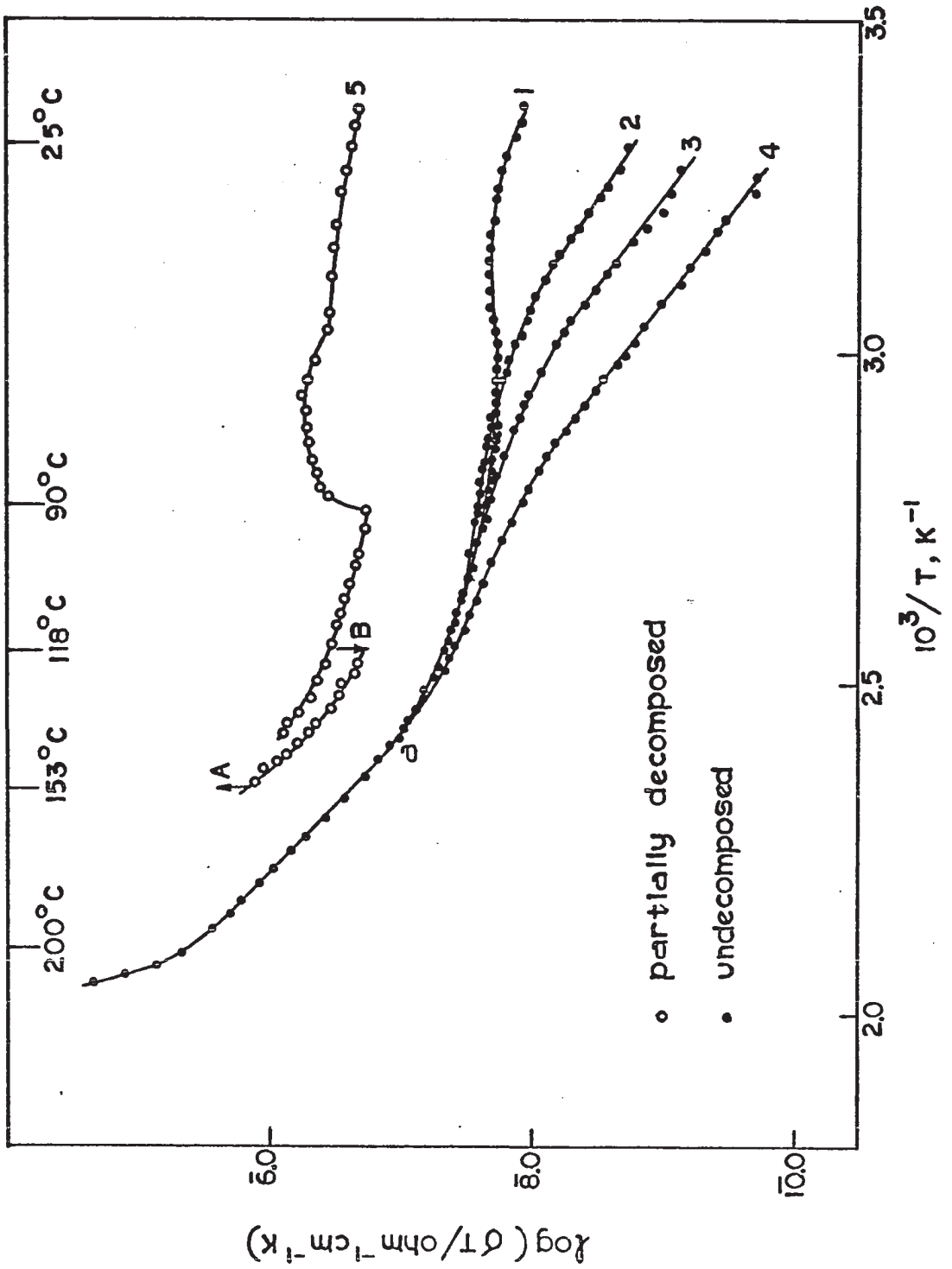

FIG. 27

CONDUCTIVITY PLOT OF PELLET AFTER 5 DAYS ANNEALING AT 120°C

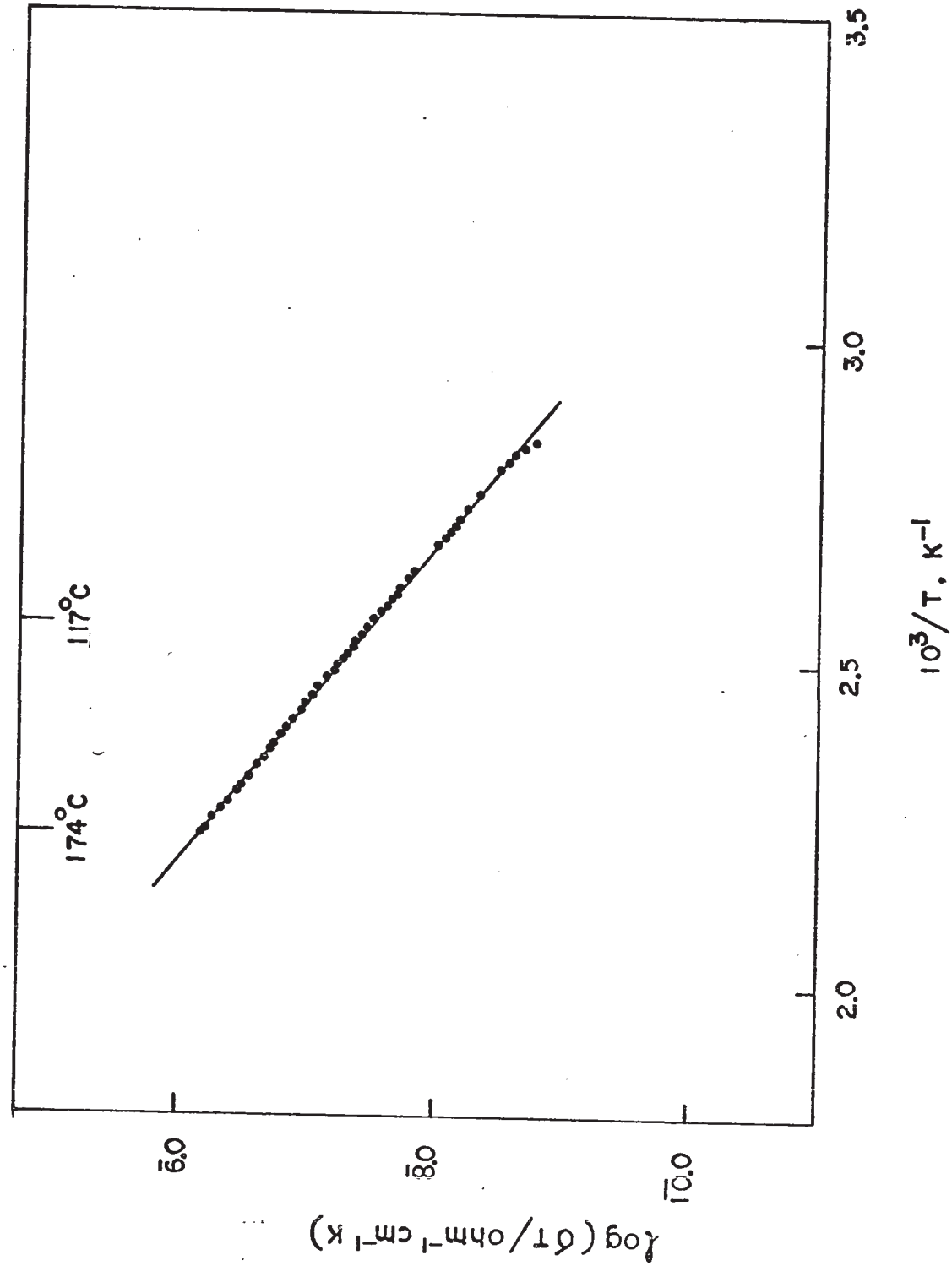

FIG. 28

EFFECT OF ONE DROP OF $HClO_4 \cdot H_2O$ ON THE CONDUCTIVITY OF AN AP PELLET

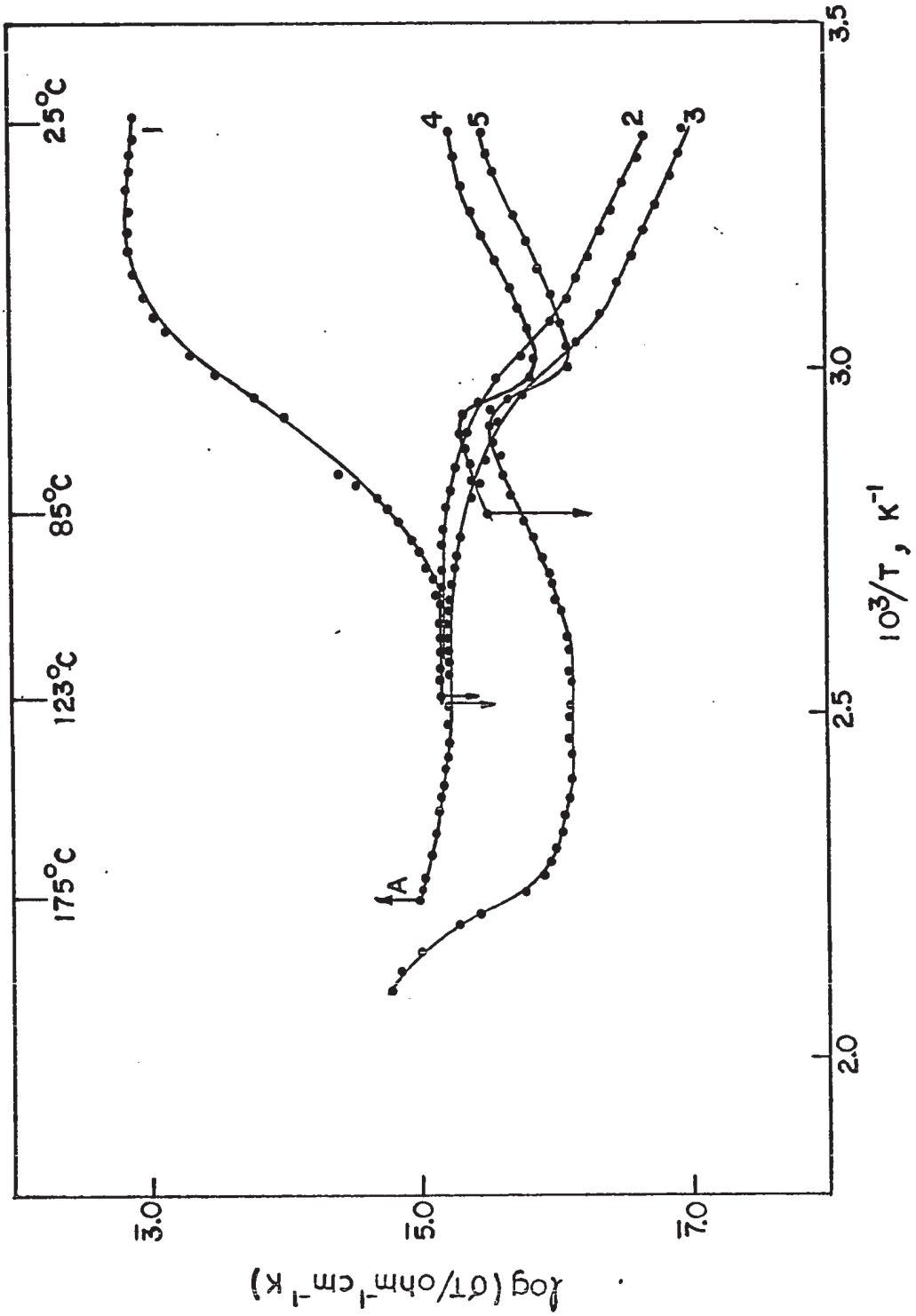

FIG. 29

EFFECT OF N_2 SATURATED WITH H_2O ON THE CONDUCTIVITY OF AN AP PELLET

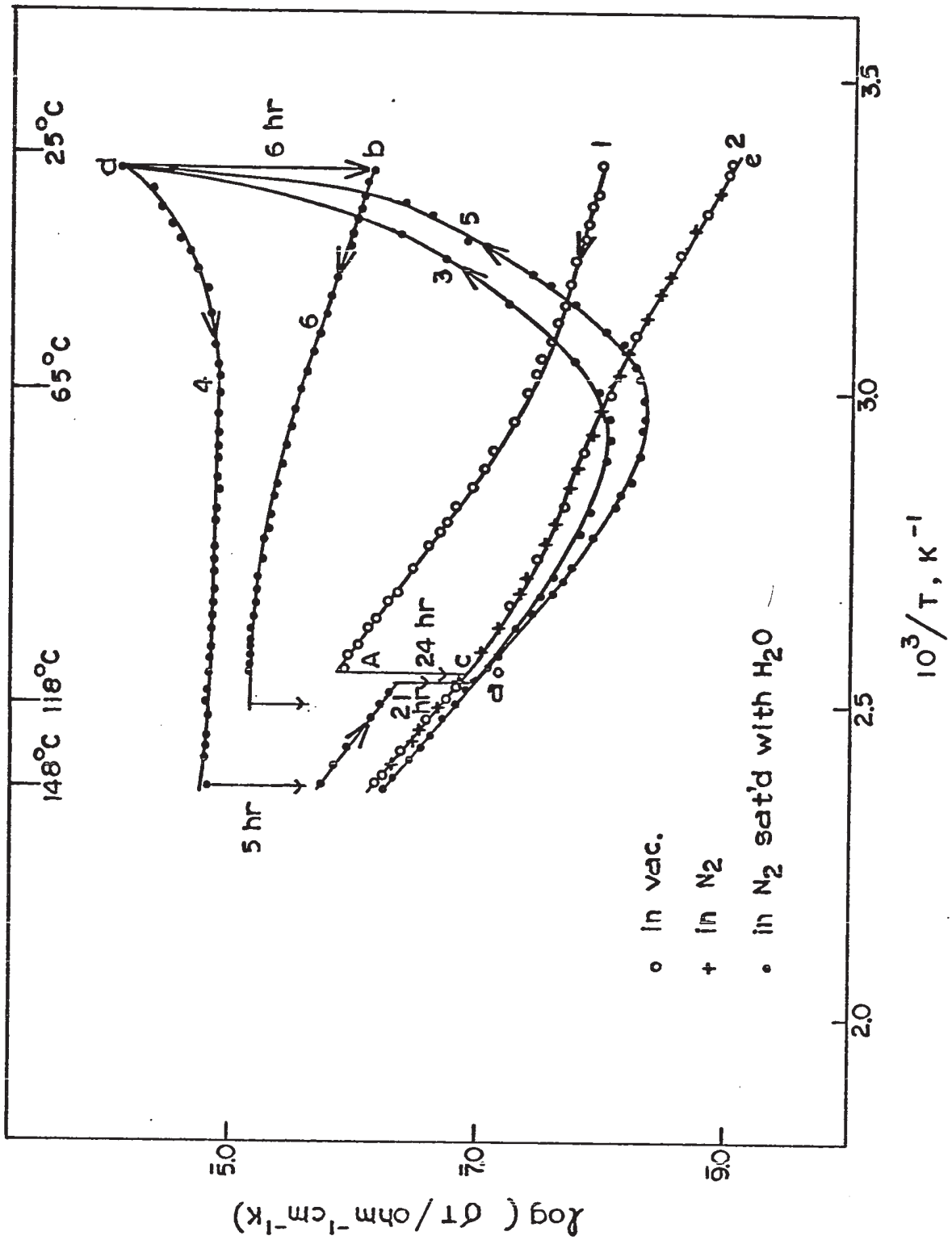

FIG. 30

EFFECT OF 760 TORR OF NH_3 ON THE CONDUCTIVITY OF PELLET AP

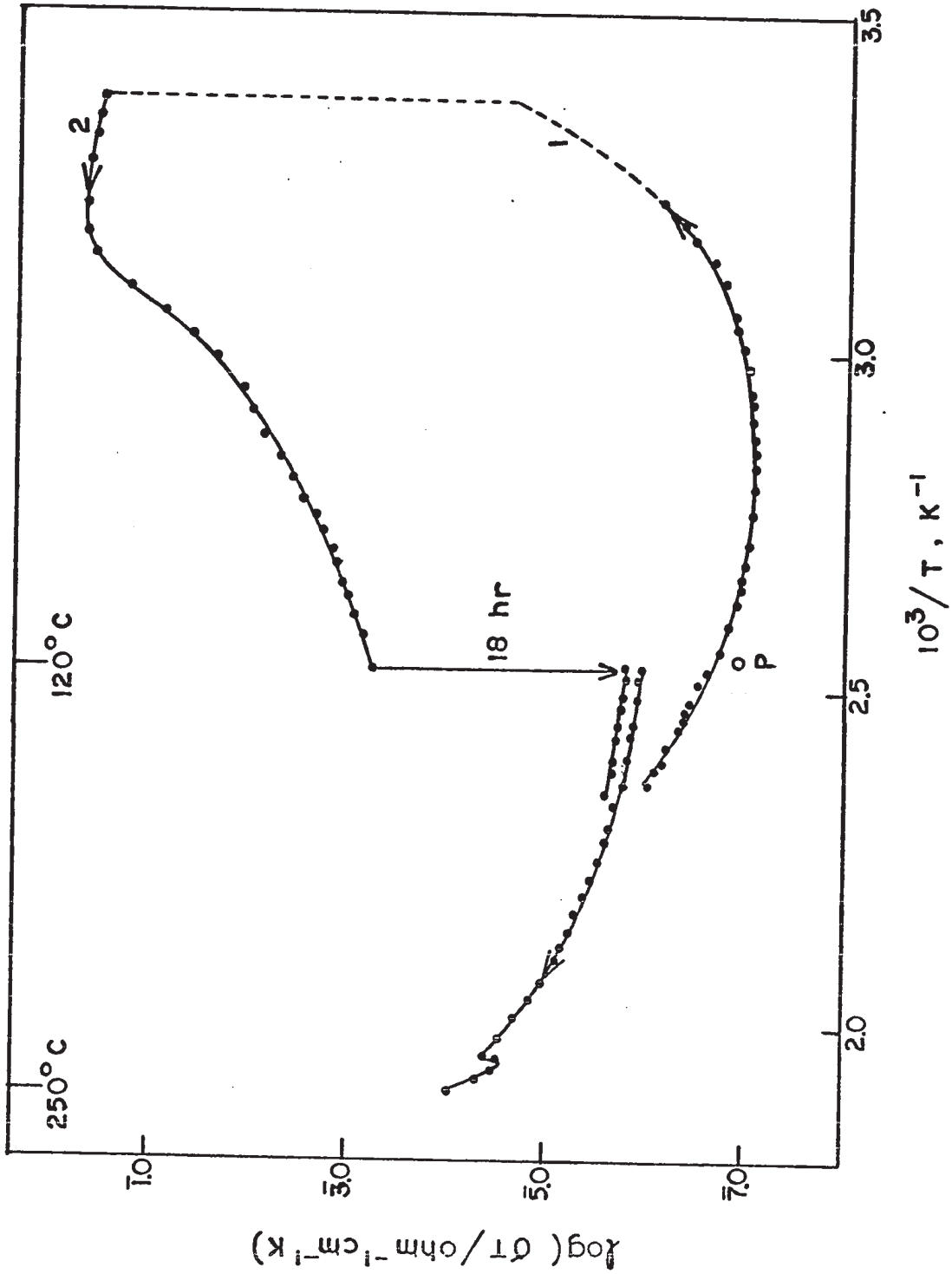

FIG. 31

EFFECT OF 80 TORR NH_3 ON THE CONDUCTIVITY OF AN AP PELLET

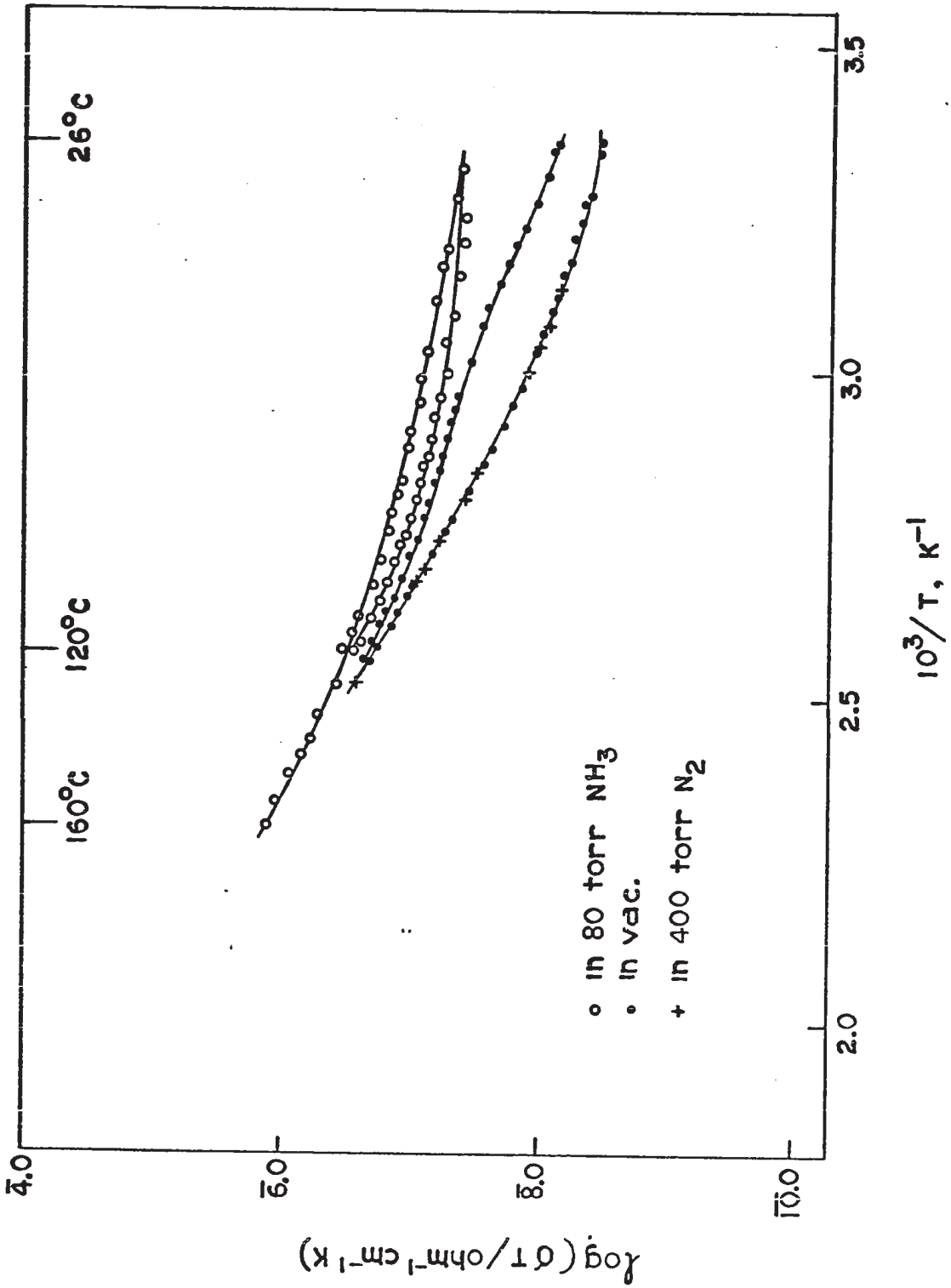

FIG. 32

CONDUCTIVITY IN THE LOW-TEMPERATURE RANGE
USING GUARD RING ELECTRODE SYSTEM

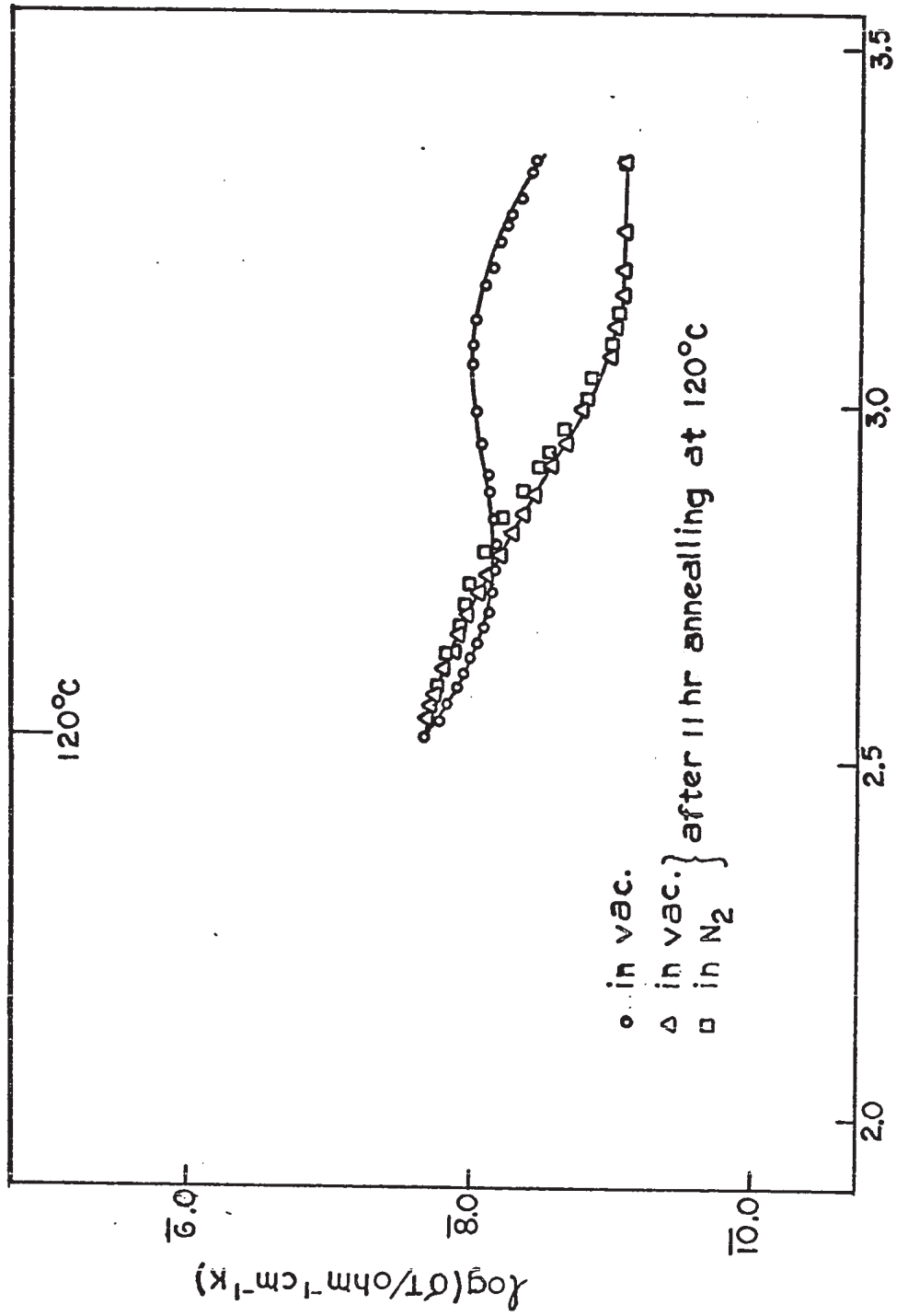

FIG. 33

EFFECT OF 107 AND 267 TORR NH_3 ON PELLET USING A GUARD RING ELECTRODE

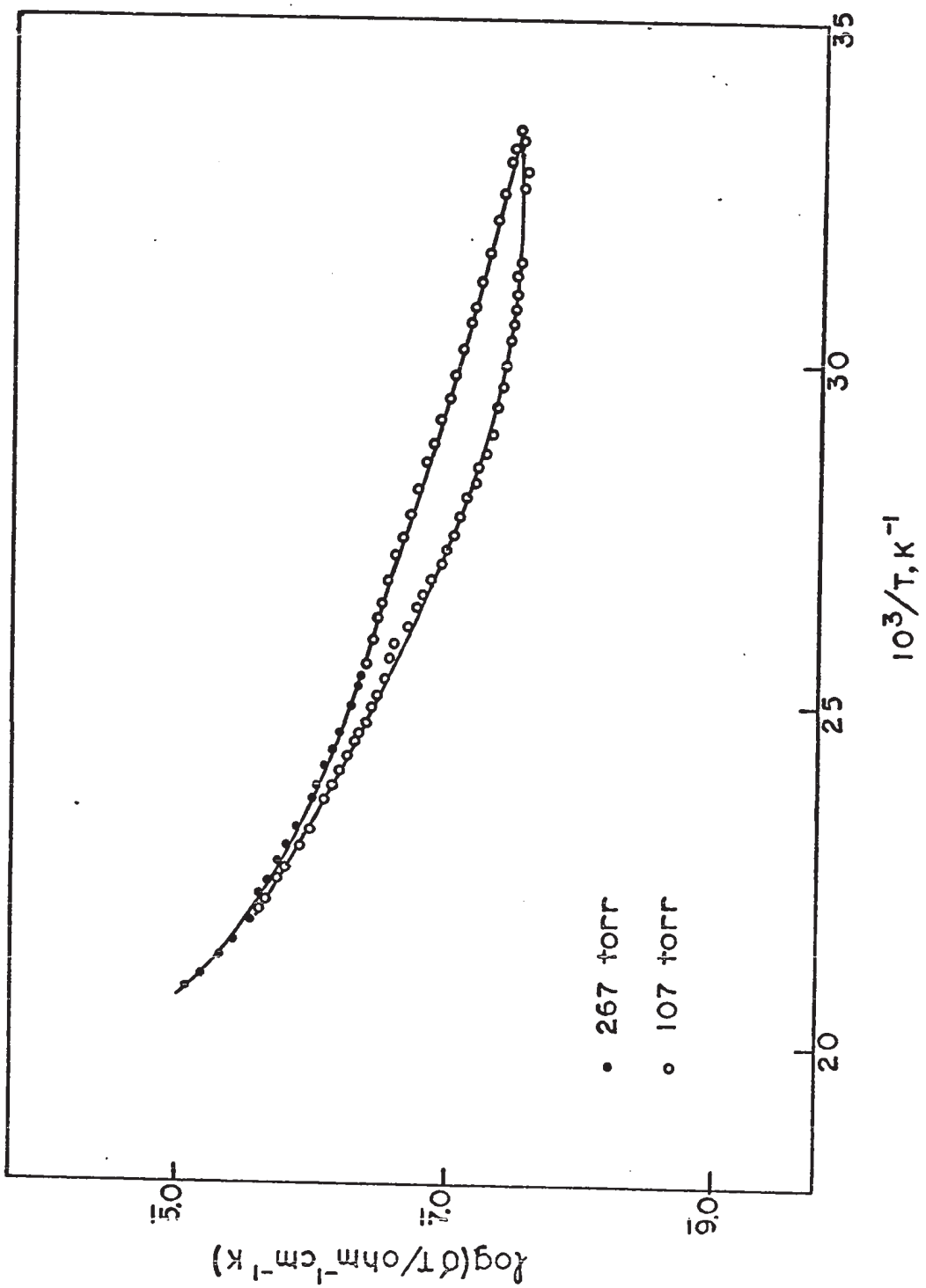

FIG. 34

CONDUCTIVITY OF SINGLE CRYSTAL AP

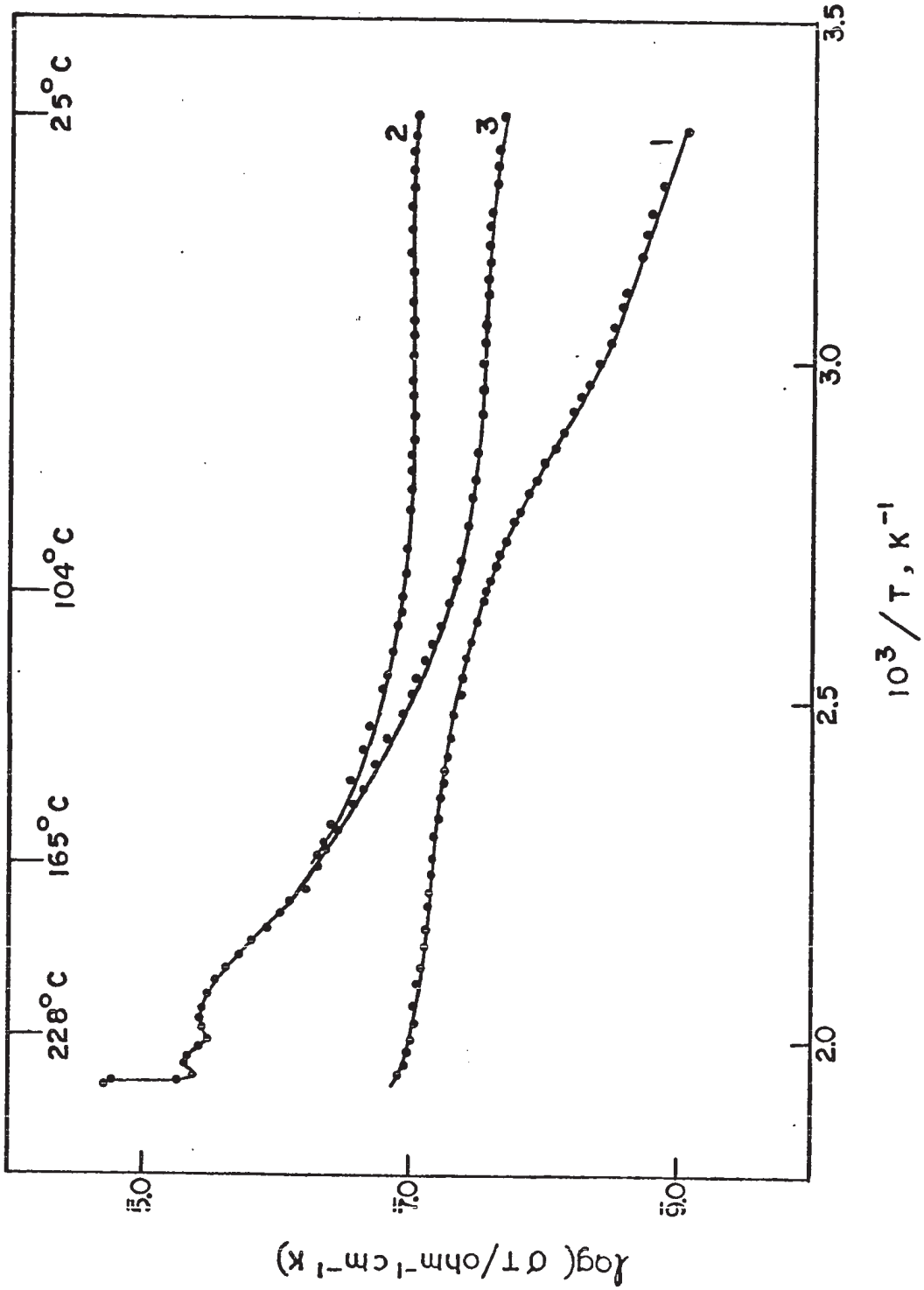

FIG. 35

CONDUCTIVITY OF A SINGLE CRYSTAL OF AP :
SUCCESSIVE RUNS WERE IN THE ORDER 1,2,3,4,5,6,7

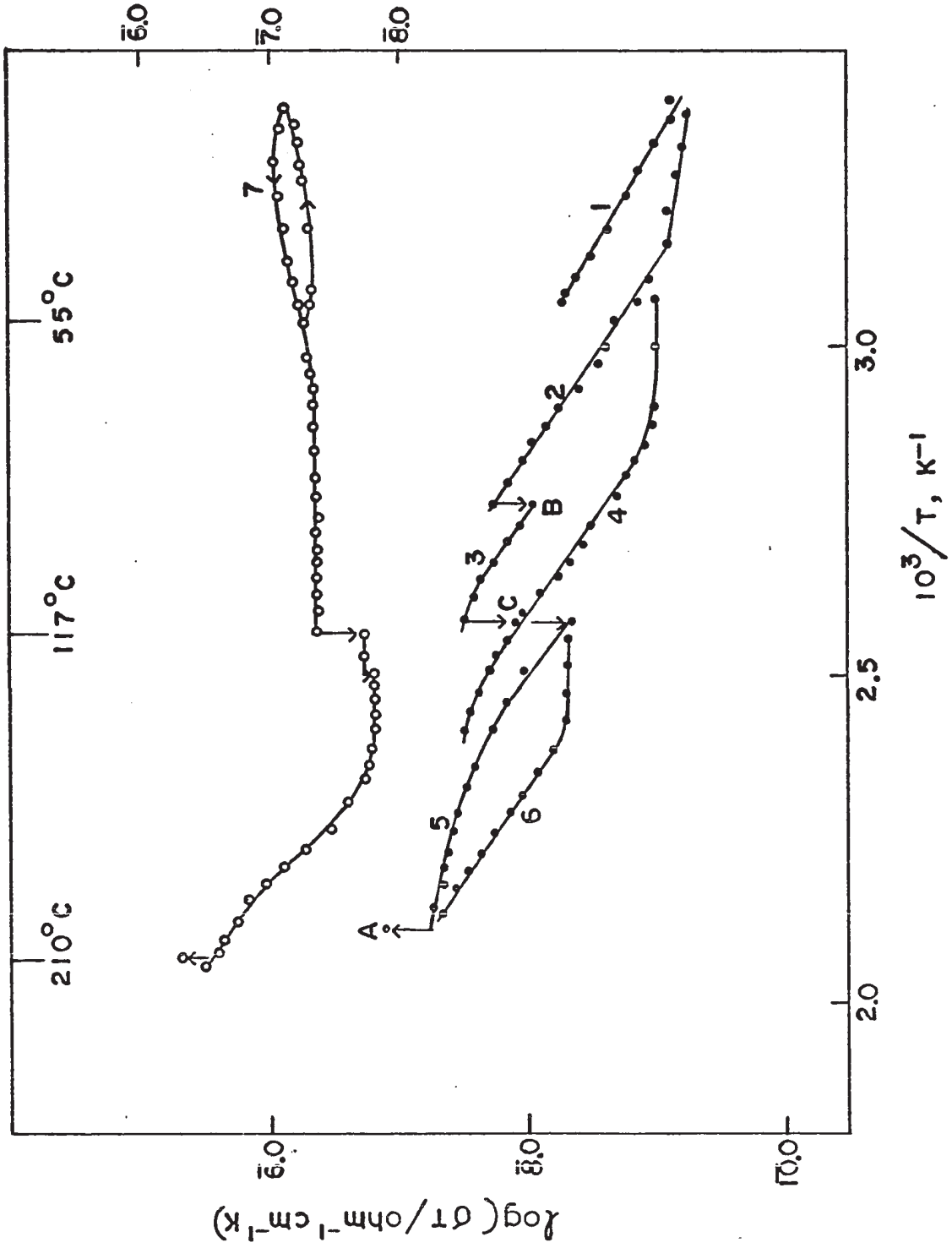

FIG. 36

CONDUCTIVITY OF A SINGLE CRYSTAL OF AP
MEASURED WITH A GUARD RING ELECTRODE

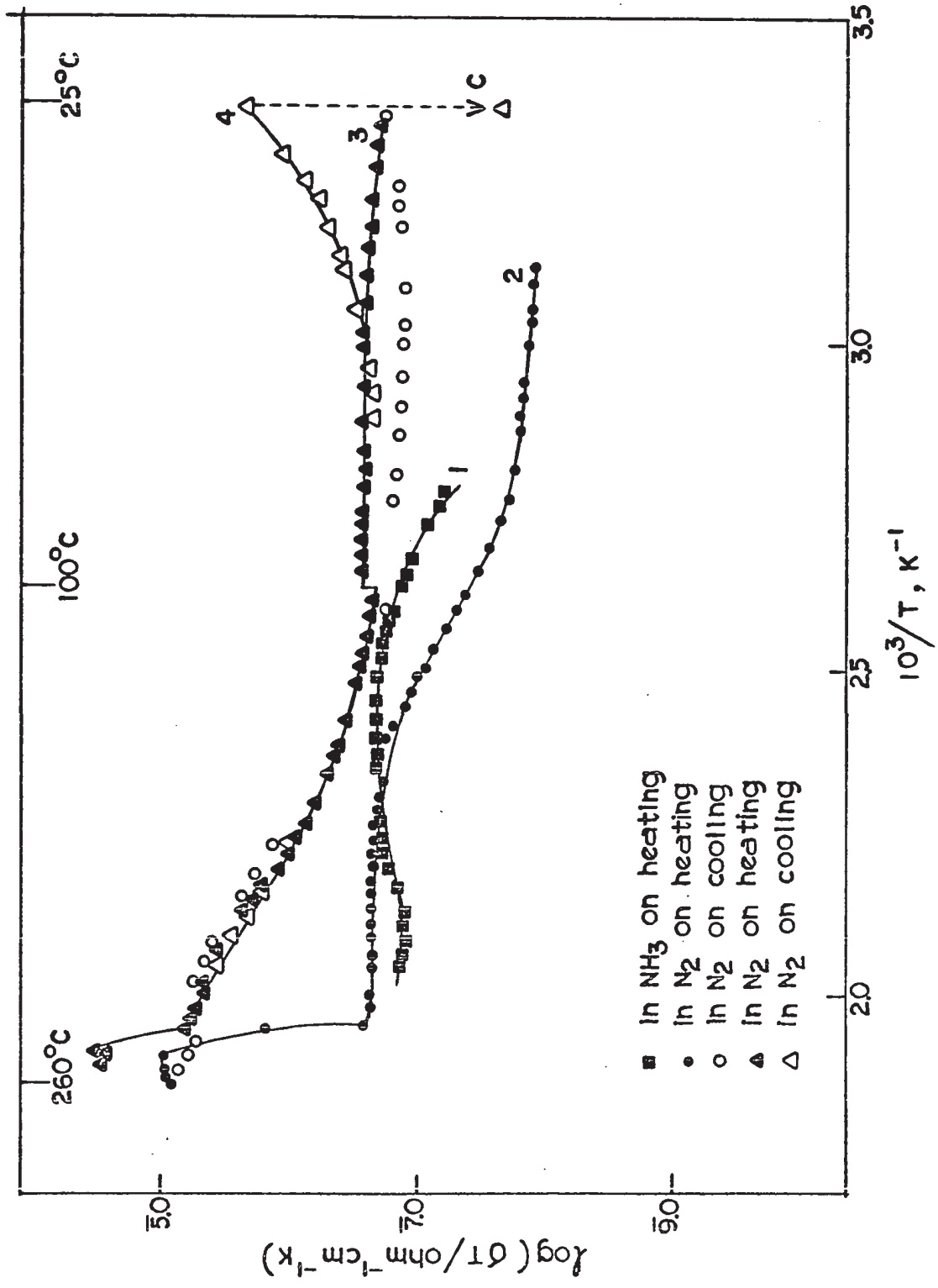

FIG. 37

TIME-DEPENDENCE OF CONDUCTIVITY DURING DECOMPOSITION AT 153°C (ARROW A IN FIG. 26)

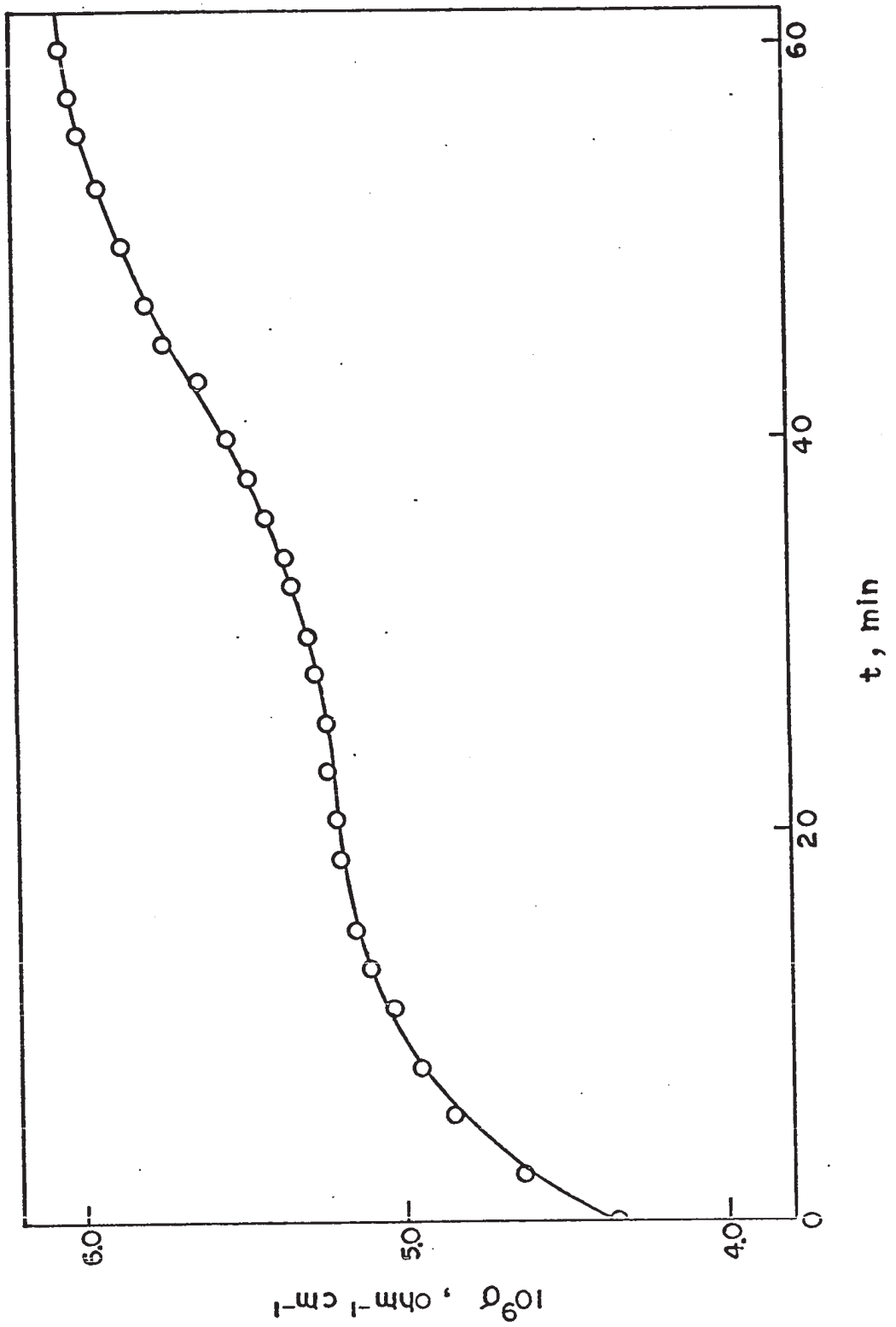

FIG. 38

ANNEALING AT 118°C OF PELLET IN VAC.
(ARROW A IN FIG. 29)

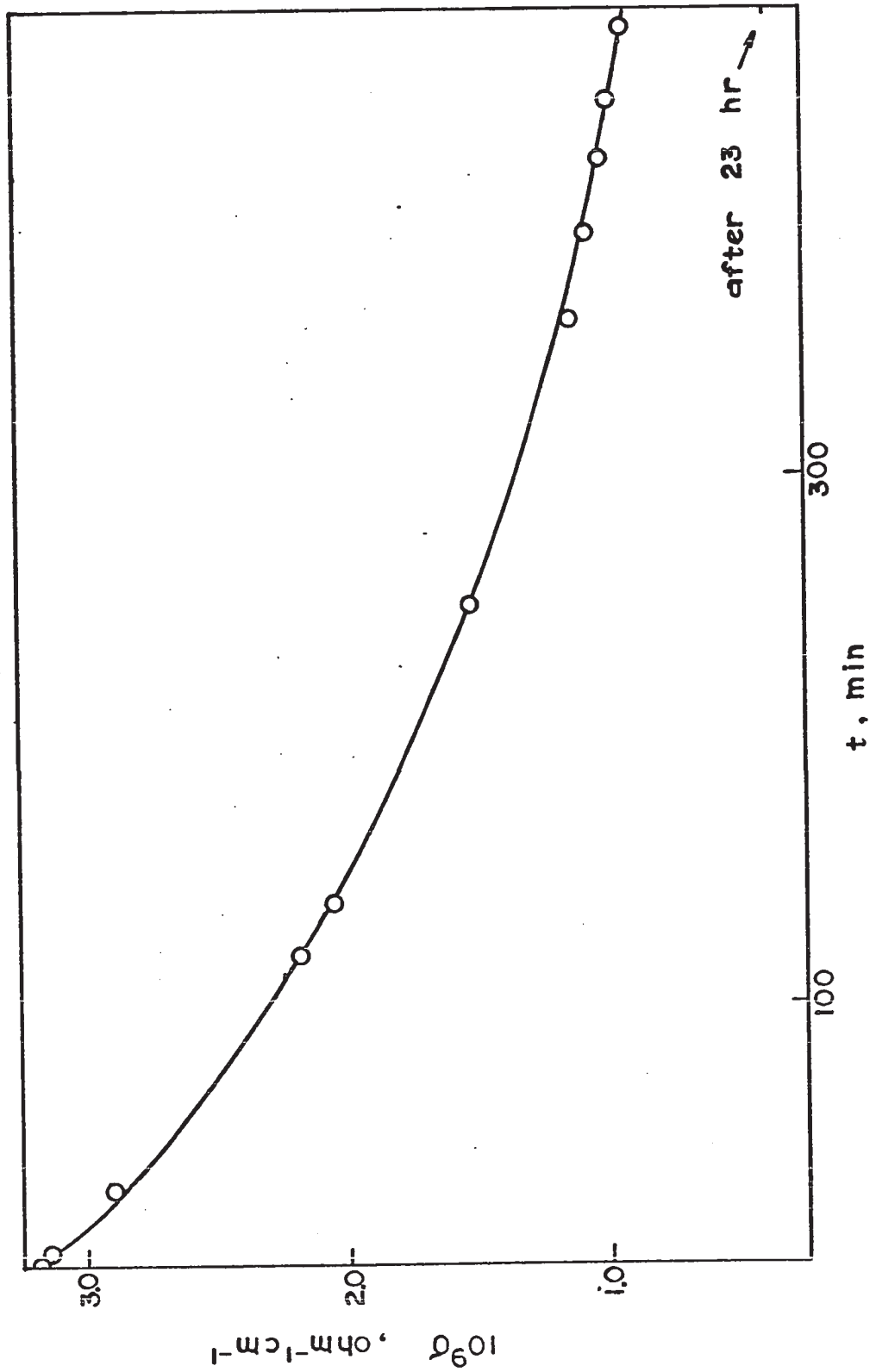

FIG. 39

PLOTS OF σ VS. $t^{\frac{1}{2}}$ AND $\log t$ FOR ANNEALING OF AN AP PELLET AT 118°C ($\sigma(t)$ IS SHOWN IN FIG. 38)

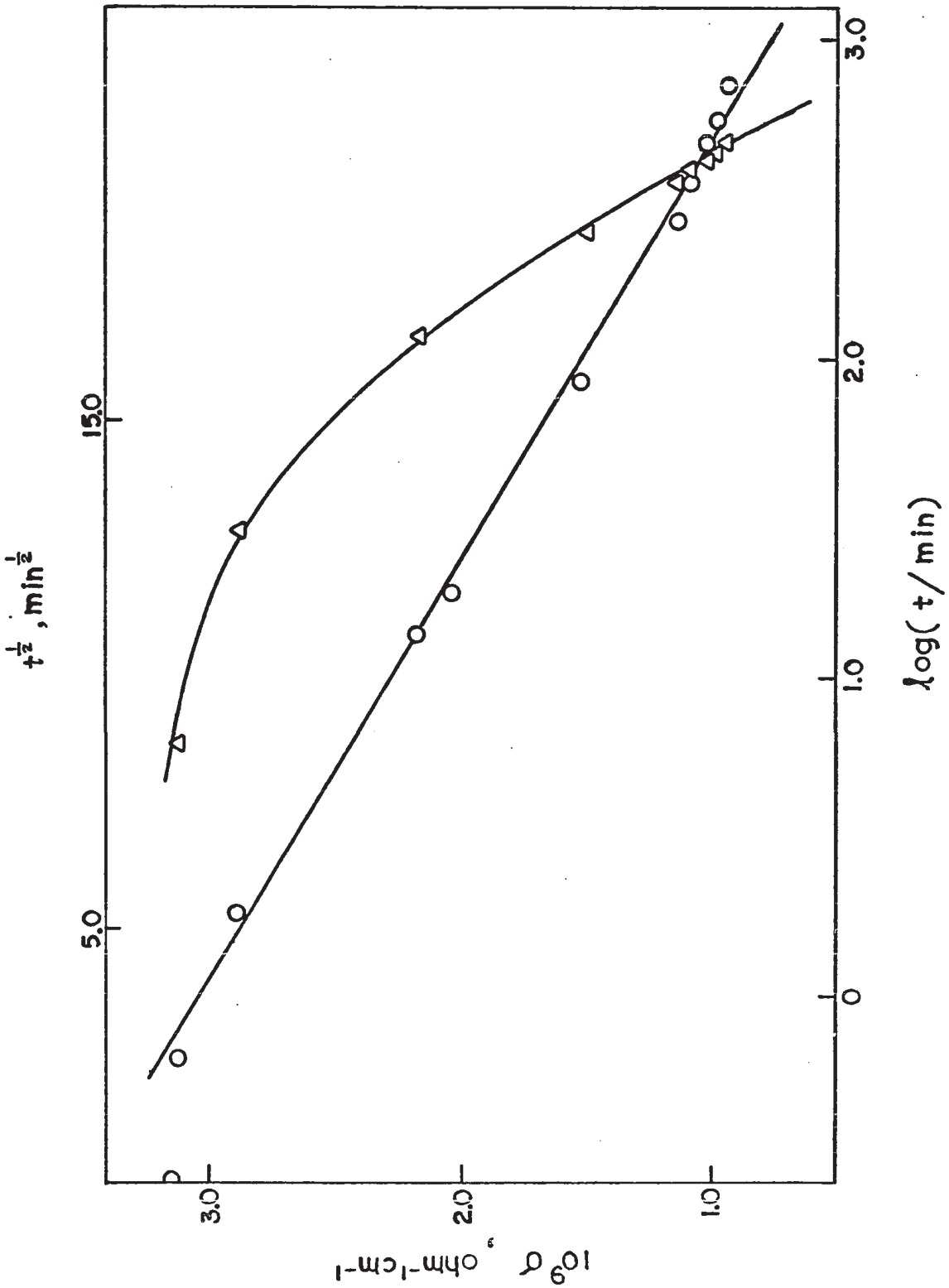

FIG. 40

CHANGE OF σ WITH TIME IN A DECOMPOSING CRYSTAL AT 193°C (ARROW A IN FIG. 35)

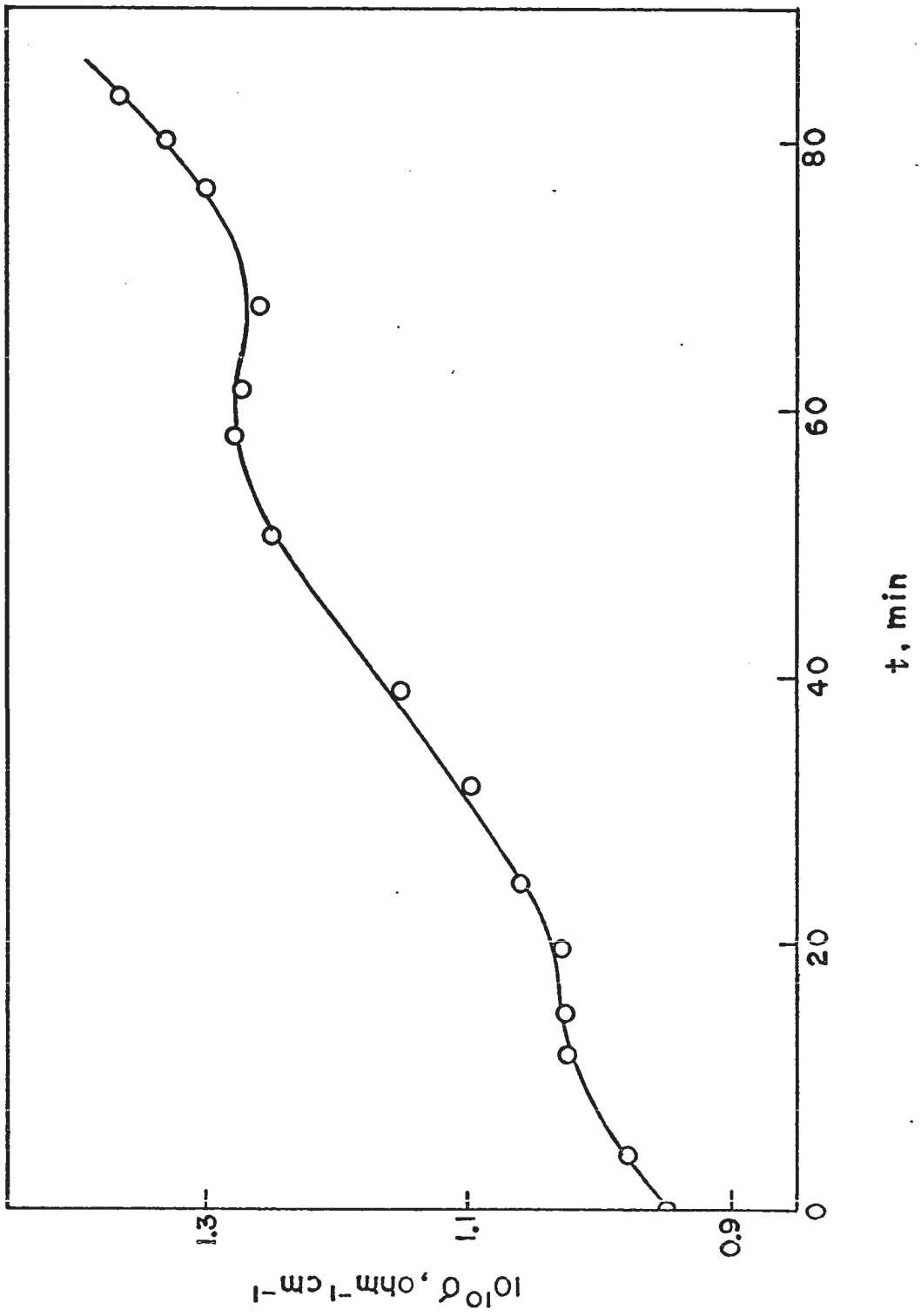

FIG. 41

CONDUCTIVITY CHANGES ON ANNEALING A SINGLE CRYSTAL AT 89°C AND 114°C (ARROWS B, C IN FIG. 35)

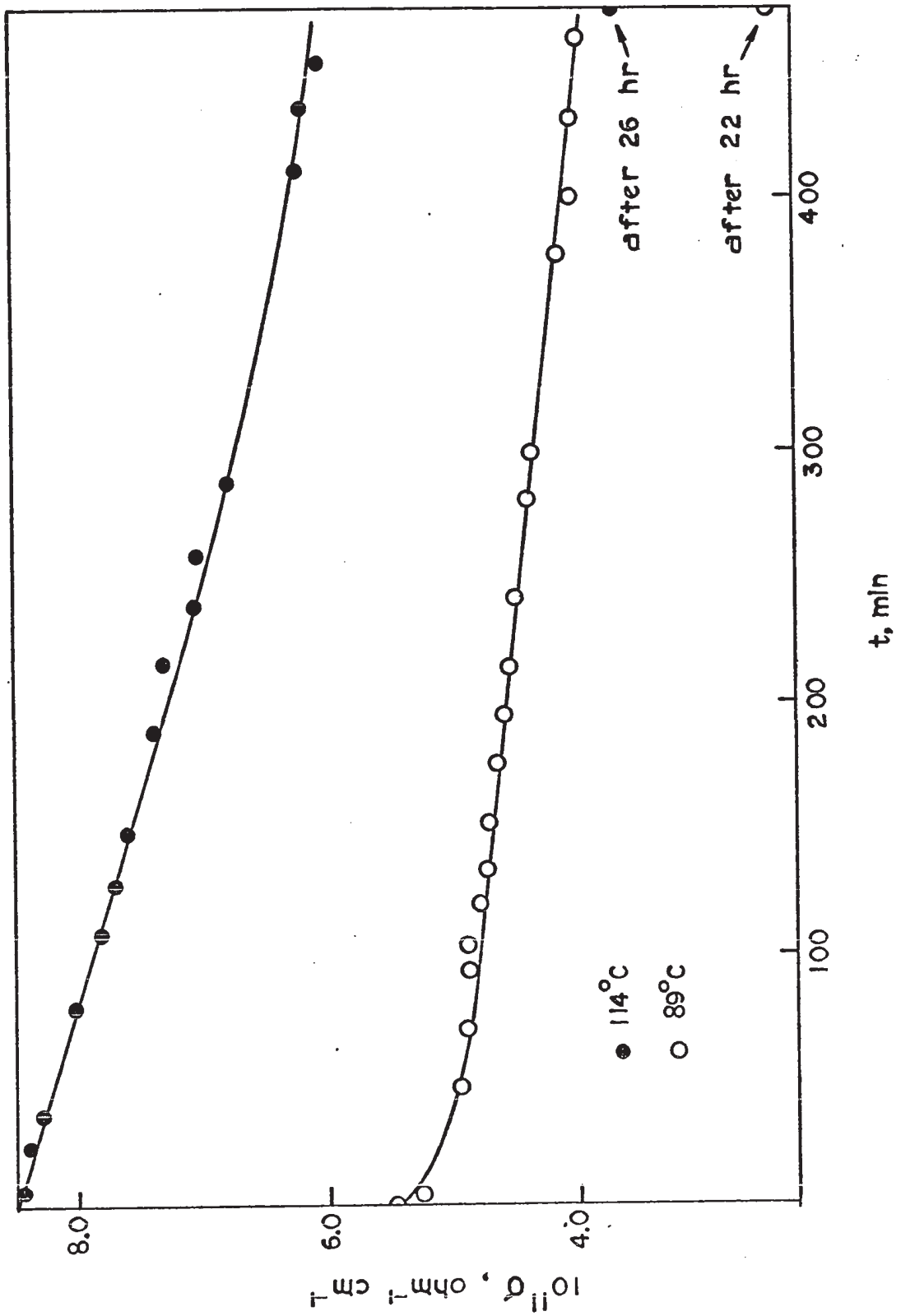

FIG. 42

PLOTS OF σ VS. $t^{\frac{1}{2}}$ AND $\log t$ FOR THE ANNEALING OF AN AP SINGLE CRYSTAL AT 89°C AND 114°C

[REFER TO FIG. 41 FOR $\sigma(t)$]

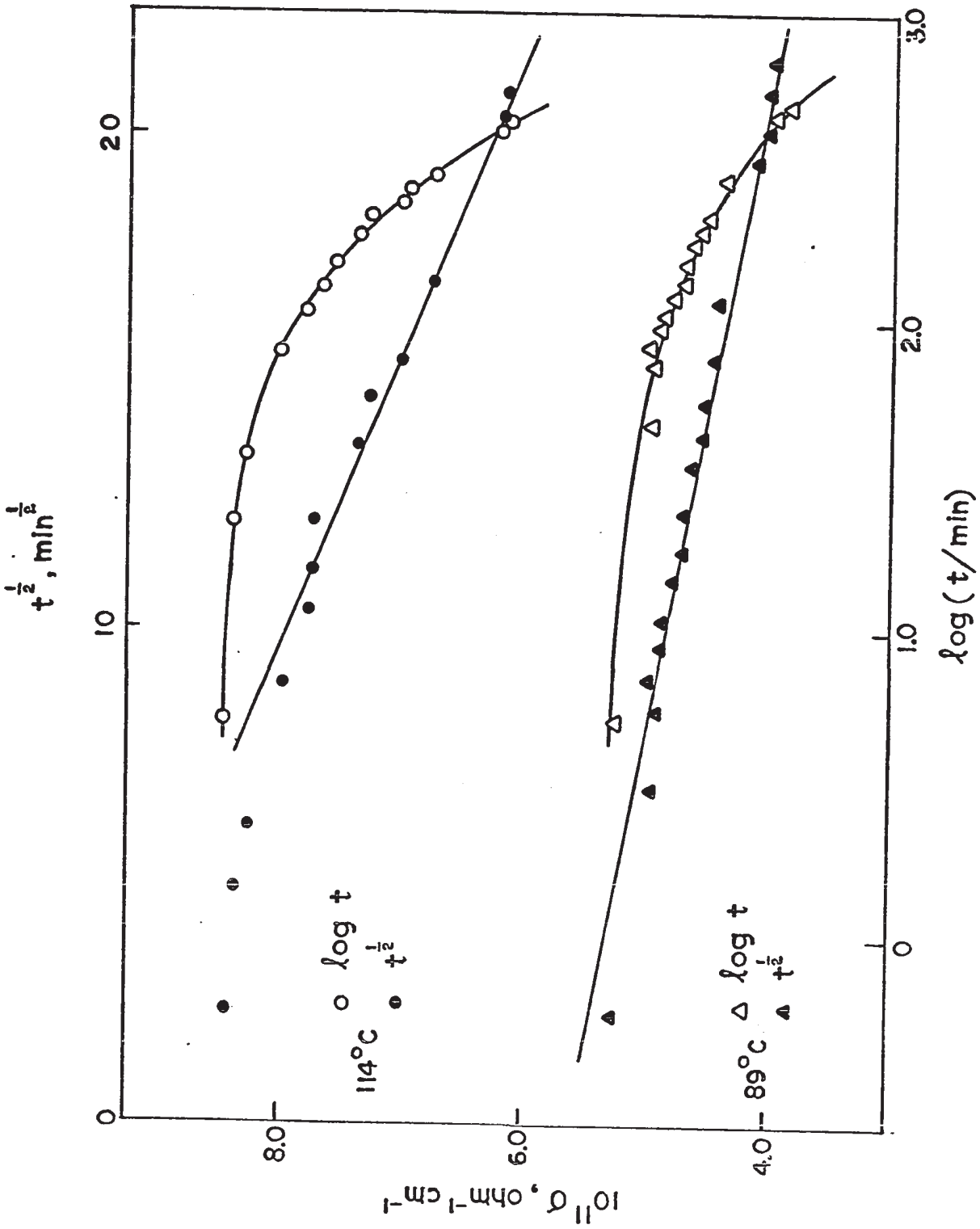

FIG. 43

ADSORPTION AND DESORPTION ISOTHERMS AT 83°C FOR AN AP PELLET IN 157 TORR NH_3

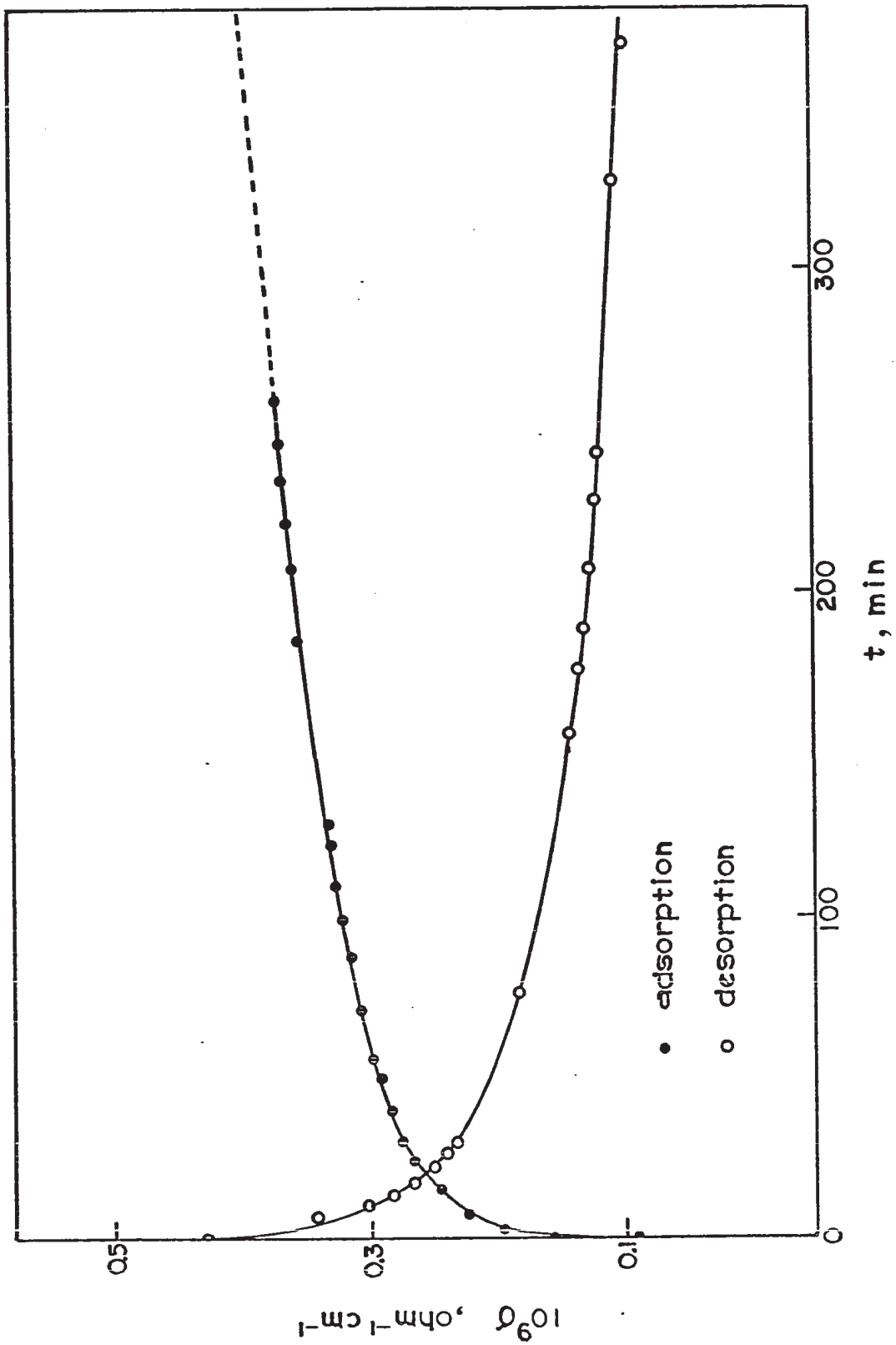

FIG. 44

PLOT OF σ VS. $\log t$, $t^{\frac{1}{2}}$ FOR AN PELLET IN NH_3 AT 83°C

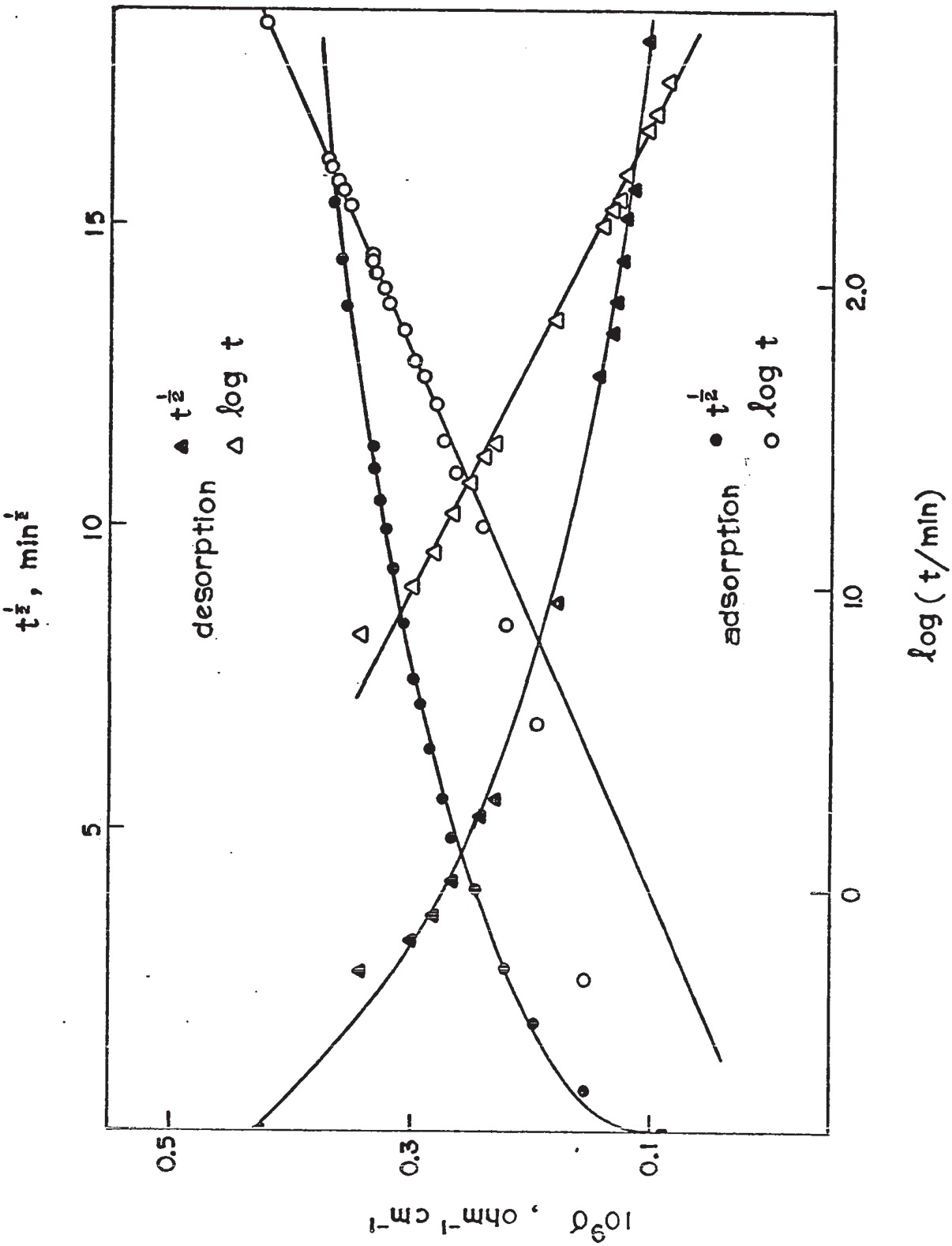

FIG. 45

ADSORPTION ISOTHERMS FOR A COMPRESSED PELLET OF AP IN NH_3

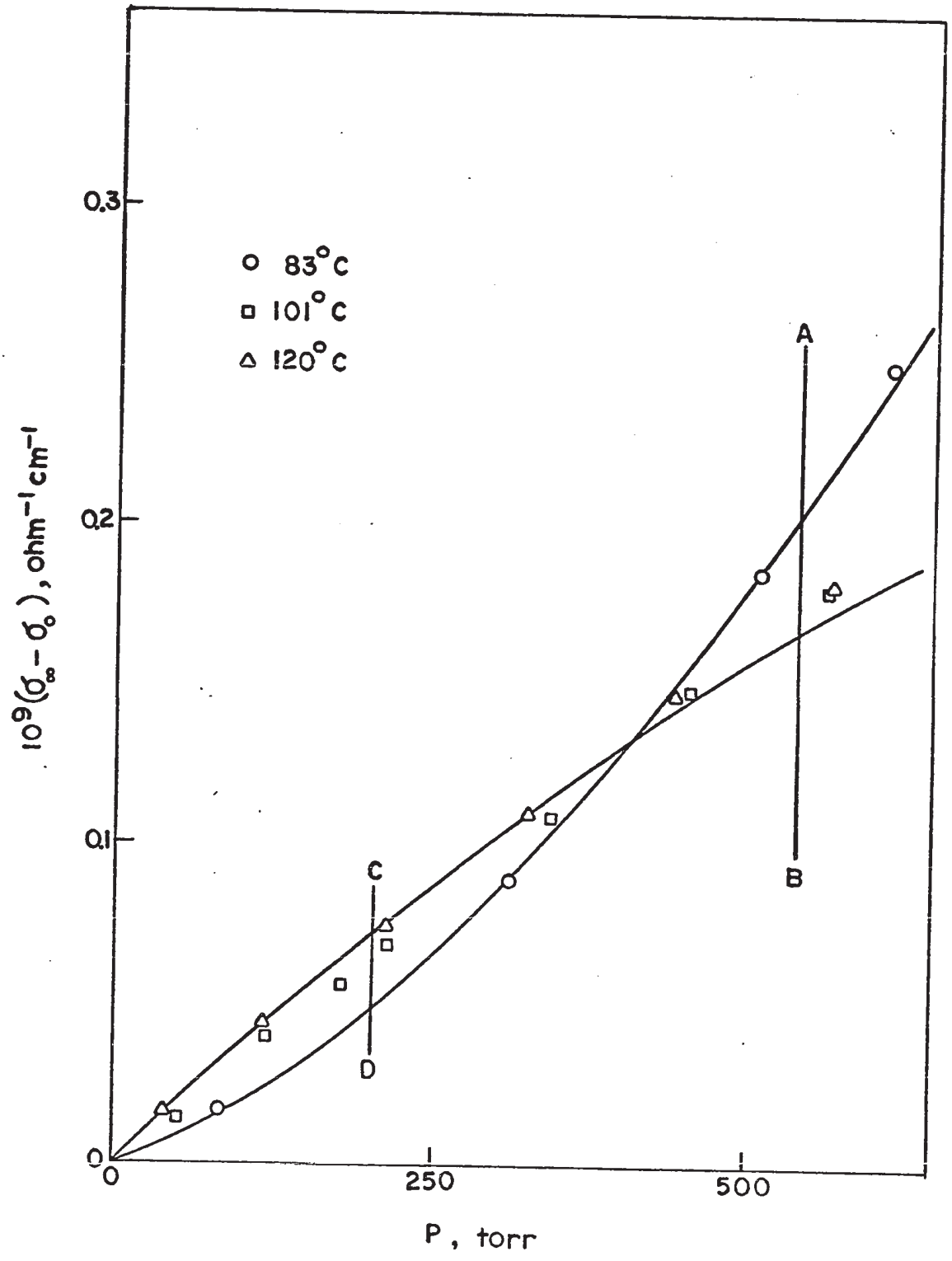

FIG. 46

DESORPTION OF NH_3 AT 116°C FROM A SINGLE CRYSTAL OF AP WHICH HAD BEEN EQUILIBRATED IN 581 TORR NH_3

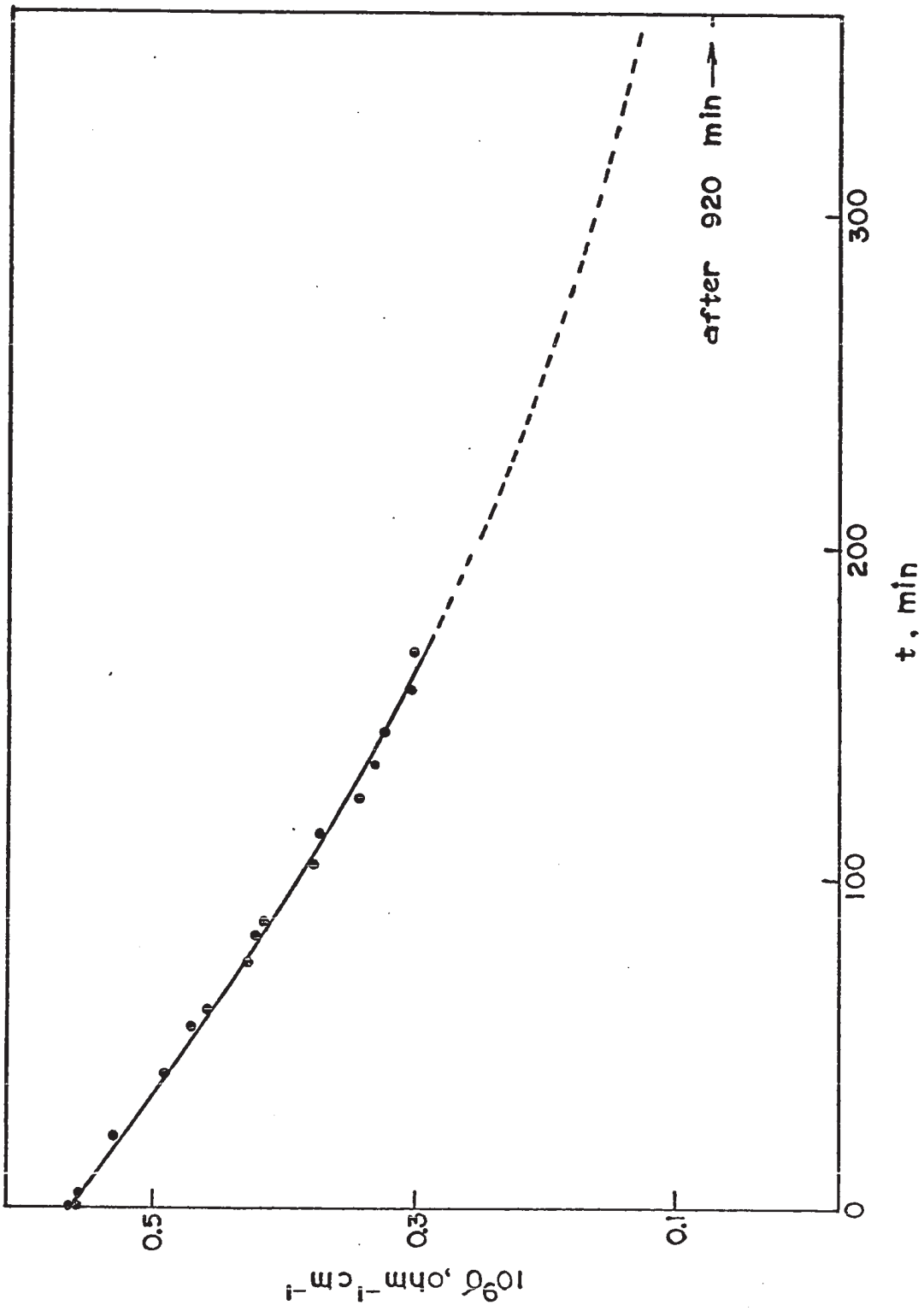

FIG. 47

PLOTS OF σ VS. $\log t$ AND $t^{\frac{1}{2}}$ FOR DESORPTION OF NH_3 FROM A SINGLE CRYSTAL OF AP AT 116°C

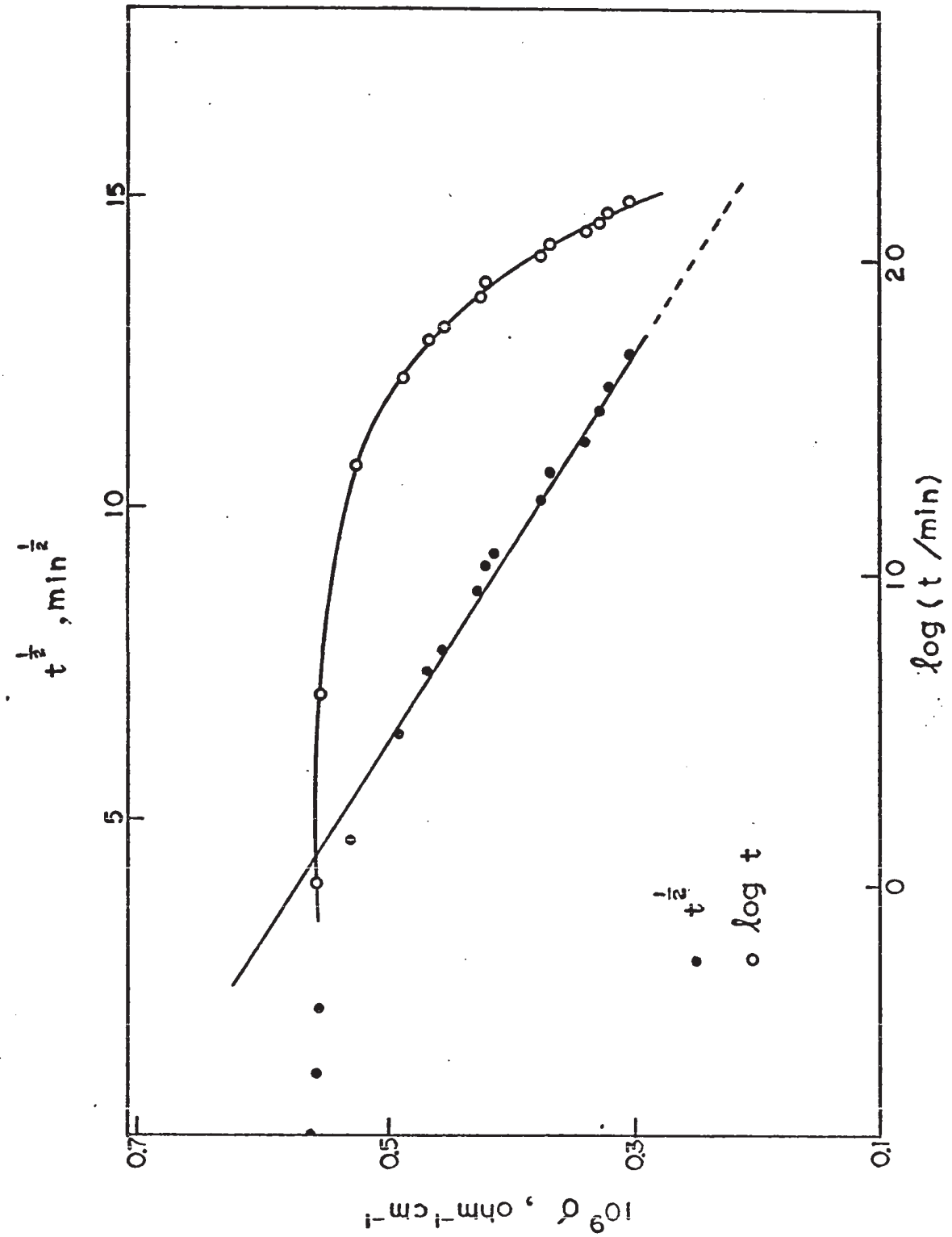

FIG. 48

PRESSURE ADSORPTION ISOTHERMS FOR SINGLE CRYSTAL AT 85°C, 102°C, 116°C

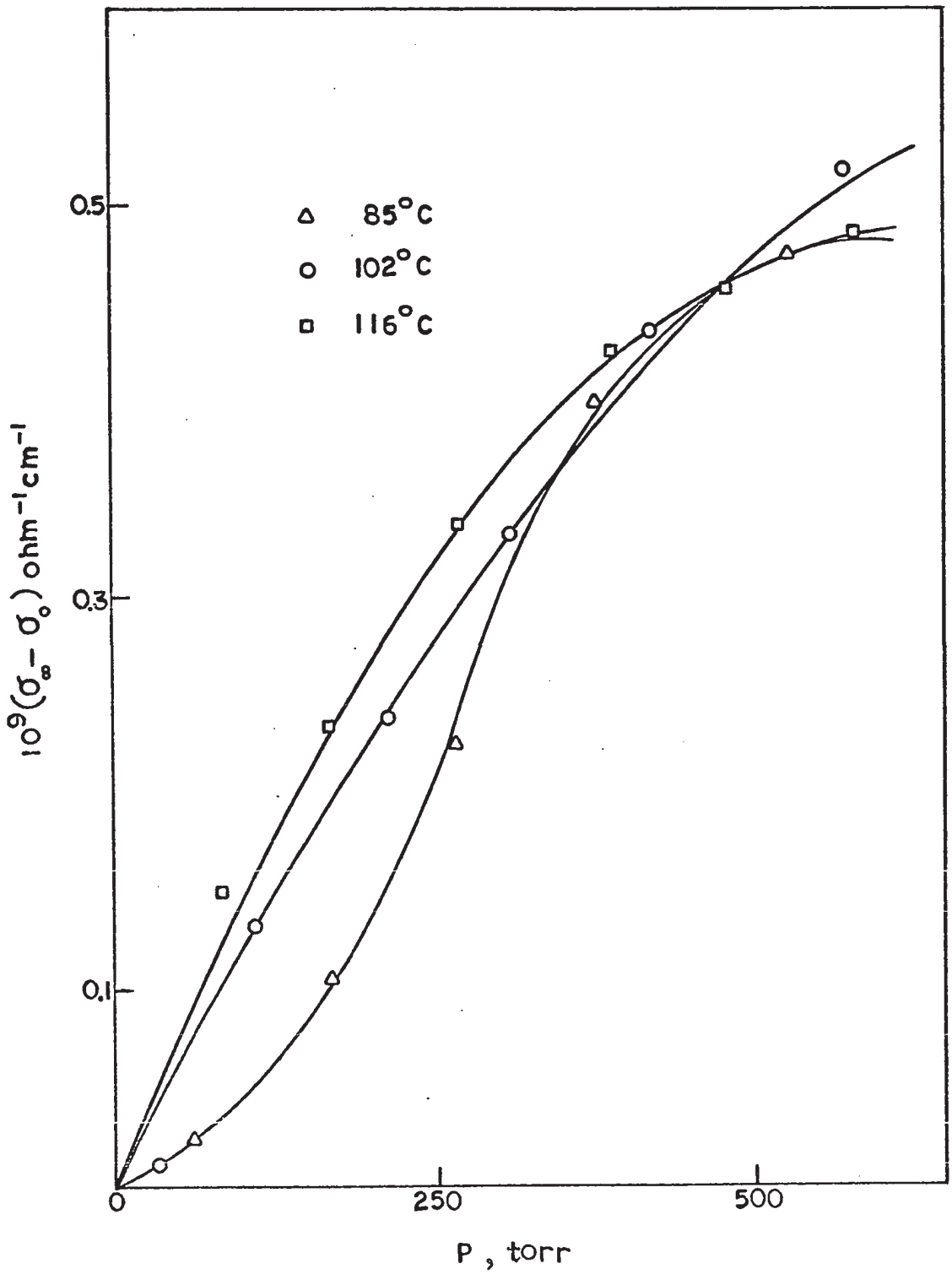

FIG. 49

PLOT OF $\ell n\ t_S$ AND $\ell n\ t_L$ VS. $10^3/T$ WHICH IDENTIFIES t_L AS THE TIME FOR COMPLETION OF SURFACE REACTION

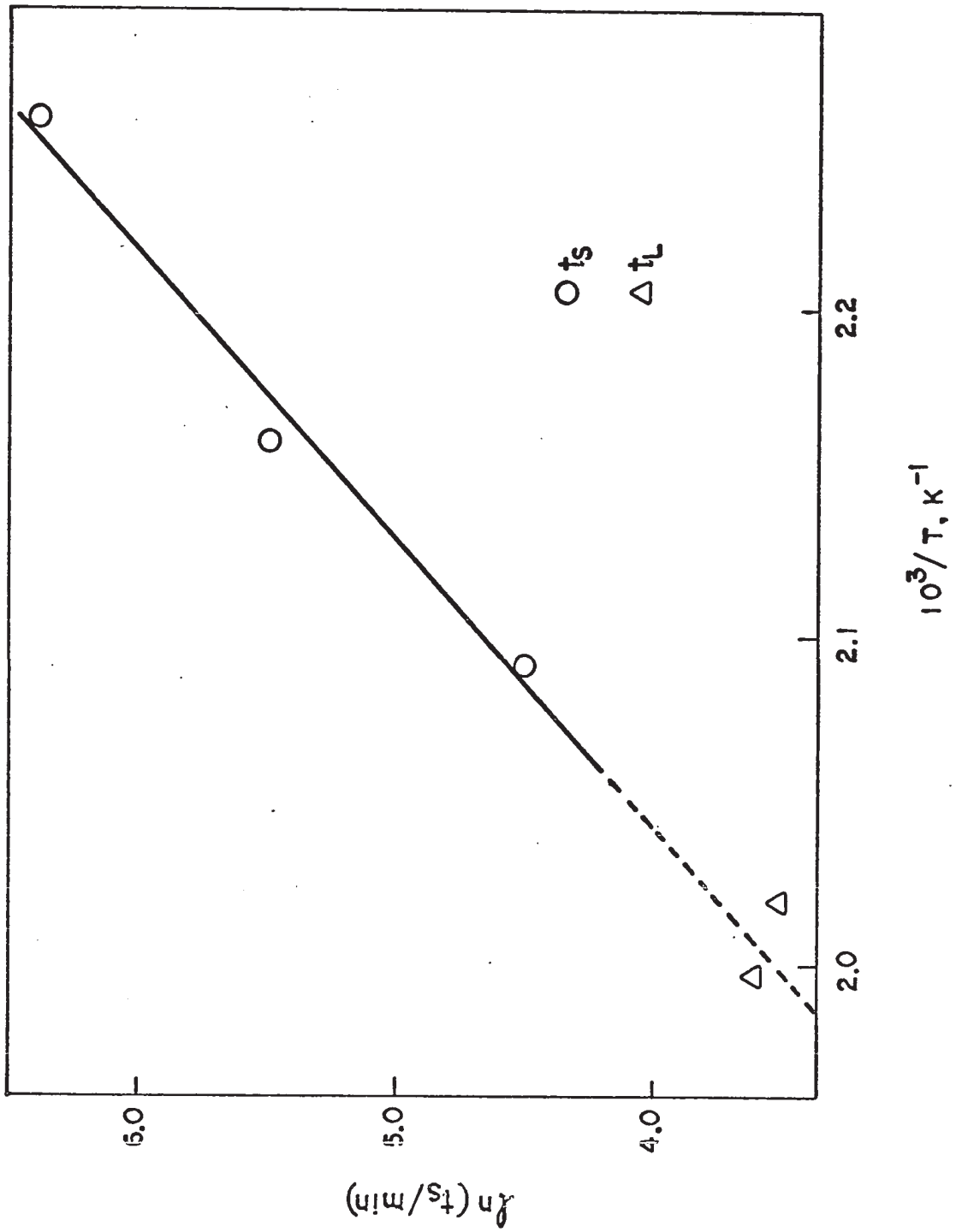

FIG. 50

DIAGRAMMATIC REPRESENTATION OF THE THREE PROCESSES OCCURRING IN THE DECOMPOSITION OF SOLID AP

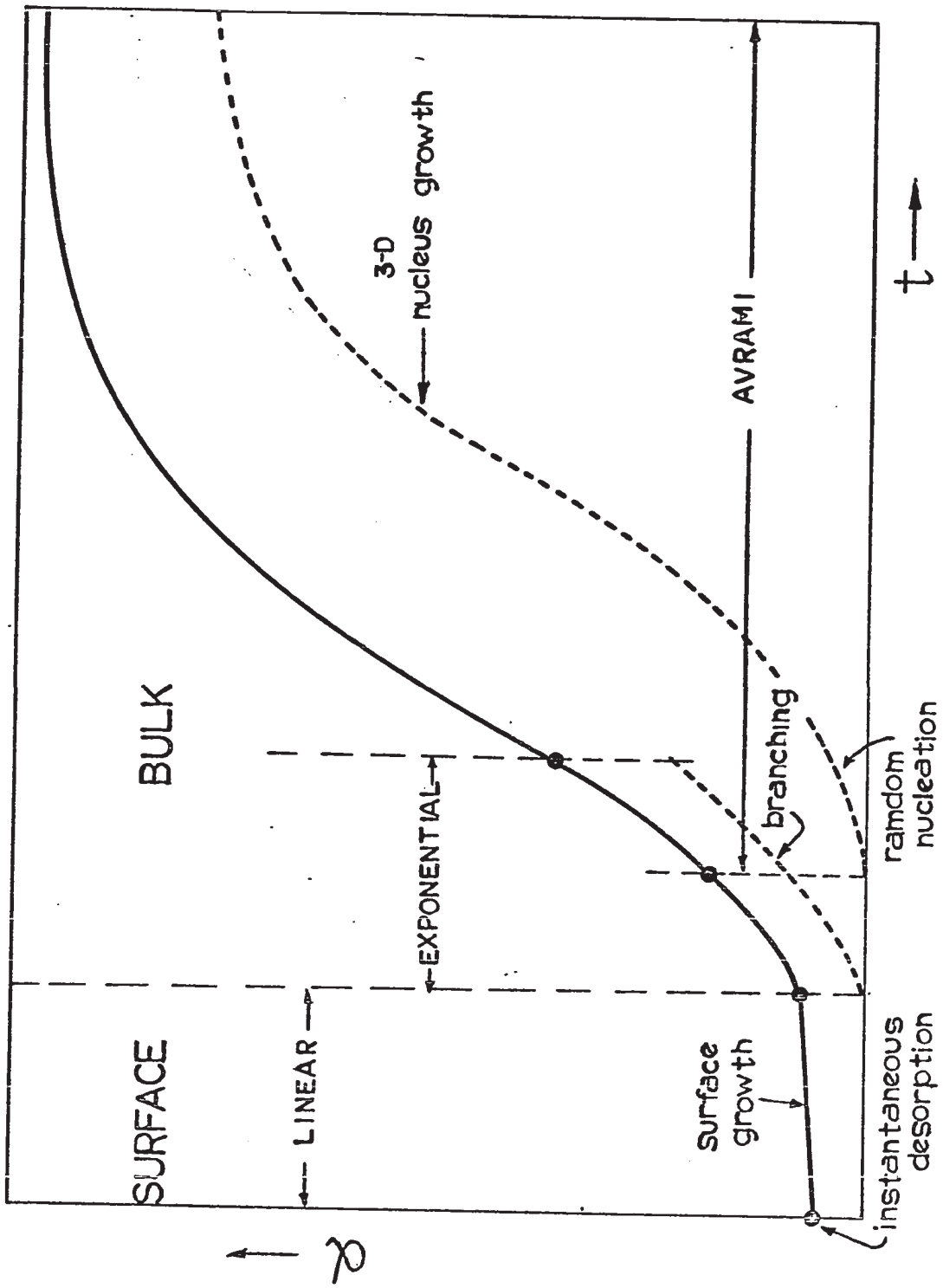

REFERENCES

1. W.E. Garner in "Chemistry of the Solid State" ed. by W.E. Garner (Butterworths, London, 1955), Chapters 8,9.

2. P.W.M. Jacobs and F.C. Tompkins, in "Chemistry of the Solid State" ed. by W.E. Garner (Butterworths, London, 1955), Chapter 7.

3. W.E. Garner and A.S. Gomm, J. Chem. Soc., 2123 (1931).

4. N.F.H. Bright and W.E. Garner, J. Chem. Soc., 1872 (1934).

5. A. Wischin, Proc. Roy. Soc., A172, 314 (1939).

6. J. Hume and J. Colvin, Proc. Roy. Soc., A125, 635 (1929).

7. M. Avrami, J. Chem. Phys. 7, 1103 (1939).

8. A.K. Galwey and P.W.M. Jacobs, Proc. Roy. Soc., A254, 455 (1960).

9. L.L. Bircumshaw and B.H. Newman, Proc. Roy. Soc., A227, 115 (1954).

10. P.W.M. Jacobs, Materials Science Research, 4, 37 (1969).

11. P.W.M. Jacobs and H.M. Whitehead, Chem. Rev., 69, 551 (1969).

12. A.R. Hall and G.S. Pearson "Ammonium Perchlorate: A Review of its Role in Composite Propellant Combustion", R.P.E. Technical Report 67/1, 1967; Oxidation Combustion Rev., 3, 129 (1968).

13. A. Seidell, "Solubilities of Inorganic and Organic Substances" (D. Van Nostrand Co., New York, 1919).

14. P.J. Herley, P.W.M. Jacobs and P.W. Levy, Proc. Roy. Soc., London, A318, 197 (1970).

15. P.W.M. Jacobs and A. Russell-Jones, J. Phys. Chem., 72, 202 (1968).

16. P.J. Herley and P.W. Levy, J. Chem. Phys., 49, 1493 (1968).

17. P.J. Herley and P.W. Levy, J. Chem. Phys., 49, 1500 (1968).

18. J.V. Davies, P.W.M. Jacobs and A. Russell-Jones, Trans. Faraday Soc., 63, 1737 (1967).

19. A.K. Galwey and P.W.M. Jacobs, Trans. Faraday Soc., 55, 1165 (1959).

20. A.K. Galwey and P.W.M. Jacobs, Trans. Faraday Soc., 56, 581 (1960).

21. S.H. Inami and J. Wise, Combustion and Flame, 12, 41 (1968).

22. E.S. Freeman and D.A. Anderson, J. Phys. Chem., 63, 1344 (1959).

23. E.S. Freeman and D.A. Anderson, J. Phys. Chem., 65, 1662 (1961).

24. E.S. Freeman, D.A. Anderson and J.J. Campisi, J. Phys. Chem., 64, 1727 (1960).

25. G. Odian, T. Acker and T. Pletzke, J. Phys. Chem., 69, 2477 (1965).

26. A.G. Keenan and R.F. Siegmund, Quart. Rev., 23, 430 (1969).

27. J.N. Maycock, V.R. Pai Verneker and C.S. Gorzynski Jr., Solid State Comm., 5, 225 (1967); Proc. Roy. Soc., A307, 303 (1968).

28. Yu. P. Savintsev, G.E. Makarova and V.V. Boldyrev, Kinetika i Kataliz, 9, 542 (1968).

29. F. Solymosi and K. Dobo in "Reactivity of Solids", ed. by J.H. de Boer (Elsevier Publishing Co., Amsterdam, 1964). Art. No. 41.

30. K.O. Hartman, paper presented at 1969 Spring Meeting of the Western States Section of the Combustion Institute, U.S. Naval Weapons Center, China Lake, California.

31. V.V. Boldyrev, Dokl. Akad. Nauk SSSR, 181, 1406 (1968).

32. P. Zirkind and E.S. Freeman, Nature, 199, 1280 (1963).

33. H. Wise, J. Phys. Chem., 71, 2843 (1967).

34. V.V. Boldyrev and E.F. Khairetdinov, J. Inorg. Nucl. Chem., 31, 3332 (1969).

35. V.F. Komarov, V.V. Boldyrev, V.K. Zhuravlev and G.V. Ivanov, Kinetika i Kataliz, 7, 788 (1966).

36. P.J. Herley and P.W. Levy, Nature, 211, 1287 (1966).

37. P.J. Herley and P.W. Levy, paper presented at the 1969 Spring Meeting of the Western States Section of the Combustion Institute, China Lake, California, April 30 - May 2, 1969;
J. Phys. Chem., 75, 191 (1971).

38. S. Fogler and D. Lawson, J. Phys. Chem., 74, 1637 (1970).

39. A.V. Raevskii and G.B. Manelis, Dokl. Akad. Nauk SSSR, 151, 886 (1963).

40. K.J. Kraeutle, J. Phys. Chem., 74, 1350 (1970).

41. J.L. Torgesen, A.T. Horton and C.P. Saylor, J. Research, Nat. Bur. Stand. C, 67C, 25 (1963).

42. A.K. Galwey and P.W.M. Jacobs, J. Chem. Soc., 837 (1959).

43. D.W. Marquardt, "Least-squares Estimation of Non-linear Parameters", Share Program No. 1428 (E.I. Du Pont de Nemours & Co., Inc. Wilmington, Delaware, 1964).

44. W.E. Garner and M.G. Tanner, J. Chem. Soc., 47 (1930).

45. E.G. Prout, J. Inorg. Nucl. Chem., 7, 368 (1958).

46. E.G. Prout and M.J. Sole, J. Inorg. Nucl. Chem., 9 232 (1959).

47. P.J. Herley and E.G. Prout, J. Inorg. Nucl. Chem., 16, 16 (1960).

48. E.G. Prout and D.J. Moore, Nature, 205, 1209 (1965).

49. W.E. Garner and H.R. Hailes, Proc. Roy. Soc., A139, 576 (1933).

50. B.V. Erofeev, Compt. Rend. Acad. Sci. URSS, 52, 511 (1946).

51. V.V. Boldyrev, Yu. P. Savintsev, and V.F. Komarov, Kinetika i Kataliz, 9, 542 (1968).

52. P.J. Herley, P.W.M. Jacobs and P.W. Levy, J. Chem. Soc. A, 434 (1971).

53. P.J. Herley and P.W. Levy, Proceedings National Symposium on Natural and Manmade Radiation in Space, American Nuclear Society, Las Vegas, Nevada, March 1971, (in press).

54. J.M. Thomas, Advances in Catalysis, 19, 296 (1969).

55. J. Frenkel, Z. Physik, 35, 652 (1926).

56. W. Schottky, Z. Phys. Chem. B, 29, 335 (1935).

57. J.M. Pollock and M. Sharan, J. Chem. Phys., 51, 3604 (1969).

58. E.J. Murphy, J. Appl. Phys., 35, 2609 (1964).

59. N. Riehl, Tran. New York Acad. Sci., 772 (1965).

60. A. Von Hippel, D.B. Knoll and W.B. Westphal, J. Chem. Phys., 54, 134 (1971).

61. S. Maricic, V. Pravdic and Z. Veksli, J. Phys. Chem. Solids, 23, 1651 (1962).

62. J.M. Thomas and T.A. Clarke, Trans. Faraday Soc., 65, 2718 (1969).

63. J.M. Pollock and M. Sharan, J. Chem. Phys., 47, 4064 (1967).

64. J.M. Pollock and A.R. Ubbelohde, Trans. Faraday Soc., 52, 1112 (1956).

65. T.M. Herrington and L.A.K. Staveley, J. Phys. Chem. Solids, 25, 921 (1964).

66. R.G. Fuller and F.W. Patten, J. Phys. Chem. Solids, 31, 1539 (1970).

67. O.P. Bahl and J.M. Thomas, J. Mater. Sci., 2, 500 (1967).

68. V.V. Boldyrev, O.P. Korobeinichev and V.N. Pan'kov, Kinetika i Kataliz, 9, 218 (1967).

APPENDIX I

VARIABLE PARAMETERS USED IN LEAST-SQUARES FITTING OF THE KINETIC RESULTS

SYMBOL		DEFINITION
b_1	=	P_o, instantaneous desorption at t=0
b_2	=	k_L, rate constant in the linear process
b_3	=	t_L, time for the completion of linear process
b_4	=	C_3, pre-exponential coefficient in the exponential process
b_5	=	k_3, branching rate constant in the exponential process
b_6	=	$t_E - t_L$, duration of the exponential process
b_7	=	P_A, final pressure at the completion of the Avrami process
b_8	=	C_1, pre-exponential coefficient in the Avrami process
b_9	=	k_1, rate constant for nucleation in the Avrami process
b_{10}	=	$t_E - t_A$, duration for the overlapping of exponential process and the Avrami process
$b_8^{1/3} b_9$	$\propto$	k_2, rate constant for nucleus growth in the Avrami process

APPENDIX II

PRINCIPAL SYMBOLS USED IN THE KINETIC ANALYSIS OF THE THERMAL DECOMPOSITION DATA

SYMBOL	UNITS	DEFINITION
P_o	torr	instantaneous desorption at t=0
P_A	torr	final pressure at the completion of the Avrami process
PF	torr	final pressure at the completion of the entire reaction
k_L	torr min^{-1}	rate constant in the linear process
k_{21}	min^{-1}	rate constant for the inward growth of surface nuclei
$\bar{k}_2$	min^{-1}	rate constant in the AE equation for n=2
$\bar{k}_3$	min^{-1}	rate constant in the AE equation for n=3
k_1	min^{-1}	rate constant for nucleation in the bulk
k_2	min^{-1}	rate constant for nucleus growth in the bulk
k_3	min^{-1}	branching rate constant in the exponential process
C_1		pre-exponential coefficient in the Avrami process
C_3	torr	pre-exponential coefficient in the exponential process
t_L	min	time for the completion of linear process
t_E	min	time for the termination of exponential process
t_A	min	time for the commencement of Avrami process

SYMBOL	UNITS	DEFINITION
N		number of nuclei formed at time t
N_o		number of potential nucleus forming sites
σ		shape factor for nuclei, e.g. $4\pi/3$ for spherical nuclei
α_{LT}		fractional decomposition at the termination of linear process
α_{ET}		fractional decomposition at the termination of exponential process
α_{AS}		fractional decomposition at the commencement of the Avrami process